Développement de procédés de gravure à base de plasmas réactifs pulsés Pulsed plasmas for etch applications

Moritz Haass

UNIVERSITÉ DE GRENOBLE

THÈSE

Pour obtenir le grade de

DOCTEUR DE L'UNIVERSITÉ DE GRENOBLE

Spécialité : **Nano-Electronique et Nano-Technologies**

Arrêté ministérial : 7 août 2006

Présentée par

Moritz Haass

Thèse dirigée par **Olivier Joubert**

préparée au sein **du LTM (CNRS/UJF-Grenoble1/CEA)**
et de **l'école doctorale EEATS**

Pulsed plasmas for etch applications

Développement de procédés de gravure à base de plasmas réactifs pulsés

Thèse soutenue publiquement le **6 novembre 2012**,
devant le jury composé de :

René-Louis INGLEBERT
Professeur, Directeur de l'Ecole Polytechnique de l'Université Grenoble-I, Président
David GRAVES
Professeur de l'University of California, Berkeley, USA, Rapporteur
Gilles CARTRY
Maître de conférences à l'Université de Marseille, Rapporteur
Efrain ALTAMIRANO SANCHEZ
Senior Researcher and R&D Engineer, IMEC, Belgium, Examinateur
Maxime DARNON
Chargé de recherche CNRS, LTM, Grenoble, Examinateur
Olivier JOUBERT
Directeur de recherche CNRS, LTM, Grenoble, Directeur de thèse

Contents

Nomenclature

AC	alternating current
αC	amorphous carbon
ARDE	aspect ratio dependent etching
ARXPS	angle-resolved X-ray photoelectron spectrometry
CCP	capacitively coupled plasma
CD	critical dimension
CW	continuous wave
DC	direct current
DPS	decoupled plasma source
ECR	electron cyclotron resonance
HDP	high density plasma
HF	hydrofluoric acid
HWP	helicon wave plasma
IC	integrated circuit
ICP	inductively coupled plasma
IEDF	ion energy distribution function
IFP	ion flux probe
ITRS	International Technology Roadmap for Semiconductors
LED	light emitting diode
LSIC	large scale integrated circuit
MBMS	modulated beam mass spectrometry
MS	mass spectrometer
NBE	neutral beam etching
PCER	power compensated etch rate

PID	plasma induced damage
PM	photo multiplier
pSi	polycrystalline silicon
REL	reactive etch layer
RF	radio frequency
RFA	retarding field analyzer
RGA	residual gas analysis (MS mode for neutral analysis)
RLSA	radial line slot antenna
sccm	standard cubic centimeters
SEM	secondary electron microscope
SIMS	secondary ion mass spectrometry (MS mode for ion analysis)
SPL	sidewall passivation layer
STI	shallow trench isolation
TCER	time compensated etch rate
TF	transmission function
UV	ultra violet (light), 200-400 nm
VUV	vacuum ultra violet (light), 100-200 nm
XPS	X-ray photoelectron spectrometry

Acknowledgements

The presented work was carried out in the Laboratoire des Technologies de la Microélectronique (LTM) that is affiliated to the National Center for Scientific Research (CNRS), to the Institute of Engineering Science and Systems (INSIS) and to the Université de Grenoble.

First of all I would like express my gratitude to the President of the University Joseph Fourrier for the allocation of a Bourse Présidentielle (MENRT) to finance this thesis.

Furthermore, I would like to thank my PhD director Olivier Joubert for his support, the very helpful discussions and for giving me the opportunity to work at the LTM.

I would also like to thank the members of the jury, Prof. David Graves and Prof. Gilles Cartry, who accepted being referees of the thesis, and Prof. René-Louis Inglebert (president of the jury), Dr. Efrain Altamirano Sanchez, Dr. Olivier Joubert, and Dr. Maxime Darnon, who agreed to be part of the jury.

A special paragraph is definetly needed to express my thanks to my PhD supervisor Maxime Darnon, who was always available for excellent discussions, brainstorming, jokes, and encouragement, who helped me with every question regarding my thesis, bureaucracy, food (especially concerning cakes in H3), music and pretty much everything else, and who, at the same time, gave me the freedom to explore my own ideas while guiding me just enough not to veer off course. Thank you very much, Max!

A tremendous help was also Jumana Boussey, who supported me in difficult questions concerning all kinds of regulations for PhD students.

I would also like to thank Gilles Cunge very much for sharing his large knowledge of fundamental plasma processes, for his contagious excitement for all kinds of plasma diagnostic systems, for our discussions about windsurfing and for lending me his surfboard for a year!

A great thanks also goes to all colleagues and friends at the LTM who made working there a pleasure.

Last but not least, none of this would have been possible without the assistance and patience of Wiebke and my close friends. An exceptional thank you is going to my family that always supports me regardless of the situation.

Abstract

The continuous downscaling in microelectronics imposes increasing demands on the plasma processes and traditional ways for process optimization reach their limits. New strategies are needed and innovations in the field of plasma processes are being developed: e. g. the use of pulsed plasmas.
In this thesis, a pulsed HBr/O_2 etch plasma is studied. Various *in-situ* diagnostics are used to characterize pulsed plasmas in an industrial 12" etch reactor. The silicon etching is investigated by XPS and electron microscopy.
We show that the plasma dissociation and temperature are reduced if the plasma is pulsed at low duty cycles. The Br radical flux with respect to the on-time of the plasma is increased and the influence of the O radical is decreased, leading to enhanced time compensated silicon etch rates, a higher selectivity towards SiO_2 and a more homogeneous etching. The pattern profiles can be controlled via the sidewall passivation layer formation that is closely linked to the duty cycle.

Keywords: microelectronics, pulsed plasma, plasma etching, silicon etching, plasma diagnostics

Résumé

Du fait de la réduction des dimensions en microélectronique, les procédés de gravure par plasmas ne peuvent plus satisfaire aux exigences de l'industrie. De nouvelles stratégies sont en cours de développement.
Ce travail consiste en l'étude de plasmas pulsés de HBr/O_2 comme une alternative pour la gravure du silicium. Divers diagnostics dans un réacteur industriel 300 mm sont utilisés pour caractériser le plasma tandis que la gravure du silicium est étudiée par XPS et par microscopie électronique.
Lorsque le plasma est pulsé à faible rapport cyclique, sa température et sa dissociation sont fortement réduits. Le flux de Br radicalaire par rapport à la période ON du plasma augmente tandis que l'influence du radical O diminue, ce qui conduit à une amélioration de la sélectivité par rapport au SiO_2 et à une gravure plus homogène. Les profils des structures gravées peuvent être contrôlés par la formation de la couche de passivation sur les flancs dépendant également du rapport cyclique.

mots-clés : microélectronique, plasma pulsé, gravure à base de plasma, gravure de silicium, diagnostic du plasma

1. Introduction

Since the invention of silicon based transistors in the 1950s, tremendous progress has been made in terms of miniaturization, cost, speed, power consumption and versatility concerning large scale integrated circuits (LSIC). By subsequent etching and deposition of patterns, the microelectronic devices like transistors and the interconnecting lines are produced on a semiconductor substrate like silicon. The main steps are sketched in Fig. 1.1.

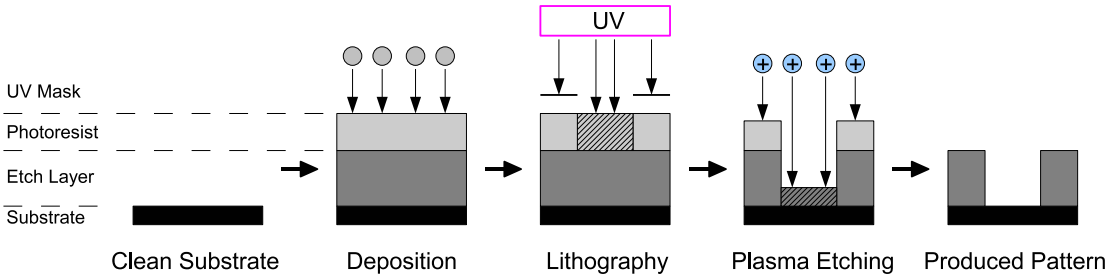

Figure 1.1.: *Sketch of the main microelectronics fabrication steps: deposition, lithography and plasma etching. A repeated sequence of these processes can be used to fabricate complicated patterns on the silicon substrate, e. g. for transistors or interconnecting lines.*

In the beginning of the microelectronic revolution, the miniaturized structures of the integrated circuits (ICs) were produced by selective chemical "wet" etching. By decreasing continuously the dimensions of the IC components, the isotropic wet etch processes reached their limits in terms of profile control. Since then, "dry" plasma etch processes are the only viable technological solution to address the critical dimension control in the micro- and nanometer range. Figure 1.2 illustrates the differences between wet and dry etching.
A plasma consists of charged (ions and electrons) and neutral (atoms, molecules) species, which have different roles in the etch mechanism. Anisotropic etching can be achieved by the acceleration of ions from the plasma onto a target, where the bombarding ions physically sputter atoms from the surface due to collision cascades in the etch layer. Often, this process lacks a good selectivity between materials and exhibits slow etch rates. In contrast, isotropic, but selective etching is induced by the radicals from the plasma that can spontaneously etch atoms from the target surface if the appropriate feedgas is used. This mechanism is very similar to the wet etch. By combining both effects synergistically, the ion assisted chemical etching can lead to highly selective, anisotropic etching [1], with etch

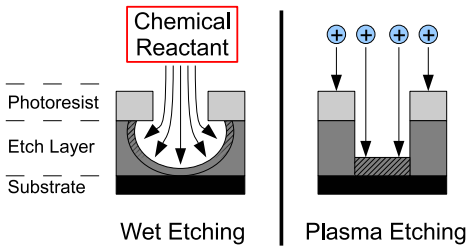

Figure 1.2.: *Sketch of an isotropic wet etch process and an anisotropic dry etch process.*

rates several times higher than the sum of both mechanisms alone.
In etch reactors, the plasma is electrically generated in low pressure chambers. A potential difference is created in the gas, which accelerates electrons that dissociate and ionize the gas molecules. The secondary electrons are accelerated in turn and increase the dissociation and ionization rate.
The first plasma reactors that were used had a barrel shape. The electric potential to accelerate the electrons was either induced by an inductive coupling, or by a capacitive coupling. The inductive coupling was realized by an electric coil placed around the barrel while for the capacitive coupling, the chamber wall and an additional electrode in the interior of the barrel act as a capacitor. In both cases, an alternating current (AC) generator, often at a "radio" frequency (RF) of 13.56 MHz, supplied the necessary plasma power.
At first, several wafers were etched at the same time in one reactor, but single-wafer reactors started to show superior performances, so that most of the later developed reactors adopted the single-wafer design.
In a next step, planar plate capacitively coupled plasma (CCP) reactors were introduced. The wafer holder acts as the RF power electrode while the chamber wall is the grounded counter electrode. An increase in the power results in an increase in ion flux as well as in ion energy. Although this device is still used for the etching of dielectrical layers during which a high ion energy is advantageous, in many processes only a low ion energy can be tolerated. At the same time, a high ion flux is desirable to increase the etch rate. Therefore, hybrid reactors were developed that produce high density plasmas (HDP) with a strongly reduced ion energy that can be controlled almost independently of the ion flux. In this design, a capacitive wafer holder is combined with a high (ion) density source, as, e. g., an inductively coupled plasma (ICP) source, an electron cyclotron resonance (ECR) plasma source, or a helicon wave plasma (HWP) source. In the modern ICP reactors a planar coil couples the RF power through a dielectric window into the plasma. The ECR and HWP reactors are powered by microwaves, often at 2.45 GHz, which are also transmitted via antennae through dielectric windows.
The continuous downscaling of the LSICs imposes increasing demands on the plasma processes in terms of etch homogeneity, profile tolerance, surface damage, etch materials, throughput and reproducibility. Especially the plasma induced

damage (PID) becomes difficult to control since the tolerance range for deformations and surface alterations decreases continuously. A short list of some of the most important types of PID (see Fig. 1.3) is given in the following:

1. **Bowing** - The broad lateral etch into the sidewalls of pattern structures is called bowing. It can be caused by spontaneous lateral etch due to radicals if the sidewall is not sufficiently passivated, or by a differential charging effect. The latter is caused by the almost isotropic electron velocity distribution that leads to a preferential charging of the sidewalls of the (dielectric) mask. Moreover, while the collection angle for electrons is reduced at the trench bottom, the anisotropic ions easily reach it. Thus, the different fluxes can lead to a positive charge on the trench bottom and a negative charge on the mask sidewalls. Further ions can then be deflected electrostatically towards the sidewalls [2–5].
2. **Notching** - The localized lateral etch at the bottom of a trench where the next layer starts is called notching. The differential charging is also thought to be one possible cause [4, 5].
3. **Micro trenching** - Often, the etch rate close to the sidewalls of patterns is increased, leading to small trenches. This feature is called micro trenching and is thought to be caused mainly by the reflection of ions on the sidewalls [6–9]. Also differential charging effects [8, 10, 11] might play a role.
4. **Surface damage** - Energetic ions, radicals and photons can damage the surface structure of materials [12–20], leading to defects, dopant deactivation, destruction of bonds, formation of dangling bonds and oxidation [21–26].

Currently, the traditional ways for process optimization to meet the increasing demands reach their limits. New strategies to overcome these limiting factors are needed and innovative approaches are being developed.
One approach is the development of advanced plasma etch devices. Recently, several different plasma reactor layouts were proposed that target the increase of ion densities and the control of the ion flux [27–30], or the reduction of plasma induced damage, e. g. due to high energy ions or UV photons [31–39]. In the following, a short overview of some of the proposed designs is given.

Advanced CCP Reactor

The modification of the traditional parallel plate CCP reactor offers new possibilities to improve the etching. High frequencies, e. g. 60 MHz, mainly control the gas dissociation and the ion density while low frequencies, e. g. 2 MHz, rather control the ion energy. Therefore, double or triple frequency CCP reactor were introduced [27–29] to combine the advantages of a CCP with an increased ion density and flux. Such tools are already used for several years now in the microelectronics fabrication. Improvements are continuously proposed, e. g. a superimposed direct current (DC) high voltage [30] that can additionally increase the ion density due to a strongly enhanced production and acceleration of secondary electrons.

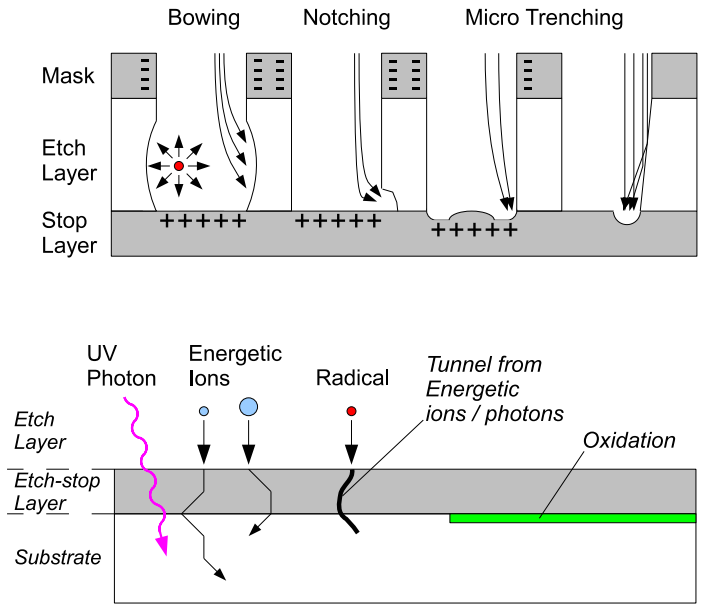

Figure 1.3.: *Examples of plasma induced damage on the pattern profile, the surface and buried layers.*

Diffusion Plasma

One approach to reduce plasma induced damage and to increase the etch homogeneity across the wafer is the use of diffusion plasma reactors. Goto *et al.* [31–33] report the development of a 200 mm high density diffusion plasma chamber, in which the plasma is excited by microwaves via a radial line slot antenna (RLSA). The ion flux and energy can be controlled individually by an additional RF bias power on the wafer holder. The authors report a very reduced electron temperature of approximately 1 eV that allows to reduce the minimal ion energy to a few eV. For certain process steps, diffusion tools are already used in the industry. However, in the last years their range of applications was strongly extended.
Another way to produce a homogeneous diffusion plasma above the wafer is the use of a broad planar electron beam sheath that ionizes the gas very efficiently above the wafer [34–36]. Up until now, only research reactors exist of this type.

Neutral Beam Etching

A solution to address UV induced damage in the surface and/or to reduce charging effects might be neutral beam etching (NBE). Samukawa *et al.* [37–40] presented an etch chamber in which ions are produced via an ICP and subsequently accelerated and neutralized by a grid. This way the UV is partially blocked and an energetic, anisotropic flux of mainly radicals reaches the wafer that is positioned behind the grid. The downside for certain processes is the much reduced particle flux and, hence, the slow etch rate. Only experimental prototypes of these reactors exist.

Pulsed ICP

Last but not least, pulsed ICP reactors are also thought to minimize plasma induced damage. Several authors reported reduced damage due to charging effects [41–46], reduced surface damage [47, 48], reduced ion energies [42, 49, 50], reduced UV damage [16,51], increased plasma uniformity [52,53] and an increased selectivity [50,54]. In such reactors, the RF for plasma generation and the optional additional RF for ion acceleration are pulsed in various modes: synchronously at various frequencies with adjustable phase lags and duty cycles or independently, e. g. with one generator in continuous wave (CW) mode. The advantage of pulsed plasmas is the possible implementation into existing, commercially available hardware. Pulsed plasma processes are already used for several years in the industry. However, it is not fully understood **how** pulsing affects in detail the processes.

This Ph.D. thesis focuses on the potential of pulsed plasma etching to meet the increasing demands on the plasma processes. In the following, a short review on the differences between CW and pulsed plasmas, as well as on HBr/O_2 etching is given. Then, the outline of this work is presented.

1.1. Difference Between CW and Pulsed Plasma

In order to understand the fundamental differences between a pulsed and a CW plasma, the most important parameters of a CW plasma are summarized in the following, before they are compared to the pulsed case. More details on the basics of plasma physics can be found in the literature [55, 56]

1.1.1. Basics of an Inductively Coupled Plasma

A summary of some important plasma parameters that are explained in the following is given in Tab. 1.1.

Basics

A plasma is a partially or fully ionized gas that is composed of electrons, ions and neutral species. As mentioned above, to generate plasmas in microelectronics applications, an externally imposed potential accelerates the few present electrons that in turn start to dissociate and ionize the gas molecules. Secondary electrons are produced and also accelerated until a balance between production and loss rates is reached. This process leads to the same amount of positive and negative charges in the plasma and hence, the plasma is macroscopically neutral. Any artificially introduced charge (e. g. from fluctuations) will attract and deflect charged species from the plasma, so that the potential from the parasitic charge is strongly reduced on a characteristic length scale λ_D, called the Debye length (see Tab. 1.1). The response to a parasitic charge is different between ions and electrons due to

the strong discrepancy in mobilities. Considering a negative parasitic charge, a positive ion approaches the charge, but its inertia pulls the ion further than the equilibrium position. The resulting oscillation frequency is called plasma frequency ω_p (see Tab. 1.1). The ability to respond to imposed potentials can thus be described by a characteristic time scale $\tau = 2\pi/\omega_p$. Often, RF voltages at 13.56 MHz or higher are used for the plasma production since they accelerate electrons but leave the ions rather unaffected due to the discrepancy in ω_p. This leads to hot electrons ($\sim 3\,\mathrm{eV}$) while the ion temperature is close to the neutral gas temperature ($< 0.1\,\mathrm{eV}$). The corresponding thermal velocities v_{th} differ, therefore, by more than three orders of magnitude.
Charged and neutral species from the plasma can traverse the interface (sheath) between plasma and a surface. At the instance when the plasma is generated, the electrons reach the wall faster than the ions due to their high velocity. This leads to a negative charge (floating potential) of the surface while the remaining ions in the plasma bulk produce a small positive space charge (plasma potential). Nevertheless, the relative differences between ion and electron density in the plasma is small and the plasma itself can still be considered as neutral. The voltage drop V_s across the sheath increases, repulsing the electrons from the wall and attracting the ions, until a balance between ion and electron flux is reached. The sheath itself is depleted of electrons and a positive space charge is imposed by the drifting ions.
In an ICP the electromagnetic energy is coupled into the plasma via large coils that are positioned, e. g., on top of a dielectric window. The current in the coils generates a magnetic field that, in turn, induces a strong circular electric field in the reactor. Since the accelerated electrons are captured by this field geometry, the electron and ion density can become quite high ($\sim 10^{10-11}\mathrm{cm}^{-3}$). By adjusting the impedance of the coils correctly with a matching network, the power coupling into the plasma becomes very efficient. In many etch process reactors, an additional RF voltage is coupled capacitively to the wafer holder on the bottom while the plasma itself holds as the counter electrode. The electrons follow the imposed potential instantaneously as if it was a constant voltage while the ions only respond to the average potential. This leads to the following situation: when the potential becomes more positive, electrons can effectively reach the electrode. During most of the time the electron flux would therefore be increased while the ion current would not change. Since the electrode is electrically blocked for direct currents by a capacitor, the charge is accumulated until a new balance between ion and electron flux is reached at a "self-bias" potential below the floating potential. Hence, the ions are accelerated by the increased sheath voltage drop and impinge with higher kinetic energy on the wafer. The RF voltage is used to control the ion energy for etch processes.

Table 1.1.: *Standard plasma parameters and typical values for an ICP.*

Parameter	Definition	Typical Value (ICP)
Ion- and electron density	n_i, n_e	$n_{e,i} \approx 10^{10-11}\,\mathrm{cm}^{-3}$
Electron temperature	$T_e[\mathrm{eV}] = \frac{k_B}{e} T_e[\mathrm{K}]$	$T_e \approx 3\,\mathrm{eV} = 66240\,\mathrm{K}$
Plasma frequency	$\omega_{p,(e,i)} = \sqrt{\frac{q_{e,i}^2 n_{e,i}}{\epsilon_0 m_{e,i}}}$	$\omega_{p,e} \approx 1\,\mathrm{GHz}$ $\omega_{p,i} \approx 3\,\mathrm{MHz}$
Debye length	$\lambda_{D(e,i)} = \sqrt{\frac{\epsilon_0 k_B T_{(e,i)}}{e^2 n_{(e,i)}}}$	$\lambda_{De} \approx 100\,\mu\mathrm{m}$
Mean thermal velocity	$v_{th} = \sqrt{\frac{8 k_B T_{(e,i)}}{\pi m_{(e,i)}}}$	$v_{th,(i,n)} \approx 500\,\mathrm{m/s}$ $v_{th,e} \approx 10^6\,\mathrm{m/s}$
Bohm velocity	$v_B = \sqrt{\frac{k_B T_e}{m_i}}$	$v_B \approx 2500\,\mathrm{m/s}$
Floating sheath potential drop	$V_s = \frac{k_B T_e}{2e}\left(1 + \ln\left(\frac{m_i}{2\pi m_e}\right)\right)$	$V_s \approx 15\,\mathrm{V}$
Child law sheath ($e\,V_s \gg k_B\,T_e$)	$s = \frac{\sqrt{2}}{3}\,\lambda_D\,\left(\frac{2\,e\,V_s}{k_B\,T_e}\right)$	$s \approx 1\,\mathrm{mm}$ (for $V_s = 100\mathrm{V}$)

k_B : Boltzmann constant
e : elementary charge
q : charge of the species
ϵ_0 : permittivity of free space
s : sheath width

Since the ICP source power generates a high ion density, it is almost unchanged by the relatively small contribution from the RF bias power if the latter is small compared to the first [57]. Hence, ion flux and ion energy are independently controllable. However, it was reported recently that in some conditions the RF bias can have a significant influence on the electron and ion density, as well as on the electron temperature [58–62].
In case of an applied RF bias voltage, the sheath potential drop can be in the order of several 100 V. A widely used model of such a sheath, called the Child law sheath, can be used to determine the sheath thickness, which is often in the order of some mm (see Tab. 1.1).

Chemical Reactions

The chemical reactions in a plasma reactor are governed (amongst others) by the nature of the gases, the dissociation products, the degree of dissociation (plasma power) and the nature of the reactor walls (sticking coefficients). In a continu-

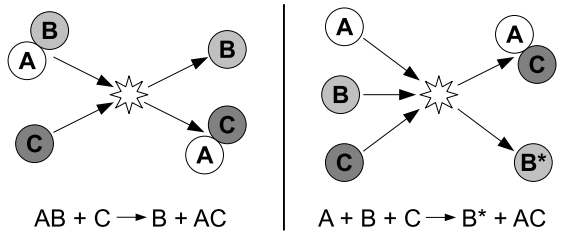

Figure 1.4.: *Sketch of a two body exchange collision and a three body recombination reaction.*

ous plasma, an equilibrium exists between ionization, dissociation, recombination, pumping, and gas inflow. The main dissociation occurs in the region close to the dielectric window, where the induced fields are the strongest.
Two main chemical reactions exist in the gas phase, illustrated in Fig. 1.4, that are of interest in the following: a two body exchange reaction during which two colliding species produce two different species and a three body recombination reaction during which two species recombine by transferring the excessive energy to a third species. In low pressure plasmas, the three body reaction is very improbable because of the very low density. In this case, recombination processes occur mainly on the reactor walls, where an adsorbed species reacts with an incoming species. The probability of such a reaction strongly depends on the nature of the species and of the reactor wall [63–70].

1.1.2. Plasma Pulsing

In contrast to CW ICPs, the RF voltage in pulsed mode is switched on and off periodically with a frequency far below the RF (< 100 kHz), modifying the overall characteristics of plasma etch processes. By varying frequency and duty cycle, the ion and radical flux can be changed, the etch rate varied, the etch selectivity between materials increased and the etch profile control augmented [45, 46, 49, 50, 71, 72].
In order to understand the fundamental differences between CW and pulsed plasmas, it is helpful to review the characteristic time scales of production and loss processes of the different plasma species.

Characteristic Time Constants

The creation of radicals, ions and electrons is based on electron impact on molecules. Considering a Maxwellian energy distribution of the electrons for $T_e = 3\,\mathrm{eV}$, it is more likely to dissociate a molecule (threshold energy $\sim 5\,\mathrm{eV}$) than to ionize it (threshold energy $> 10\,\mathrm{eV}$). A typical characteristic time for the production of these species is 0.1-1 ms with a faster creation of radicals than ions.
The loss of particles is caused by pumping, or by reactions in the gas phase and on boundary walls. The residence time τ_{pump} of the species in the chamber due to pumping is typically in the range of several 100 ms (at 20 mTorr, 200 sccm) and

can be estimated from the gas inflow Q (in mol/s), the reactor volume V_R, pressure p_R and temperature T_g:

$$\tau_{pump} = \frac{1}{Q} \cdot \frac{p_R V_R}{k_B T_g}. \tag{1.1}$$

However, this does not include the dependence on the nature of the species, which can change the residence time considerably. Nevertheless, the order of the time scale remains valid in comparison to the other loss mechanisms.
The characteristic loss time of radicals caused by diffusion and sticking to the wall can be estimated with respect to the sticking coefficient β by using the approximation from Chantry [73]:

$$\tau_{wall} \approx \frac{\Lambda_0^2}{D} + \frac{V_R}{A_R} \cdot \frac{2(2-\beta)}{v_{th}\beta}, \tag{1.2}$$

where D is the diffusion constant, V_R/A_R the ratio of the reactor volume to its surface and Λ_0 an approximation of an effective reactor length that can be calculated for a cylindrical geometry (with height h_R and radius r_R) by

$$\frac{1}{\Lambda_0^2} = \left(\frac{\pi}{h_R}\right)^2 + \left(\frac{2.405}{r_R}\right)^2. \tag{1.3}$$

The resulting characteristic loss time is typically in the order of 1-10 ms.
If the right precursors are available in the plasma, two body reactions in the gas phase can be extremely fast, almost at the collision frequency of the gas molecules (~ 100 kHz). Characteristic time scales of ~ 100 µs have been reported [74].
The ion loss during the plasma discharge is governed by ambipolar diffusion. Since the electron temperature is quite high, the ions are lost significantly faster compared to the radicals. When the plasma is switched off, the electrons cool down quickly due to inelastic collisions (high collision frequency) and to the loss of fast electrons to the wall (if energy is greater than the sheath potential drop). This occurs on time scales of several µs due to the high velocity. Consequently, the ambipolar diffusion is decelerated and the ion and electron loss rates decrease.
The characteristic timescales for particle production and loss are summarized in Tab. 1.2 (next page).

Table 1.2.: *Approximated time scales for particle generation and loss for a pressure of 20 mTorr.*

Species	Process	Cause	Time scale [ms]
all	loss	pumping	> 100
radicals	production	electron impact	0.1-1
	loss	diffusion and sticking (wall)	1-10
	loss	2-body reaction (gas phase)	0.1
ions	production	electron impact	0.1-1
	loss	ambipolar diffusion	0.1 (high T_e)
	loss	ambipolar diffusion	0.4 (low T_e)
electrons	production	electron impact	1
	loss	fast electrons traverse sheath	0.01 (high T_e)
	loss	ambipolar diffusion	0.4 (low T_e)

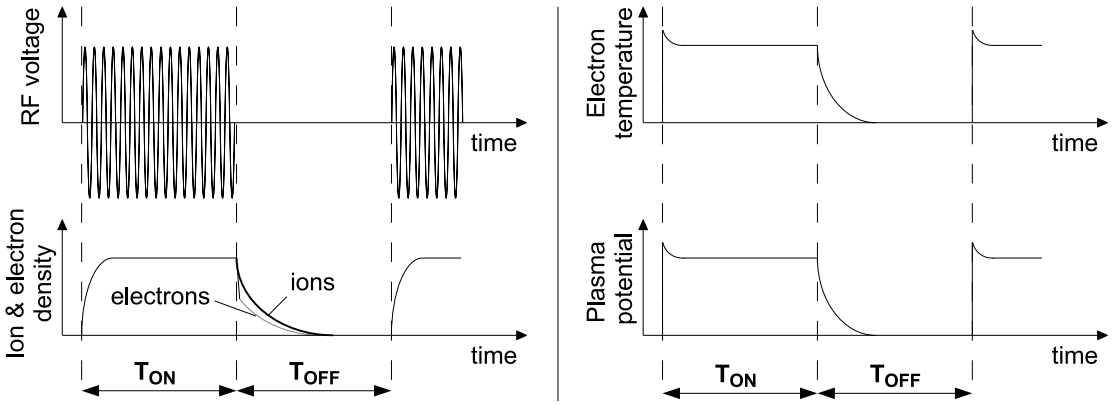

Figure 1.5.: *Sketch of the expected evolution of characteristic properties during a pulse period: electron and ion density, electron temperature and plasma potential.*

Pulsed ICP (Source Only)

In a pulsed ICP, several aspects change compared to a CW discharge. In Fig. 1.5 the expected evolution of charge densities, electron temperature and the plasma potential are sketched for one pulse period.
In the beginning of the on-time T_{ON} of the plasma, the remaining electrons from the previous pulse absorb the total power (few electrons but high electron temperature T_e) and start to ionize the gas molecules, leading to an increased electron and ion density (n_i, n_e) and a decreased T_e. Depending on the process parameters, this can lead to a strong overshoot of T_e at the beginning of the pulse. The plasma potential follows the evolution of T_e, considering Tab. 1.1. If T_{ON} is long enough, a steady state is reached after a certain time, similar to CW mode. When the plasma is switched off, the electrons quickly cool down and the ions and electrons

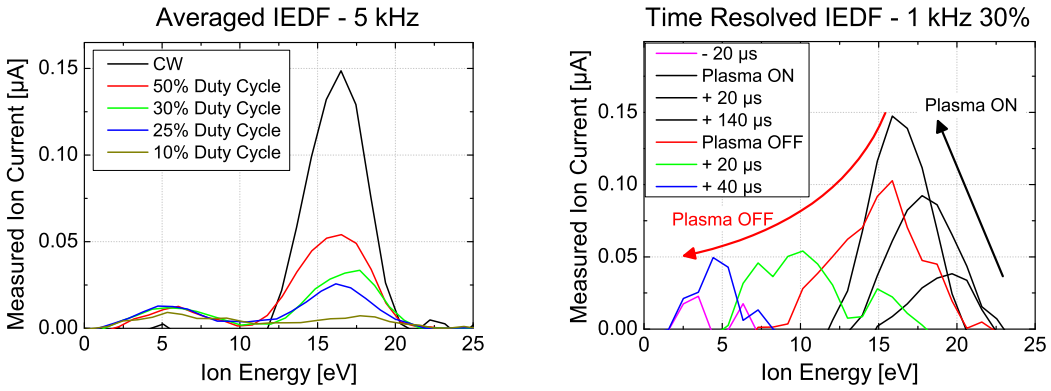

(a) **(b)**

Figure 1.6.: ***(a)*** *Time-averaged and* ***(b)*** *time-resolved IEDFs of a pulsed argon plasma at 5 mTorr and 800 W source power (no bias power).*

are lost mainly by ambipolar diffusion towards the plasma boundary walls until the plasma power is switched on again.
The radicals, which are produced by dissociation during the on-time, are lost continuously due to recombination or adsorption at the walls. If the characteristic loss and production rates are slow compared to the pulse frequency, the particle densities do not change significantly during one pulse period.
An example of the ion energy distribution function (IEDF) in an Ar plasma is presented in Fig. 1.6. The time-averaged measurements show that the amount of high energy ions from the on-time of the plasma is dependent on the duty cycle while the contribution from the low energy ions from the off-time remains constant. The time-resolved IEDFs show the fast shift in ion energy and the slight energy overshoot at the beginning of the on-time. The change in ion energy is linked to the fast change of electron temperature (see Tab. 1.1).

Additional Synchronous RF Bias Pulsing

In the following discussion a synchronous pulsing of the source and an additional bias voltage is assumed. When the bias power is switched on, the ion and electron density is quite low. The characteristic time to establish a constant self-bias voltage depends on the capacitor that couples the RF to the wafer holder, the ion flux, the electron flux, and the electron temperature. The (small) capacity is unknown and the other parameters change strongly in the first instants after the start of the pulse. Therefore, it is difficult to give a reliable prediction on the self-bias evolution for this period. If, after this period, the ion energy is high (several 100 eV), the energy deposition due to additional ionization from the RF bias is small, and the power coupling losses are insignificant, the RF bias power P_{bias} is approximately proportional to the ion flux Γ_i and the ion energy E_i [55]:

$$P_{\text{bias}} \propto \Gamma_i \cdot E_i. \tag{1.4}$$

Considering a high frequency where the ion density does not reach the steady state value of the CW case, the ion flux is lower compared to the CW case, leading to a higher ion energy if the RF power is held constant.
After the plasma is switched off, the strong self-bias voltage prevents electrons from reaching the wafer and only ions arrive, which neutralize the accumulated charge. The self-bias increases towards the floating potential, reducing the sheath voltage drop. Depending on the capacity and the ion flux that decreases during this period, the sheath voltage could be reduced very fast. Consequently, the average ion flux has two main contributions: the rising ion flux with high ion energy from the on-time of the pulse and the decreasing ion flux with low energy from the off-time.

1.2. A Sample Process - HBr/O_2 Etching of Silicon

The influence of plasma pulsing on an etch process is studied in an HBr/O_2 plasma for silicon etch applications. Such a process is used, e. g., for shallow trench isolation (STI) applications, where the etched trenches are filled with a dielectric and act as an electrical isolation between neighboring transistors. Another application for such a chemistry is the etching of transistor gate structures. An illustration of both applications is presented in Fig. 1.7.
Many authors have investigated the etch mechanisms of HBr/O_2 plasmas for silicon and SiO_2 [22, 26, 65, 75–81]. The fundamental mechanisms for Si and SiO_2 etching are summarized in the following, considering a very small percentage of oxygen in the feedgas.

Silicon Etching

Bromine, hydrogen, and, to a minor extend, also oxygen containing ions hit the silicon surface, dissociate, destroy bonds, and form an amorphous layer, also called reactive etch layer (REL), with incorporated H, Br, and some O atoms. Depending on the ion energy, the amorphous layer can vary in thickness. Since H atoms are considerably smaller than the other particles, they might penetrate deeper into the silicon layer. Si atoms can desorb due to a collisional impact or if they are incorporated into volatile species, like $SiBr_4$. It is also known that hydrogen containing molecules, like SiH_2Br_2, are even more volatile [81]. Less volatile species can also desorb due to physical sputtering. However, the silicon etching is not spontaneous and an ion threshold energy of $\sim 10\,\text{eV}$ is needed [81], which allows to etch anisotropically. Since the Si-O bond is stronger than the Si-Br bond [78] and oxygen containing molecules are less volatile, the desorption rate can be decreased if oxygen atoms bind silicon to the layer. On the other hand, Br and H radicals from the gas phase additionally adsorb on the surface of the amorphous layer

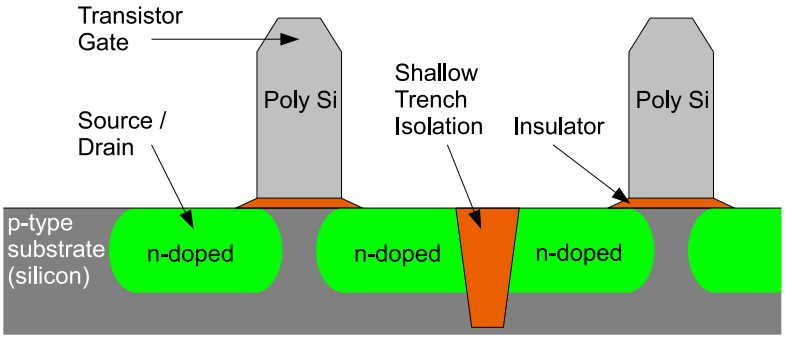

Figure 1.7.: *Sketch of the applications for an HBr/O_2 silicon etch process. The transistor gate (polycristalline silicon) and the isolation trenches (bulk silicon) are often etched in this kind of chemistry.*

and strongly increase the formation of volatile Si molecules. While the role of Br radicals is fairly understood, the role of hydrogen in the etching remains vague.

Silicon Oxide Etching

In contrast to the silicon etching, the SiO_2 is etched very slowly. Since the formation of Si-O bonds is thermodynamically favored compared to Si-Br bonds, no chemical enhanced etching mechanism exists. Oxygen atoms are preferentially sputtered from the surface [79, 82], leaving free spaces for Br to form Si-Br bonds and, subsequently, volatile molecules. However, since oxygen atoms from the gas phase can replace Br spontaneously [65, 75, 79], this mechanism seems to be rather inefficient. Only at the surface, where a lot of bromine is adsorbed, the sputtering of an oxygen can lead to the formation of a volatile silicon etch product. If SiO_2 is used as an etch mask for silicon, silicon containing species with a high sticking coefficient, like SiBr, can be deposited on the surface. While this has only little effect on the silicon etch, these products can bind strongly on dangling bonds of the SiO_2 surface, decreasing the effective etch rate [65]. Oxygen from the gas phase can further harden this deposited layer. Therefore, an increased oxygen flow and/or an increase of depositing species can slow down the SiO_2 etch rate.

Comparison - Si vs. SiO_2 Etching

The silicon etch is strongly enhanced by a large surface coverage of Br radicals and the activation energy is rather low. In contrast, the SiO_2 etching needs quite a lot of energy, even if the surface is fully covered with Br radicals [83]. Therefore, it is likely that in real process conditions, the etch rate for silicon is limited by the Br radical flux while the SiO_2 etch rate is limited by the ion energy and the ion flux.

1.3. Outline

In the framework of this Ph.D. thesis, the impact of synchronous pulsing on silicon etching in an HBr/O_2 plasma is studied. The work is focused on the fundamental differences between a continuous and a pulsed plasma, and on the role of the pulse parameters (duty cycle and frequency).
At first, in Chap. 2, the industrial etch tool is described and the used diagnostic systems are introduced: mass spectrometry, UV absorption spectrometry, a capacitive ion flux probe (IFP), a retarding field analyzer (RFA), X-ray photoelectron spectrometry (XPS), ellipsometry and scanning secondary electron microscopy (SEM). For each diagnostic system, the basic principles of operation are given. In addition, we present a newly developed angle resolved XPS technique to investigate the sidewall passivation layer (SPL), formed at the pattern sidewalls during etching. It allows to obtain profiles of the SPL in terms of thickness and chemical composition.
Then, in Chap. 3, the HBr/O_2 process plasma is investigated **without** applied bias power (no silicon etching, clean reactor). This allows to understand the general influence of the pulse parameters on radical and ion fluxes and their composition.
Chapter 4 deals with the impact on the plasma and on the plasma-surface interaction during silicon etching **with** applied bias power. The species fluxes and their compositions are very different since a large amount of silicon containing etch products are present in the gas phase and the reactor walls are coated differently.
The presented results serve as the basis for the analysis of the actual impact of plasma pulsing on the pattern etching, presented in Chap. 5. Etch rates of blanket wafers are presented to show the impact on the different mechanisms of the etching for various materials. Then, the impact of pulsing on the etched patterns is presented and the observed evolution with the pulse parameters is explained.
In Chap. 6, all results are discussed and the impact of synchronous pulsing on silicon etching is elaborated. In addition, the general potential of pulsed plasmas is presented and an outlook on future experiments is given.
Finally, a conclusion is given in Chap. 7.

2. Diagnostic Systems and Experimental Setup

All experiments are carried out in a plasma reactor suited for 300 mm wafers. In addition, several diagnostic techniques are used to study the impact of pulsing on the plasma and on the plasma-surface interaction. In the following, the basic concepts of each diagnostic tool are discussed and the hardware is described.

2.1. Plasma Reactor and Reference Process

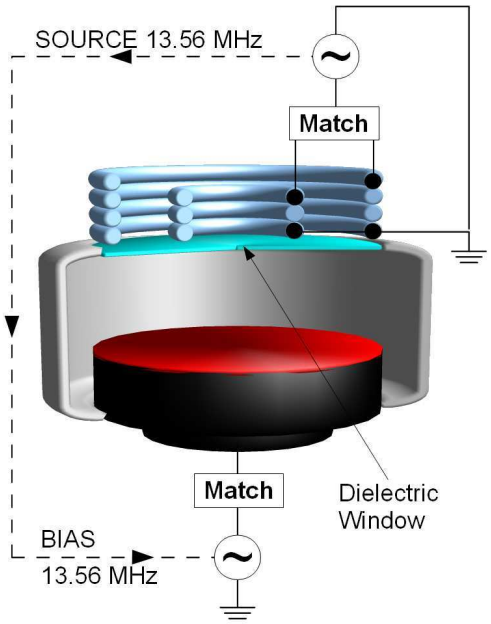

Figure 2.1.: *Sketch of the plasma reactor.*

The etch reactor in which the experiments were carried out is a commercially available 300 mm AdvantEdge™ decoupled plasma source (DPS) from Applied Materials, Inc. [84]. The plasma chamber, made of anodized aluminum, is part of an Applied Materials Centura platform. The reactor has an inner diameter of 500 mm and a height above the wafer holder of 172 mm. The inductively coupled plasma (ICP) is sustained via two antenna coils situated on top of the reactor, which are

connected to each other by a variable capacitance in order to improve the plasma homogeneity across the processed wafers. An RF power supply (13.56 MHz) is connected via an impedance matching network to the coils, which in turn transmit the energy through a dielectric alumina window to the plasma. The thermally regulated wafer holder, also called "chuck", is capacitively coupled to a second RF power supply ("bias"), including an additional impedance matching system. The RF voltage at the chuck is used to produce a self-bias voltage at the wafer in order to change the energy of the impinging ions.
Both power supplies are further modified with the Pulsync™ system to allow individual pulsing of the source and the bias RF voltages at frequencies between several Hz and 10 kHz and duty cycles between 10 and 90 %. It is also possible to pulse synchronously at the same frequency with an adjustable phase delay and an individual duty cycle. This Ph.D. thesis is focused on synchronized pulsing with the same duty cycle, phase and frequency for source and bias.
The reactor is extensively modified to allow several *in-situ* diagnostic systems. The chamber ports are used for real-time ellipsometry, absorption spectroscopy, ion flux measurements, ion energy analysis, and mass spectroscopy. In addition, an angle resolved X-ray photoelectron spectroscopy system is connected to the vacuum transfer platform for quasi *in-situ* analysis of the wafer surface directly after processing.
The reference silicon etch process of this work uses a gas flow of 200 sccm HBr and 5 sccm O_2 at a constant pressure of 20 mTorr. The source and bias powers are set to 750 W and 200 W, respectively. During the etch process, the wafer and the reactor wall temperatures are held constant at 55 and 60° C, respectively.

2.2. Mass Spectrometry

Mass spectrometry is a powerful diagnostic technique, which allows in principle to

1. sample neutral species/radicals from the plasma,
2. sample positive and negative ions from the plasma,
3. study the ionization cross section of a neutral species, and
4. study the ion energy distribution function for an ionic species.

In this work, a modified EQP 500 mass spectrometer from Hiden Analytical is used (Fig. 2.2). It is equipped with a beam chopper and two differential pumping stages. The entrance orifice is in plane with the reactor sidewall, at a height of approximately 5 cm above the wafer holder. The basic theory of mass spectrometry is given based on the design of this tool.

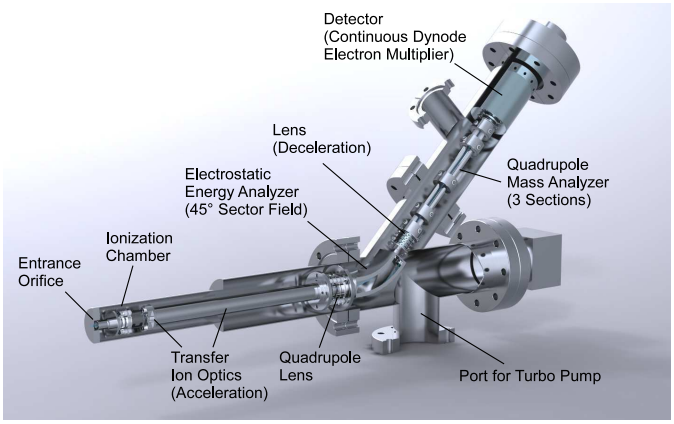

Figure 2.2.: *Sketch of the Hiden Analytical EQP 500 mass spectrometer (www.hidenanalytical.com).*

2.2.1. Basics

Two diagnostic modes of the mass spectrometer (MS) are used, the so-called residual gas analysis (RGA) mode for the analysis of neutral species and the so-called secondary ion mass spectrometry (SIMS) mode for ion analysis. In RGA mode, neutral species diffuse into an ionization chamber in the spectrometer. The entrance hole of the spectrometer is biased positively to prevent ions from the plasma to reach the interior. The neutrals are then ionized by a mono-energetic electron beam, which is thermally generated by a wolfram filament and accelerated to a tunable energy. The created ions are in turn accelerated to a known kinetic energy towards the end of the MS. In SIMS mode, the potential of the entrance hole is tuned negatively to attract the plasma ions and to tune the obtained signal to a maximum. Obviously, a further ionization is not necessary and the ions can be analyzed directly.
The next stage of the MS is a 45° sector field electrostatic energy analyzer, which consists of two parallel electrostatic plates that form a curve of 45°. By applying a potential difference between the plates, a linear homogeneous electric field is produced that deflects the ion trajectory. With the electric field $\mathcal{E}$, the length of the sector field l and the ion charge q, the ion pass energy for such an energy analyzer is

$$E_{kin,pass} = \frac{1}{2} q \mathcal{E} l. \tag{2.1}$$

All ions that have the required energy are deflected into the exit slit, independent from their mass. The mono-energetic ions are subsequently focused into a quadrupole mass analyzer, sketched in Fig. 2.3.
A quadrupole analyzer consists of four usually circular rods that are placed parallel to each other. Opposing rods are connected electrically. An RF voltage is

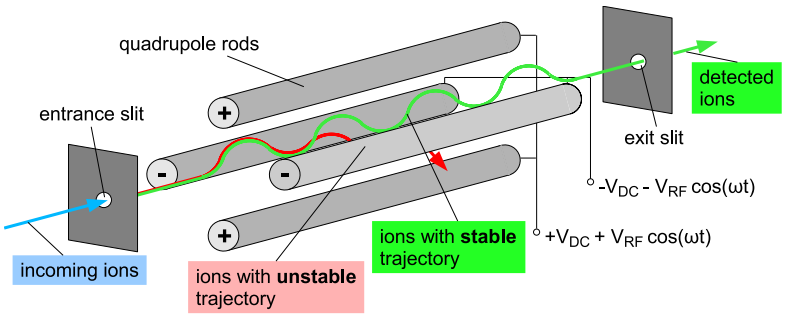

Figure 2.3.: *Sketch of a quadrupole mass analyzer.*

applied together with opposing potential offsets to each pair of connected rods ($\pm[V_{DC} + V_{RF}\cos(\omega t)]$). Hence, the trajectory of passing ions is periodically deflected, so that only ions with a specific charge to mass ratio q/m can pass for a given voltage ratio V_{DC}/V_{RF}. Other ions have instable trajectories, are strongly deflected, collide with the rods, and are neutralized.
The final stage of the MS is a photo multiplier (PM), which detects the ions that pass the energy and mass filters. When an ion hits the photosensitive first electrode of the PM one or more secondary electrons are produced. These electrons are accelerated to a dynode where they produce in turn secondary electrons. By adding several dynodes, or in a continuous-dynode design, the electrons that are detected at the last electrode (anode) produce a signal that is large enough to detect even single ions.
However, the resulting signal is only accurate if the ion trajectory is collision-free. Thus, the pressure needs to be low enough to assure a long mean free path for the ions ($< 10^{-3}$ mTorr). On their way through the MS the ions are repeatedly focused by different electrostatic lenses. A good tune of the applied potentials is essential to maximize the final signal to noise ratio. Still, the optimal tune can shift slightly from experiment to experiment, e. g. due to different plasma conditions or different background pressures. Moreover, this tune is also dependent on the energy and mass of the ion that is analyzed. Therefore, the parameters need to be re-tuned for each plasma species and before each experiment.

2.2.2. Analysis of Neutral Species

Removing the Background Signal

In RGA mode, the neutrals of the plasma need to be ionized in the MS. A priori, at this point we cannot distinguish between species that come directly from the plasma and neutrals that remain in the ionization chamber as a background signal. One technique that allows to remove the background signal is modulated beam mass spectrometry (MBMS). In such a setup, a chopper is installed between the entrance hole of the mass spectrometer [85–87] and a second orifice that seperates the plasma from the chopper. The hereby created chamber is differentially

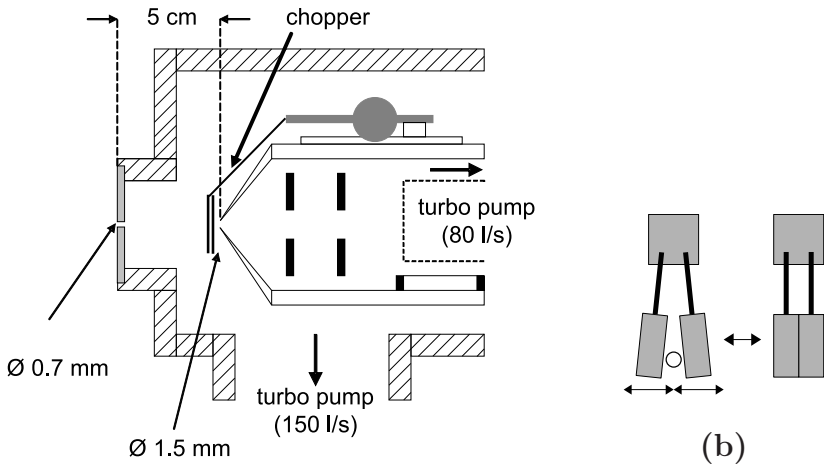

Figure 2.4.: *Sketch of the mass spectrometer entrance and the tuning fork chopper.*

pumped by a turbomolecular pump to reduce the background density and, thus, also the background signal. For a sufficient reduction of the background signal, a double or even triple differential pumping system is necessary [85].
A schematic overview of the spectrometer entrance used in this work is shown in Fig. 2.4. The neutrals pass through the first orifice of diameter $\varnothing = 0.7\,\mathrm{mm}$ and reach the first stage of differential pumping. The entrance hole to the spectrometer ($\varnothing = 1.5\,\mathrm{mm}$) is covered by a tuning fork resonant chopper, which allows in principle to reduce the dimension of the first stage to a minimum to increase the signal to background ratio. In our case, the distance between the two orifices was set to 5 cm in order to place the first entrance hole in plane to the reactor wall.
Often, the background signal is assumed to be constant during the chopper period [85, 86]. However, Cunge *et al.* [88] showed that this is not always the case since part of the background can originate from the beam itself. Therefore, it is necessary to measure the time resolved intensity variation of the signal for one chopping period (in our case 100 ms). In the original setup, this can be done by a boxcar that averages the signal at one point of the period until the signal to noise ratio is sufficient and then moves to the next point (in time) of the pulse period. A more efficient way of measurement is the use of a multi-channel (1000) pulse counter [89] that measures all points of the chopper period in parallel. A comparison between both techniques with the same acquisition time is shown in Fig. 2.5.

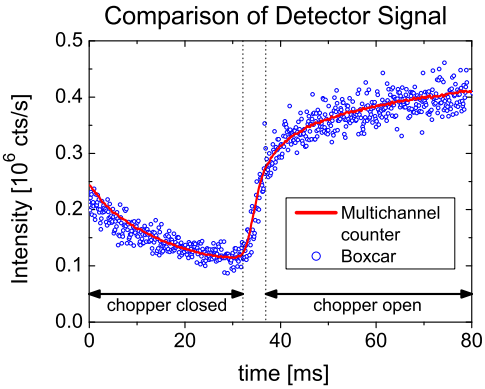

Figure 2.5.: *Comparison between detector signals: boxcar vs. multi-channel pulse counter.*

Appearance Mass Spectrometry

In a mass spectrometer, it is often possible to produce the same ion from different parent molecules, e. g. by dissociative ionization, giving rise to a false measurement. Usually, the lowest threshold energy to form an ion A^+ is found for direct ionization of A. Considering that A^+ can also be formed by dissociative ionization, e. g. of A_2 with a slightly higher threshold energy, a differentiation between the two processes can be achieved by setting the electron beam energy for ionization to the adequate threshold energy [86, 90–93].
In the standard HBr/O_2 process without bias, the only (main) species that can be produced by dissociative ionization are the radicals Br, O and OH (H cannot be detected by our MS, see below). In the experiments, O or OH radicals were not detected, probably due to the high dilution of O_2 in HBr gas (1:40) and a possibly high sticking coefficient, which increases the loss rate on the reactor walls (see Sec. 3.1.1). The signal of the Br radical on the other hand is just detectable. The threshold energy for direct and dissociative ionization of Br is obtained by scanning the electron beam energy for ionization in an HBr gas and in an HBr plasma. In the first case, Br radicals are only produced by dissociative ionization in the spectrometer. In the second condition, some Br radicals are created in the plasma and can be ionized directly. Both measurements are shown in Fig. 2.6.

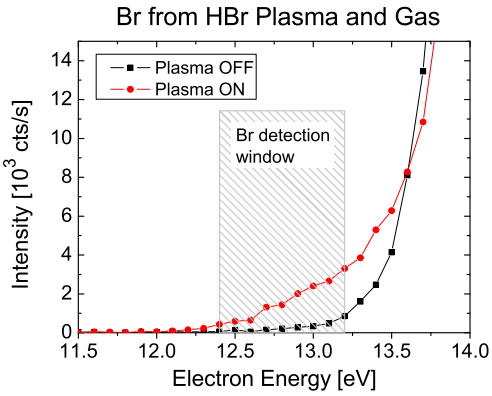

Figure 2.6.: *Dissociative ionization (Plasma OFF) and combined dissociative/direct ionization (Plasma ON) of Br from an HBr plasma/gas.*

The grey hatched area indicates the energy window where the Br flux is large enough to be detected and where the dissociative ionization of HBr molecules is still low. Based on this graph, an ionization energy of 13.2 eV is used for all measurements of the Br radical. Although there is already a small contribution from dissociative ionization at this point, it is more important to obtain a strong signal in order to increase the signal to noise ratio. Moreover, assuming that the contribution from the dissociation of HBr is approximately proportional to the measured HBr density, the so-produced Br is estimated and subsequently subtracted from the measured Br signal.

Measurement Procedure

The basic measurement procedure in RGA mode for a series of plasma conditions is the following. Before each series of experiments, a reference measurement is acquired, e. g. for Ar gas at 10 mTorr, in order to account for any shift between experiments. It consists of a MS tune to Ar, a measurement of the ionization cross section, and a measurement of the Ar atom. This allows to normalize slightly different experimental conditions. Then, the spectrometer parameters need to be re-tuned to the species of interest, which is subsequently measured using the neutral beam chopper in all plasma conditions, if necessary, at threshold ionization energy. In a next step, the MS is tuned to another species.
For entire mass spectra the chopper is not used. Instead, a background spectrum is acquired separately in order to remove the signals from residual species. This technique gives rise to several sources of error:

1. The background from the real process does not necessarily have the same intensities (or at least intensity ratios) as the residual measurement.
2. The MS is tuned to only one species (e. g. Ar) instead of an individual tune for each species.

3. The ionization cross sections differ between molecules. Therefore, the same intensity could indicate different species densities.
4. Direct ionization and dissociative ionization cannot be distinguished (ionization energy 70 eV).
5. The mass dependent transmission function (see below) is unknown, but it remains approximately constant for changing plasma conditions.
6. The measured intensities depend on the plasma temperature (see below).

Consequently, the signals of different species in one spectrum cannot be compared. However, the intensity of one species can still be compared between different plasma conditions, provided that this species can only be produced by direct ionization and changes in temperature are taken into account. Despite all these disadvantages, entire mass spectra can still give a rough overview on the species in the plasma.

2.2.3. Analysis of Ions

In contrast to the RGA mode, the ions can be studied without the use of a chopper since no background exists. However, the measurement of the ion flux is rather complicated since the plasma ions can have a very different ion energy distribution function (IEDF) compared to the mono-energetic IEDF in the RGA case. Moreover, depending on the ion energy that is used for the MS calibration, the obtained IEDF can change strongly [94]. Finally, it would also be possible that different species have different IEDFs, but in the studied conditions all analyzed species showed only insignificant differences between their IEDFs.
A great disadvantage of such a measurement is that the resulting IEDFs do not necessarily represent the real energies of the ions that hit the chamber wall: the reference potential is different since the reactor wall is floating while the MS is connected to the laboratory ground. Hence, the measured IEDFs should be used very carefully.
Nevertheless, the approximate composition of the total ion flux can still be obtained by taking the integral from each species' IEDF.

Measurement Procedure

In SIMS mode, the basic measurement procedure for a series of plasma conditions consists of three steps. At first, the spectrometer is tuned to an ion of intermediate mass, including tune of the pass energy to find the maximum of the IEDF and to increase the signal. Experiments carried out to investigate the influence of the choice of the ion species used for the tune, showed no observable impact on subsequent measurements. In a next step, an Ar reference plasma is analyzed to account for spectrometer shifts between measurement sessions, similar to the analysis of neutrals. Finally, the IEDF of each ion in each plasma condition is measured. The total flux can be deduced via integration from the acquired IEDFs.

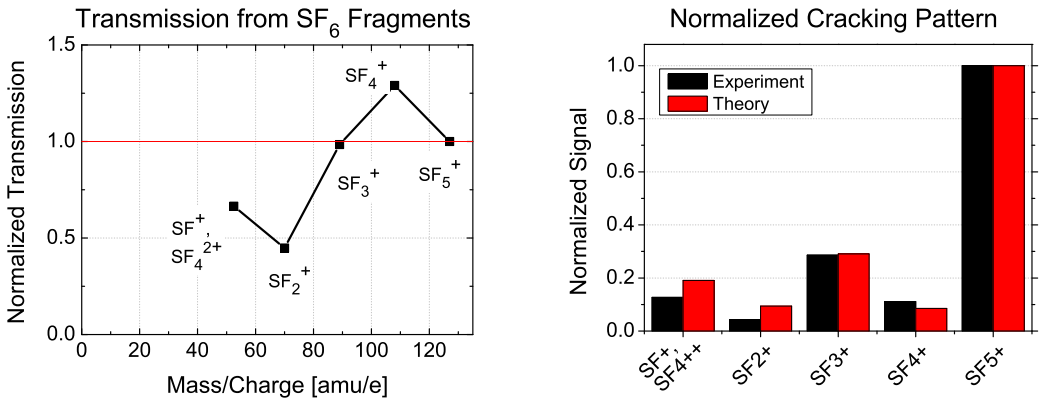

(a) (b)

Figure 2.7.: ***(a)*** *Transmission function obtained from SF_6 cracking pattern and* ***(b)*** *direct comparison of measured and theoretical cracking pattern.*

Since the transmission function of the orifice for ions is approximately constant with the mass (see Sec. 2.2.4), we can compare the ion fluxes of the different species directly.

2.2.4. Mass Spectrometer Transmission Function

The transmission of neutrals and ions from the plasma to the detection device in the mass spectrometer depends mainly on the species mass, but in SIMS mode also on the ion energy [94]. The mass dependence is due to the transmission function (TF) of the quadrupole mass filter and the mass dependence on the production of secondary electrons on the detector. The entrance orifice of an MS can also alter the detected signal.

Mass Analyzer and Detector Device

One way to determine the TF of the mass analyzer and the ion detector is the use of the cracking pattern of a large molecule, e. g. SF_6.
Following this approach, the signal intensity for each species in the cracking pattern of SF_6 was measured and divided by the corresponding cross section for electron impact ionization [95,96], shown in Fig. 2.7 a. For many MS systems, the combined TF of the quadrupole mass analyzer and the detector device is approximately proportional to the inverse of the mass (m^{-1}) [93, 97, 98]. However, the measured transmission function does not follow this dependence. Instead, the relative TF varies around a mean value. As Fig. 2.7 b shows, the greatest differences are found for molecules with a low signal strength and hence, also a low signal to noise ratio. Thus, it might be possible that the actual TF is approximately constant, at least

up to a mass of 127 amu. Since the MS is equipped with an improved quadrupole mass analyzer (length of 9 cm instead of 6 cm) that is supposed to have a strongly reduced mass dependence, a constant transmission function might indeed be close to reality.
Unfortunately, the used MS has a very much reduced transmission for ions with masses of 1 and 2 amu. The RF frequency of the quadrupole mass analyzer is optimized for a large range of mass values up to 500 amu, but the drawback is the insensitivity for very low masses. Hence, it is not possible to investigate H or H^+ with the current system. Furthermore, the strong attenuation and the very low signal to noise ratio at low masses (see below) also prevent an accurate measurement of H_2, although its signal is detectable. Consequently, hydrogen species are not investigated by mass spectrometry in the framework of this thesis.

Orifice

The transmission function of the orifice for the analysis of **neutrals** can be approximated theoretically [85, 99]. The transmission for a diffusing gas in a molecular regime is altered due to a different gas conductance of the orifice, which is proportional to $(T/m)^{1/2}$ [85, 100]. Since in our setup two orifices are placed in series, the temperature and mass dependence are even stronger.
For MBMS, the modulated beam of neutral species can be assumed to be collision-free. In this case, the conductance of the orifice plays only a role in the composition of the background. Since the background is removed by the modulated chopper, the transmission factor for the neutrals is in this case constant with the mass and temperature. However, Singh *et al.* [85] showed that both parameters influence the beam-to-background signal ratio: in case of a two stage differential pumping system, the ratio is proportional to $m/\sqrt{T}$. Consequently, it is rather difficult to accurately measure light species like H_2. Still, the measured densities of the species in the beam are directly proportional to the densities in the plasma, as explained by Benedikt *et al.* [101].
If the chopper is not used, e. g. in case of an entire mass spectrum, the mass and temperature dependence has to be taken into account.
Also the **ions** that traverse the orifice are affected, namely by collisions with neutral species and by the deflection due to the changes in potential lines induced by the orifice geometry. The attenuation of the MS signal in low pressure conditions caused by collisions can be calculated to be less than 0.5 % [102, 103]. The impact of the distorted equipotential lines was investigated by several authors [103, 104] and is usually found to be small for ion energies larger than 5 eV [104, 105], which is usually given in standard plasma processes. In addition, the mass dependency of the attenuation of the signal is rather weak ($\propto m^{1/4}$). Since both the overall attenuation and its mass dependence are small, these effects are neglected and the ion transmission will be assumed to be constant for different masses.

Determination of the Absolute Neutral Density

Two possibilities exist to approximate the absolute neutral density from the measured neutral flux. Either the transmission factor can be calculated by estimating several MS parameters, or it can be found experimentally [86, 101, 106]. One way to measure the total TF for neutrals is the use of a mixture of noble gases (He, Ne, Ar,...) of known composition ratios [106]. From the ratio of the noble gases and the appropriate ionization cross sections, the spectrometer signal can be calibrated up to $m/q = 131\,\mathrm{amu/e}$ (if Xe is part of the mixture) assuming that the TF depends only on the mass and the ionization cross sections.
Alternatively, the conversion factor for a neutral species can be found by calibrating the signal with a reference measurement [85, 86, 93] of a gas of known density with similar molecular mass as the species of interest (e. g. Br and HBr). If the ionization cross section of the gas molecule and the species of interest is known, an estimate of the absolute density in the plasma can be obtained [86], assuming the absence of other sources of ionization (e. g. by using the adequate threshold energy).

2.3. (V)UV Absorption

Absorption spectroscopy can be used to measure line integrated densities of absorbing species in liquids, gases or plasmas. Incoming photons are absorbed with a certain probability by atoms and molecules, which change in turn their rotational, vibrational or Rydberg states. The absorption of the incident light is characterized by the Beer-Lambert law

$$\frac{I_T}{I_0} = e^{\sigma\, l\, n}, \tag{2.2}$$

where the ratio of the intensities of the incident light I_0 and the transmitted light I_T is expressed in terms of the absorption cross section of a single molecule/atom σ, the path length l in the medium and the atomic density of the absorbing species n. In this study, we use ultra violet (UV) and vacuum ultra violet (VUV) light to investigate the species densities in reactive etch plasmas. UV light is usually associated with wavelengths between 200 and 400 nm while the VUV region goes down to approximately 100 nm. In this region of wavelengths many different species can be studied, including, but not limited to Cl_2, SiCl, $SiCl_2$, SiBr, CF, CF_2 (UV) and HBr, BrCl, Br_2, $SiCl_4$, BCl_3, SF_6, O_2 (VUV).
The main difference between the experimental setups for UV and VUV absorption spectroscopy, described in the following, is linked to the absorption of VUV light by the ambient air.

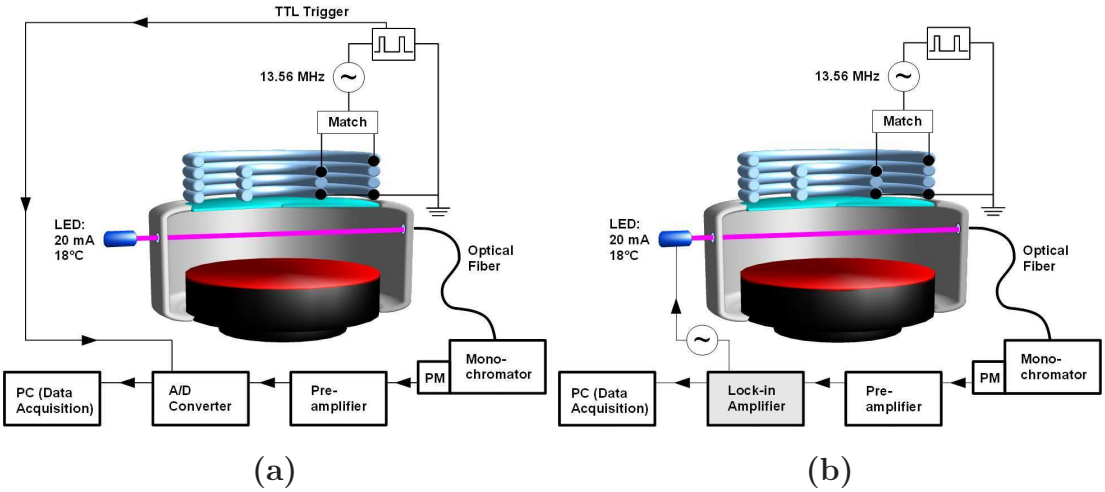

Figure 2.8.: *Sketch of the UV absorption setup for* ***(a)*** *time-resolved and* ***(b)*** *time-averaged measurments.*

2.3.1. Setup of UV Absorption Experiments

In contrast to mass spectrometry, absorption spectrometry can be used to measure the densities in the bulk of the plasma, just below the plasma generation coils.
In the past, xenon or deuterium light sources were often used to generate UV light. Recently, Cunge *et al.* [107] started to use light emitting diodes (LED) instead. The advantage of such a light source is its increased stability of the emitted intensity, increasing the signal-to-noise ratio of one to two orders of magnitude. In general, even species that have a very small absorption cross section can be studied. In the present case, the LED technique is used to study SiBr in an HBr/O_2 etch plasma. Kogelschatz *et al.* [108] examined the absorption structure of SiBr between 270 and 310 nm and report a strong absorption line at 292 nm that we target with a temperature controlled LED from THORLABS, whose Gaussian-like intensity distribution is centered at 290 nm with a full width at half maximum of 12 nm. The LED emits the light isotropically at an angle of 120°. A lens with a focal length of 9 mm creates a parallel beamthat passes into the plasma reactor through a MgF_2 window. After the transit of the reactor, behind a second window, the beam is focused into an optical fiber by a lens with a focal length of 50 mm. The fiber is connected to a monochromator and the resulting signal is measured by a photo multiplier. The Acton series monochromator is fabricated by Princeton Instruments and has a diffraction grating of 1200 grooves/mm with a focal length of 20 cm. A pre-amplifier converts the measured current into a voltage and increases its signal by a factor of $10^5\,\mathrm{VA}^{-1}$.
Depending on the information we want to obtain, two different setups can be realized, shown in Fig. 2.8.
In the first setup (a), which allows to follow the time-resolved density variation in pulsed plasmas, the signal from the amplifier is directly connected to an acquisition

card from National Instruments. The acquisition process has to be synchronized with the plasma pulses in order to allow an averaging of the signal for a high signal-to-noise ratio. Therefore, the outgoing TTL signal from the plasma power supply is measured with a second National Instruments card and synchronized with the absorption measurement in a LabView program. Five different measurements of the pulse period are needed to obtain the absorption of the target species:

1. lamp **without** plasma (incident signal, $I_{l,1}$),
2. plasma **and** lamp **on** (measured absorbed signal, I_{pl}),
3. plasma **without** lamp (plasma emission, I_p),
4. lamp **without** plasma ($I_{l,2}$) and
5. both plasma **and** lamp **off** (background, I_b).

The density of the studied species can then be calculated by

$$n = \frac{1}{\sigma\, l} \cdot \ln\left(\frac{I_{pl} - I_p}{(I_{l,1} + I_{l,2})/2 - I_b}\right). \tag{2.3}$$

The measurements of the lamp intensity in the beginning and at the end account for possible lamp intensity drifts due to deposition on the windows. Such an increase of absorption by the reactor windows can be observed during HBr/O_2 etching of silicon.
The second setup (b) is used to obtain time-averaged data. The output of the amplified PM signal is connected to a lock-in amplifier that controls the LED intensity by a built-in wave generator. The signals from the wave generator and the PM measurement are multiplied and integrated over a specified time. All components of the PM signal that have a different frequency compared to the wave generator are attenuated to zero. Thus, the contribution from the background and the plasma emission are directly removed. In consequence, only three measurements have to be carried out ($I_{l,1}$,I_{pl} and $I_{l,2}$) to determine the averaged species density. For its calculation Eq. 2.3 can be used with $I_p = I_b = 0$.

2.3.2. Setup of VUV Absorption Experiments

In principle, the VUV absorption technique is similar to UV absorption, but gives access to additional absorbing species (see Fig. 2.9). Especially close-shell molecules are usually not detectable in the UV region. However, several components of the hardware setup have to be changed. First of all, the total path of the VUV light has to be under vacuum; otherwise the ambient air would absorb the photons immediately. Furthermore, no adequate LEDs exist that could be used for VUV light emission, so that a less stable 75 W high pressure deuterium lamp (X2D2, Hamamatsu) is used. It emits a continuous light spectrum between 115 and 400 nm with a high VUV intensity in the range of 115-200 nm, shown in Fig. 2.9 b. The light is collimated by a parabolic mirror, passes through the reactor via MgF_2 windows and is thereafter focused by a second parabolic mirror into the

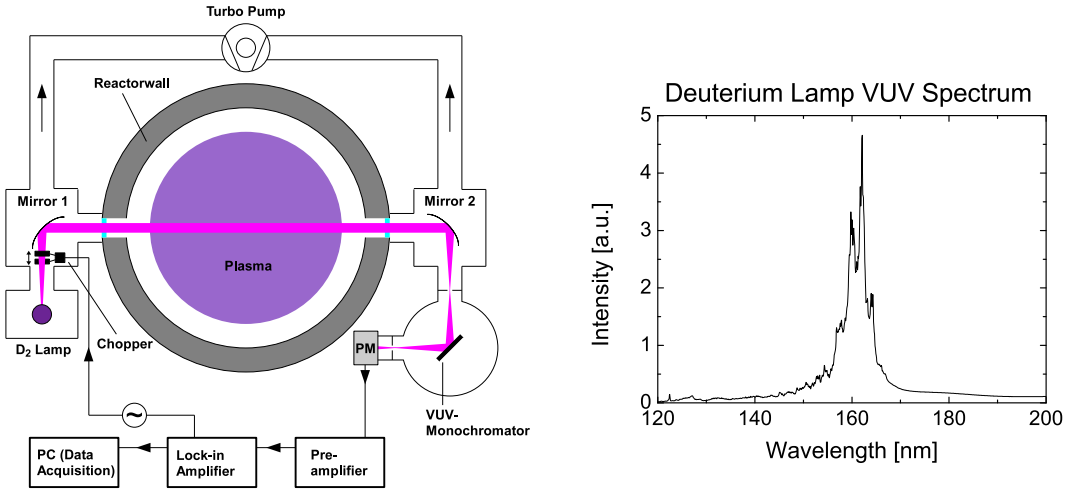

Figure 2.9.: ***(a)*** *Sketch of VUV-absorption setup and* ***(b)*** *VUV spectrum of D_2 lamp.*

entrance slit of a VUV spectrometer (Jobin Yvon H20-UVL, HORIBA). The latter is equipped with a diffraction grating of 1200 grooves/mm and has a focal length of 20 cm. A PM converts the optical signal into a current, which is afterwards amplified by a factor of $10^6\,\mathrm{VA}^{-1}$ and recorded by a PC via an acquisition card from National Instruments. Figure 2.10 shows the absorption spectrum of an HBr gas and plasma.

The three major absorption lines of HBr at 138, 143 and 150 nm correspond to the $4p\pi \rightarrow 5s\sigma$ transition in the two Rydberg states $C^1\Pi$ (138 and 143 nm) and $b^3\Pi$ (150 nm) [109]. The continuous absorption between 155 and 200 nm is due to the transition of the $4p\sigma$ orbital to the antibonding $4p\sigma^*$ orbital (into the dissociative $a^3\Pi$ and $A^1\Pi$ states). The broad absorption peak at around 150-160 nm in the plasma spectrum can be attributed to Br_2, which cannot be seen in HBr gas [88, 110]. Even for low densities of HBr, the absorption lines are saturated [88] and thus, it is difficult to deduce the absolute HBr density from their intensities. One possibility, described by Cunge *et al.* [88], is the use of experimentally obtained reference spectra of HBr gas at different pressures. By fitting the appropriate reference spectrum to the obtained plasma spectrum, the absolute density of HBr can be found. After subtraction of the HBr contribution to the spectrum, the same procedure can be used to obtain the density of Br_2 molecules in case of the plasma.

However, several problems of this technique have to be addressed. One of these is linked to the tubes in the reactor wall with a length of several cm in which the MgF_2 windows are inserted. HBr and Br_2 can recombine more easily in these tubes due to the increased surface area and the absence of dissociation processes. The magnitude of the contribution to the line integrated density is difficult to

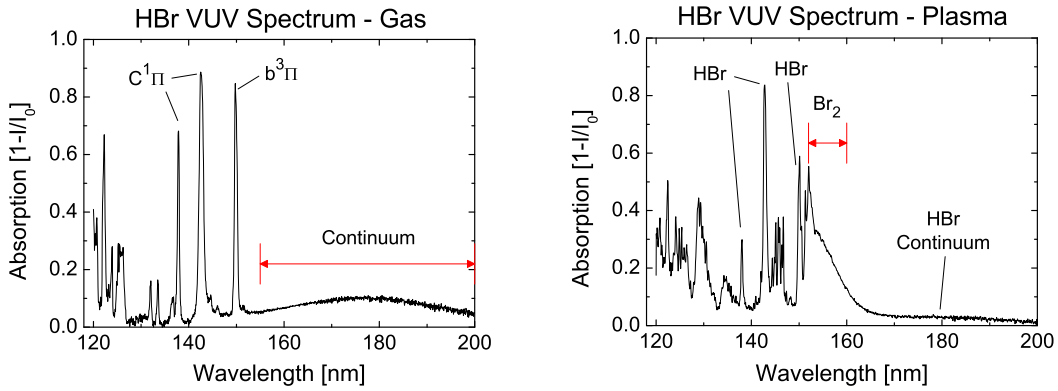

Figure 2.10.: *VUV absorption spectra from* ***(a)*** *an HBr gas and* ***(b)*** *an HBr plasma*

determine, but it could have a considerable impact. Moreover, the non-linearity of the peak intensity with a change of density can lead to a misinterpretation of the spectrum. Even a small change in peak intensity (in the margin of error) could lead to a significant change in density.
Finally, compared to reference HBr gas spectra, we observe different peak intensity ratios in the spectra from the plasma. This could be linked to different populations of the energetic states, temperature changes or small changes in the hardware setup. In general, the resulting error becomes rather large, allowing in our case only qualitative information on the HBr and Br_2 density.

2.4. Ion Flux Probe

The ion flux is a crucial parameter for etching processes. In this study a planar probe, developed by Braithwaite *et al.* [111], was used to measure directly the ion flux onto its surface. In principle, it is also possible to gain information on the electron flux and energy distribution function, once the ion flux is known [112]. The probe itself consists of a large area ($1\,cm^2$) planar single-sided disk, which is positioned in plane to the plasma reactor wall just above the wafer, at the same position as the mass spectrometer. A guard ring with the same surface is placed around the probe to avoid edge effects of the sheath (see Fig. 2.11).
A pulsed RF source is coupled to the probe and the guard ring via capacitors. For a measurement, the capacitively coupled probe surface is charged by the electron and ion flux to a negative potential V_{bias} compared to the natural floating potential V_{fl}. This effect is equivalent to the self-bias effect of the powered electrode in a CCP. After the RF voltage is turned off, the accumulated charge on the plasma side of the capacitor remains. If V_{bias} is sufficiently negative with respect to the

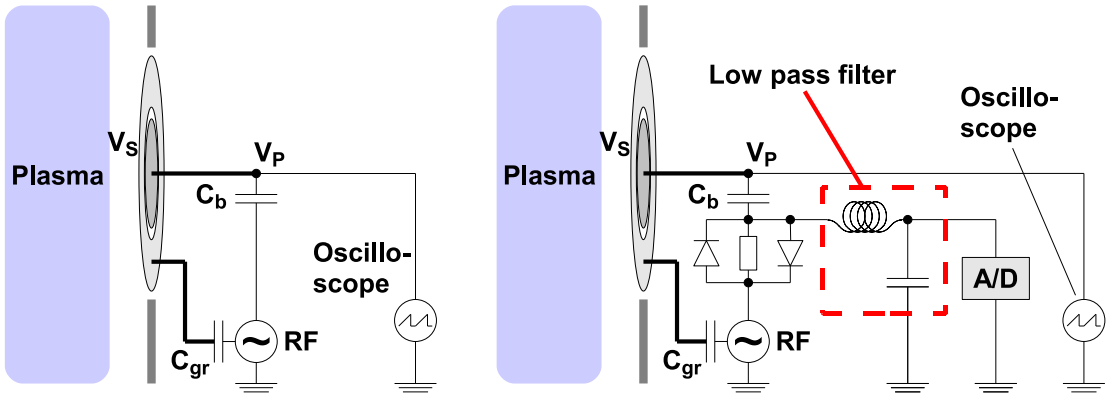

Figure 2.11.: *Sketch of the ion flux probe with* **(a)** *traditional and* **(b)** *newly developed direct current measurement system.*

plasma potential (several 10 V), the electron flux Γ_e will be negligible compared to the ion flux Γ_i on the probe surface. In this case, the probe potential will increase proportionally to the ion flux. When the potential difference between probe and plasma is small enough, the electron flux becomes important and finally V_{bias} approaches V_{fl}. During the discharge of the blocking capacitor C_b, the change in potential is essentially described by

$$\frac{\mathrm{d}V_{bias}}{\mathrm{d}t} = \frac{eA\left([\Gamma_i - \Gamma_e(V_{bias})]\right.}{C_b}\,, \tag{2.4}$$

where e is the elementary charge and A is the probe surface. In order to avoid sheath edge-effects on the probe, the guard ring has to follow the same potential discharge as the probe itself. Hence, the blocking capacitor of the guard ring needs to be chosen accordingly.
The ion flux can be measured in two different ways. The "traditional" way is to record the capacitor voltage with an oscilloscope, as shown in Fig. 2.11 a. The measured voltage corresponds to the combination of the potential drop over the blocking capacitor and the low impedance of the RF generator. By removing the calculated leak current from the RF generator and by neglecting the electron flux, we can obtain the ion flux using Eq. 2.4. A disadvantage of this method is the need to differentiate the measured data to obtain the flux from the voltage measurement, leading to a considerably increased noise. A way to improve the signal to noise ratio is the direct current measurement proposed by Booth *et al.* [112] and presented in Fig. 2.11 b. In between the blocking capacitor and the RF generator, two head-to-tail diodes are placed with a resistor in parallel. During the bias generation, the RF high voltage can pass through the two diodes without significant loss. When the RF voltage is switched off, the potential drop over the resistor, which is directly proportional to the current, is very small compared to

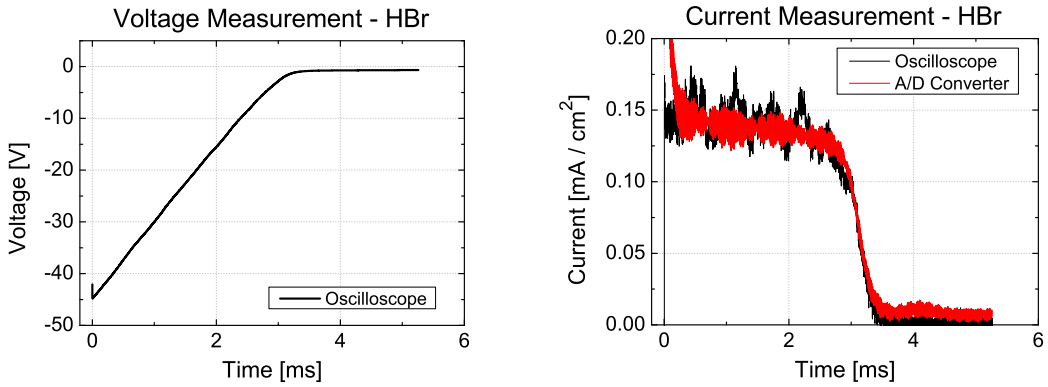

(a) **(b)**

Figure 2.12.: ***(a)*** *Voltage measurement with an oscilloscope for an HBr plasma at 20 mTorr and 750 W source (blocking capacitor of 10 nF).* ***(b)*** *Comparison between current calculation from oscilloscope data and direct current measurement.*

the diode threshold voltage. It is measured with a high resolution analog-digital converter from National Instruments with a maximum voltage input of 10 V. An example of an ion flux measurement with both methods is shown in Fig. 2.12 for an HBr plasma at 20 mTorr and 750 W source power.
In some conditions, the plasma can deposit a dielectric layer on the probe surface, introducing an additional capacitance C_L. If the effective total capacitance C_{eff}, given by

$$C_{eff} = \frac{C_L C_b}{C_L + C_b}, \tag{2.5}$$

is large compared to the sheath capacitance between probe and plasma, the current measurement is still correct [111, 112].
However, if the probe potential V_P (observed by the oscilloscope) is different from the real probe surface potential V_S, given by

$$V_S = V_P \frac{C_L + C_b}{C_L}, \tag{2.6}$$

we cannot control the bias voltage at the probe surface, which is crucial to repel the plasma electrons. To get a valid measurement of the probe surface voltage, we need to ensure that $C_L \gg C_b$. Considering a 100 nm thick layer of SiO_2 on a planar probe with a surface of 1 cm^2, we can calculate a needed capacitance of $C_b \ll 35$ nF. At the same time, C_b should be as large as possible to reduce the influence of parasitic capacitances of cables and electronic components and to slow the bias discharge for longer measurements.
This technique can easily be used to study pulsed plasma discharges. In this case,

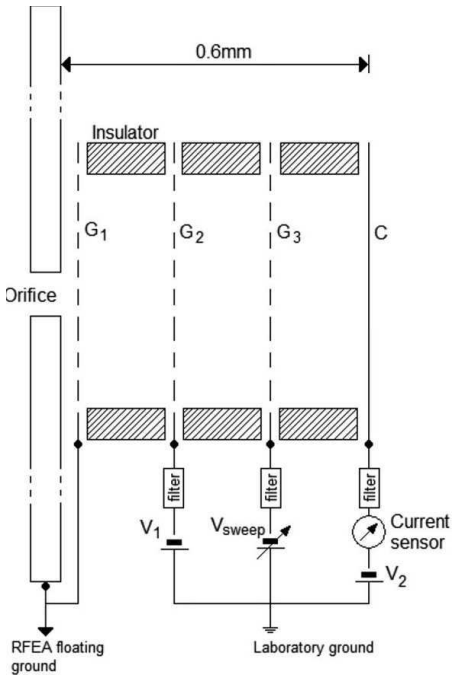

(a)

(b)

Figure 2.13.: ***(a)*** *Example of an RFA with four grids (from [113]) and* ***(b)*** *a photo of the used probe with anodized aluminum cover.*

the time during which the self-bias discharge is linear needs to be at least as long as one entire period of the plasma RF pulse. Hence, an appropriate compromise for the blocking capacitor needs to be made. Also, in order to average over several pulse cycles, the biasing of the probe needs to be synchronized with the plasma pulses.

2.5. Retarding Field Analyzer

An alternative diagnostic tool to measure the ion flux, but in addition also the ion energy distribution function, is a retarding field analyzer (RFA). In this thesis several prototypes of the commercially available SEMION probe from Impedans Ltd. were used [113, 114]. In Fig. 2.13 a scheme of such a four grid analyzer is shown.
The first grid G_1 is a floating grid to simulate the potential of the floating wall or the wafer. If the RFA is positioned on a biased wafer, the self-bias potential is transmitted via the metallic frame to G_1. The second grid G_2, called the discriminator grid, is biased with a potential ramp to discriminate the ion energy. The third grid G_3 functions as a suppression grid to repel electrons from the plasma and to prevent secondary electrons from the ion bombardment of the collector to escape. The fourth grid (or plate) C is the collector. The current from the incoming ion flux is measured at each step of the potential ramp.
All grids are connected via high impedance low-pass filters to an external power

supply, which is controlled through a USB connection by a PC. The floating potential of G_1 is measured externally with an oscilloscope. All grids follow the RF component of the plasma power supply and the changes during the pulse periods of this time scale, but only G_1 follows also the averaged DC bias/floating potential of the substrate. The non-floating grids G_2,G_3 and C are set with respect to the external ground while the incoming ions arrive on a surface with floating potential (G_1). Hence, the floating voltage needs to be subtracted from the discriminator voltage values to obtain the ion energy with respect to the floating surface. Under these conditions, the measured current-voltage (I-V) data from C (collector current) and G_2 (varied discriminator voltage) represents the total flux of ions and can be differentiated to obtain the IEDF.
In a first version, the SEMION probe was capable to measure the averaged and time-resolved IEDF of pulsed discharges **only without** bias power applied to the wafer and probe. In a second version, the filter system was changed and it was possible to measure averaged IEDFs with bias. However, the plasma pulsing disturbed strongly the measurements in this setup and only CW conditions could be analyzed. In a third, further improved setup, it was possible to obtain averaged IEDFs of pulsed plasmas with self-bias. A drawback during the third measurement session was a short circuit between the first two grids (G_1, G_2). After different tests and after consulting Impedans Ltd., the final setup was chosen as follows:

1. G_1 - floating (short circuit with G_2)
2. G_2 - floating (short circuit with G_1)
3. G_3 - discriminator potential ramp
4. C - negative collector potential (less than minimal discriminator voltage).

The collector potential needs to be less or equal to the minimal discriminator voltage of G_3 in order to collect **all** ions that pass G_3. This setup suppresses plasma electrons, but does not prevent secondary electrons from escaping the collector, appearing as incoming ions in the measured current. Therefore, the absolute current measurement might be slightly altered while the IEDF should not be influenced significantly [114].
For all experiments presented later, the RFA is placed in the center of a silicon wafer. For the first two measurement sessions, a thin ceramic shield (few mm) with 0.8 mm holes for ion collection was used to prevent the metallic body from etching. In the third session, the aluminum body itself was anodized (same material as reactor walls) and thereby converted to a dielectric shield. Only measurements with the same setup are compared since the transmission function might change between different hardware designs.
An example of the measured I-V curve and the resulting IEDF are shown in Fig. 2.14. In some cases, the I-V measurement is very noisy, so that no information can be obtained from the derivative (IEDF). In this case the I-V curve can be fitted with a combination of several logistic (Boltzmann) functions and, if necessary, with an additional linear term accounting for the escaping secondary electrons in order to obtain a smooth IEDF.

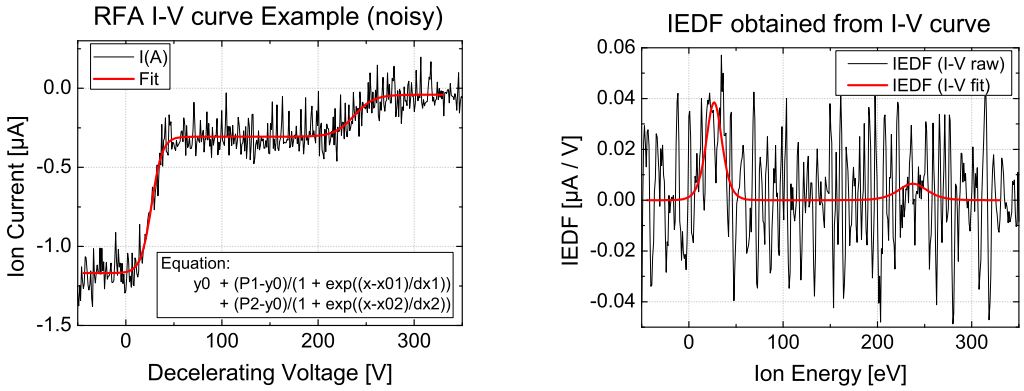

(a) **(b)**

Figure 2.14.: ***(a)*** *Measured I-V curve of the RFA with fit.* ***(b)*** *Direct derivative (IEDF) of raw data and derivative of fit.*

2.6. X-ray Photoelectron Spectroscopy

X-ray photoelectron spectroscopy (XPS) is a very powerful diagnostic method for surface analysis since it is able to probe the first few nm of a sample for a chemical analysis.

2.6.1. Basic Concept

XPS is based on the photoelectron effect, sketched in Fig. 2.15 a. An energetic (X-ray) photon transfers its energy to a core electron, which in turn leaves the shell with a certain kinetic energy. The binding energy E_B of the electron in the sample can be obtained by measuring the kinetic energy E_{kin}:

$$E_B = h\nu - E_{kin} - W_{spec} - \phi, \tag{2.7}$$

where $h\nu$ is the known photon energy, ϕ is the sample surface potential, and W_{spec} is the spectrometer work function. The latter corresponds to the potential difference between the Fermi-level (equal for sample and spectrometer) and the free vacuum level of the spectrometer [115]. In some cases, e. g. for dielectric materials, the loss of electrons can lead to a positive sample surface potential ϕ, which inhibits the electrons from escaping, so that the resulting binding energy is increased. Figure 2.15 b shows the corresponding band diagram.

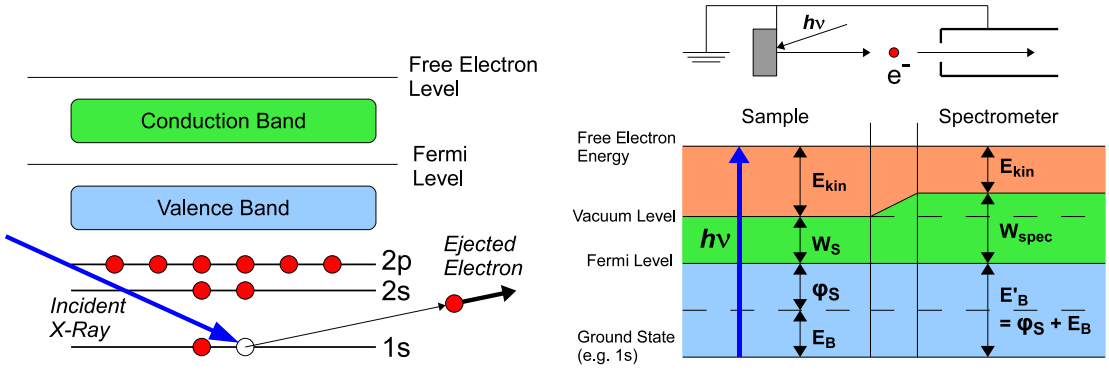

(a) (b)

Figure 2.15.: *Sketch of the photoelectron effect and the spectrometer work function.*

Chemical Shift and Spin Orbital Splitting

Since each element has different binding energies for its orbitals, the elements that contribute to the photoelectron emission can easily be identified from an XPS spectrum (Fig. 2.16 a). Each region of the spectrum that shows characteristic peaks can then be scanned with high resolution, as shown in Fig. 2.16 b for silicon. The separation of the signal of one element into multiple peaks has two reasons. First, the signal from most of the atomic orbitals is separated into two peaks, due to the two different electron spins (spin orbital splitting). For a given orbital and element, the area ratio (1:2, 2:3, 3:4, ...) and the energy difference between the two peaks are nearly unaffected by the atomic environment. The binding energy, on the other hand, is very well affected by the neighboring atoms. If the valence electron charge is reduced (oxidized element), the binding energy for the remaining electrons increases. In the same manner, an increase of the valence electron charge leads to a decrease in binding energy. This effect is called chemical shift and allows to separate signals coming from different compounds in the sample, e. g. Si and SiO_2.

Analysis of a Single Overlayer

Although the X-ray photons penetrate quite deeply into the surface, the produced photoelectrons can be easily scattered and reabsorbed by the sample material. If the photoelectron intensity of a thin layer is emitted in a depth d of the sample at a take-off angle θ with respect to the surface normal, the measured intensity is attenuated according to the Beer-Lambert law to

$$\mathrm{d}I = k\,\Gamma\,n\,\sigma\,\gamma\,e^{(-d/\lambda\cos(\theta))}\,\mathrm{d}z, \tag{2.8}$$

where λ is an effective attenuation length, Γ is the X-ray photon flux, n is the atomic density, σ is the photoionization cross section (Scofield factor [116]), and γ is

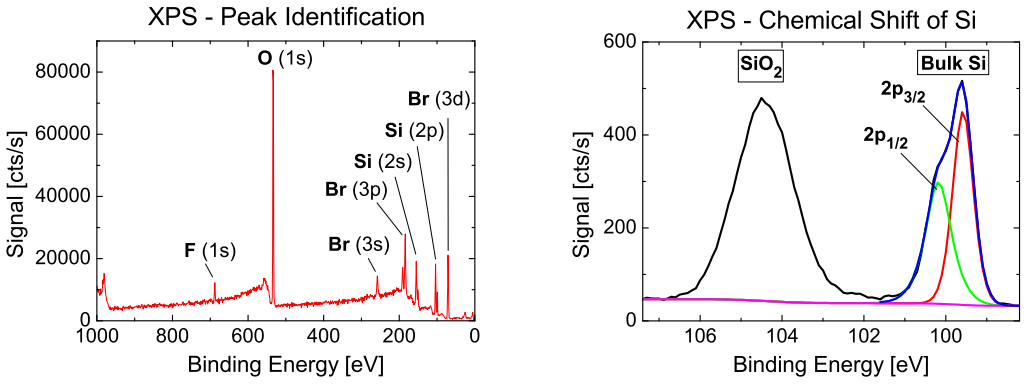

(a) (b)

Figure 2.16.: ***(a)*** *Overview spectrum to show identification of elements.* ***(b)*** *Spectrum of a thin layer of SiO_2 on the silicon bulk to show the chemical shift and the spin orbital splitting.*

the efficiency to generate photoelectrons without energy loss due to, e. g., plasmon excitation [115, 117]. k includes all spectrometer factors like the transmission function and the electron detection efficiency. Consequently, the total measured intensity I_0 for a homogeneous material is

$$I_0 = k\,\Gamma\,n\,\sigma\,\gamma\,\lambda\,\cos(\theta). \tag{2.9}$$

Considering a thin homogeneous overlayer O of thickness d on a substrate S, both containing the same element, as it is the case, e. g., for SiO_2 on Si, we obtain by integrating Eq. 2.8 and assuming $\lambda_O \approx \lambda_L$

$$I_L = I_{L,0} \cdot \left(1 - \exp\left(\frac{-d}{\lambda_L \cos(\theta)}\right)\right) \text{ and} \tag{2.10}$$

$$I_S = I_{S,0} \cdot \exp\left(\frac{-d}{\lambda_L \cos(\theta)}\right). \tag{2.11}$$

When both intensities of the chemically shifted peaks are known, the thickness of the overlayer can be determined by

$$d = \lambda_L \cos(\theta) \ln\left[1 + \frac{I_L}{I_S} \cdot \frac{1}{R_0}\right], \tag{2.12}$$

where $R_0 = I_{L,0}/I_{S,0}$. Several authors have provided equations to calculate the attenuation length, depending on the density, stoichiometry, and electronic bandgap [117–119]. The most popular set of equations, also used throughout this work, is the one from Tanuma, Powell and Penn, called TPP-2M [118, 120]. R_0 can be

determined experimentally or estimated as shown, e. g., by Seah and Spencer [121].

2.6.2. Instrumentation

All the XPS measurements were carried out in a customized Thermo Fisher Scientific Theta 300 spectrometer, which is connected under vacuum to the wafer transfer system of the etch chamber, allowing to analyze 300 mm wafers quasi *in-situ* [122]. The system is equipped with a high resolution monochromatic Al Kα source at 1486.7 eV. In this system, the size of the analyzed area of the sample is determined by the X-ray spot, set to 400 µm, and not by the detector. The detector can analyze emission angles in parallel between 20° and 76° with respect to the wafer surface normal. For most measurements, this acceptance angle was divided into 8 equal detection angles, ranging from 23.5° to 72.5°, each with an acceptance angle of ±3.5°. The spectra were recorded with a detector pass energy of 60 eV and with a step size of 0.1 eV. In addition, the spectrometer is equipped with an electron beam system for charge neutralization.

2.6.3. Sidewall Passivation Layer Analysis Technique

One of the most important factors that influence the profile of etched structures is the formation of the sidewall passivation layer (SPL) that protects the structures from lateral etching [123–125]. A balance between continuous deposition and etching produces a specific etch slope [125, 126]. Hence, the control of the SPL is essential. Unfortunately, it is rather difficult to analyze SPLs in terms of thickness and chemical composition without air exposure in order to better understand their formation.

The chemical composition of the SPL is often studied by XPS [123, 126–133]. A homogeneous pattern of lines and trenches is perpendicularly analyzed by an XPS system, so that the signals from the trench bottom and the bottom part of the sidewalls are shadowed by adjacent lines. The signal from the mask can be identified thanks to a technique of differential charging: an electron flood gun charges dielectric materials and shifts their peak positions (binding energies) in the XPS spectra [134].

As explained above, it is also possible to estimate the thickness of a thin overlayer on a substrate from XPS measurements using Eq. 2.12 [117–120, 135]. Following this approach, Pargon *et al.* [136] compared the XPS signal of a blanket resist layer to the signal of a resist pattern and calculated therewith the signal from the sidewall by subtraction. This way, they could estimate the average SPL thickness, but no profile of the SPL was obtained.

During this thesis a non-invasive angle resolved XPS (ARXPS) technique was developed that provides simultaneously profiles of the SPL thickness and profiles of the chemical composition [137]. The quasi *in-situ* analysis allows to investigate the passivation layer directly after the etch process without exposure to air (which would possibly alter the results).

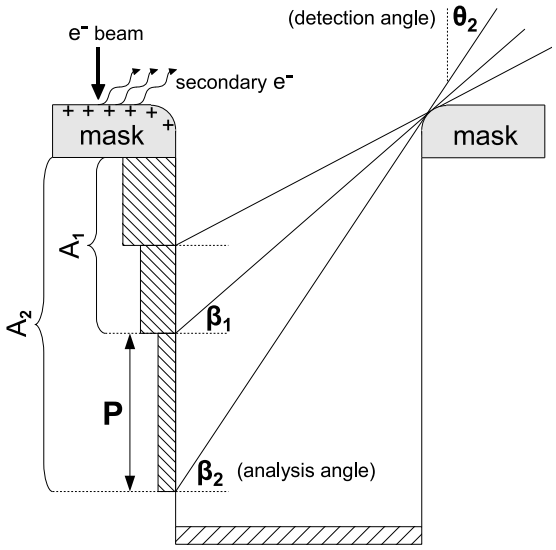

Figure 2.17.: *Sketch of the XPS technique to analyze the sidewall passivation layer.*

Technique

In order to study the chemical composition and the thickness of the SPL, several conditions have to be fulfilled.
First of all, it is necessary to collect as much signal as possible originating from the sidewalls in order to reduce the signal to noise ratio. For this purpose, a pattern consisting of lines and trenches with equal widths is very convenient. This pattern should be larger than the X-ray spot size from the ARXPS system and needs to be positioned in such a way that the plane of detection of the ARXPS system is perpendicular to the orientation of the trenches. Thus, the average XPS signal originates both from the mask and the pattern sidewalls (Fig. 2.17). Each detection angle θ corresponds to a different observed area of the SPL while the signal from the rest of the SPL and from the trench bottom never reach the detector since they are obstructed by adjacent lines. For large detection angles, all photoelectrons from the SPL are blocked and the measured signal originates only from the mask. Therefore, the number of data points for the SPL is reduced, especially for thinner trenches. The detection angle defines the maximal aspect ratio that can be analyzed. The aspect ratio is the ratio of the probed trench depth (including the mask) over its width. It is a more convenient parameter for the study of trenches with different widths than the probed depth.
In a second step, the SPL signal has to be isolated from the mask signal. This can easily be done if the pattern stack consists of a dielectric mask (e. g. SiO_2) on top of a conducting bulk material (e. g. trenches in bulk silicon). In this case, it is possible to charge the dielectric mask separately from the trench walls, resulting in a shift of the binding energies in the mask material. Consequently, the peak positions from

the mask signal in the XPS spectra are also shifted [134]. The differential charging is carried out by applying an electron beam dedicated to neutralize accumulated charges on dielectric surfaces. Depending on the electron beam energy, the mask can be charged either negatively due to an accumulation of electrons (low energy beam) or positively due to the loss of secondary electrons (high energy beam). A positive mask charge shifts the XPS peaks to higher binding energies and vice versa [138].
The extracted signal gives information on the average chemical composition of the SPL of the measured area along the trench sidewall. The average SPL thickness is calculated with Eq. 2.12.
Using the average thickness and chemical composition, it is possible to obtain the signal intensities from each part P of the sidewall using the angle resolution of the XPS system (see Fig. 2.17). P is defined as the area that is observed additionally going from a rather flat detection angle (θ_1) to a steeper angle (θ_2). However, the signal intensities of the observed sidewall areas (A_1 and A_2) at different angles cannot be subtracted directly to obtain the signal from P due to their dependence on the detection angle [117]. Thus, it is necessary to calculate the theoretical signal from area A_1 at the detection angle θ_2. Taking this into account, we can estimate the substrate and overlayer signal intensities of part P of the SPL:

$$I^{\theta_2}_{OL,p} = I^{\theta_2}_{OL,A_2} - I^{\theta_1}_{OL,A_1} \cdot \frac{1 - \exp\left[-d_1/\lambda \cos(\beta_2)\right]}{1 - \exp\left[-d_1/\lambda \cos(\beta_1)\right]} \tag{2.13}$$

and

$$I^{\theta_2}_{S,p} = I^{\theta_2}_{S,A_2} - I^{\theta_1}_{S,A_1} \cdot \frac{\exp\left[-d_1/\lambda \cos(\beta_2)\right]}{\exp\left[-d_1/\lambda \cos(\beta_1)\right]}, \tag{2.14}$$

where the emission angle β_i is defined with respect to the surface normal, so that $\beta_i = 90° - \theta_i$ (assuming a vertical trench sidewall). From the obtained signal intensities the chemical composition and the thickness can be calculated for each part P of the sidewall, resulting in a profile along the sidewalls.

Assumptions and Possible Errors

Although this technique proves to be quite accurate, as shown in the next section, we still need to keep in mind the assumptions that are made to determine the SPL thickness and the possible errors that they imply.

1. We need to assume that the XPS measurement procedure itself results in reliable data. Seah [139] evaluated uncertainties in thickness measurements using XPS for ultrathin SiO_2 on Si and reported an uncertainty of 0.4 nm over the range $2.5 < d < 7.8$ nm only due to the analysis procedure and hardware. However, since the data is always obtained in the same system, the relative change between different samples should be unaffected.

2. Furthermore, we assume the presence of vertical sidewalls. In our case the sidewall slope is changing by not more than 3° (from the vertical case) between trench top and bottom. Nevertheless, this leads to an error in the thickness estimation of between 2 and 14 %, depending on the detection angle (see Eq. 2.12).

3. Also, we use a simple bilayer model in which the overlayer is treated as a homogeneous material. Since the formation of the passivation layer is a continuous process in a rather stable environment, this assumption might be quite accurate, but due to a lack of information on the SPL, we can neither validate it at this point, nor estimate an error.

4. The attenuation length λ is calculated using the stoichiometry of the XPS measurement as well as the density and the bandgap data from SiO_2, due to the lack of information on the bromine rich silicon oxide passivation layer. For the same reason, R_0 is determined experimentally for SiO_2. Seah and Spencer [121] discuss in detail the errors in the determination of a thin SiO_2 overlayer thickness that are related to theoretical and experimental values of R_0 and λ. They cite a variation of R_0 between 0.67 and 0.87 for previously published experimental values. In addition, they determine themselves R_0 experimentally and theoretical and find values of 0.88 and 0.53, respectively. Regarding the attenuation length λ, they report an agreement between the theoretical and experimental values within an error of 10 %. Other studies state a root mean square deviation of the estimated values from experimentally obtained attenuation lengths in a range between 1 and 20 % [120, 135], depending on the probed materials and the used material properties. Moreover, the experimental results presented later indicate that the chemical composition changes slightly with the aspect ratio (but not significantly with the trench width), reducing additionally the confidence in R_0 and λ.

Considering all the above, we estimate the corresponding uncertainties by very conservative values, namely by $R_0 = 0.778 \pm 0.30$ and $\lambda = 3.367 \pm 0.7\,\text{nm}$. These values lead to an uncertainty of the thickness of 21-28 % (depending on the ratio of I_{OL}/I_S) and 20 %, respectively. It should be mentioned that an error in λ results only in a constant offset for all sets of data points and, thus, the relative behavior should remain unaffected.
The resulting probable total error is calculated to 29-40 % by using the Gaussian error propagation.

Limitations

The presence of both a dielectric mask and a conducting sidewall is necessary to charge the mask differentially in order to distinguish between the two signals. For large detection angles (small angle with respect to the sidewall surface), the

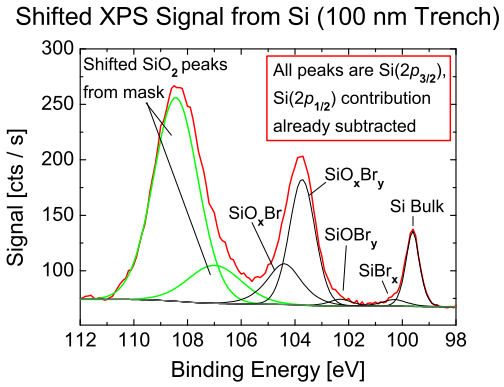

Figure 2.18.: *XPS signal from Si: the signal from the oxide mask is shifted to the left towards higher binding energies due to the secondary electrons produced from an electron beam with an energy of 300 eV.*

photoelectron refraction will increasingly disturb the XPS measurement [117,140], so that the maximal analyzable aspect ratio is approximately 3. Also, for SPL thicknesses larger than ~ 10 nm, the signal originating from the substrate is too small to estimate the thickness. Furthermore, it is necessary to have access to the relevant hardware, namely the quasi *in-situ* XPS system and adequate pattern structures. Finally, the time of acquisition for one pattern is quite high and ranges in the order of two hours, depending on the targeted signal to noise ratio. Despite these limitations, this technique is a powerful method to analyze the SPL.

Experimental Validation

The sidewall passivation layer formed during the plasma etching of silicon trenches in an HBr/O_2 chemistry is studied using the presented technique. Each analyzed pattern consists of lines and approximately 300 nm deep trenches with equal widths. The lines are patterned by electron beam lithography and form areas of 1 mm x 1 mm. The X-ray spot size was set to 400 µm, which is small compared to the size of the pattern area and the acceptance spot size of the detector (for all angles). The electron beam energy is set to 300 eV to charge the dielectric mask, a single layer of 50 nm silicon oxide, positively due to the loss of secondary electrons. This results in a shift of the peaks of the thin oxide mask of around $4-6$ eV towards higher binding energies, as shown in Fig. 2.18 for the Si signal. In this figure, the Si($2p_{1/2}$) contribution of each designated double peak was subtracted beforehand to simplify the identification of the peaks. After identifying the shifted contribution of the mask, it can be removed, so that only the signal from the sidewalls remains.

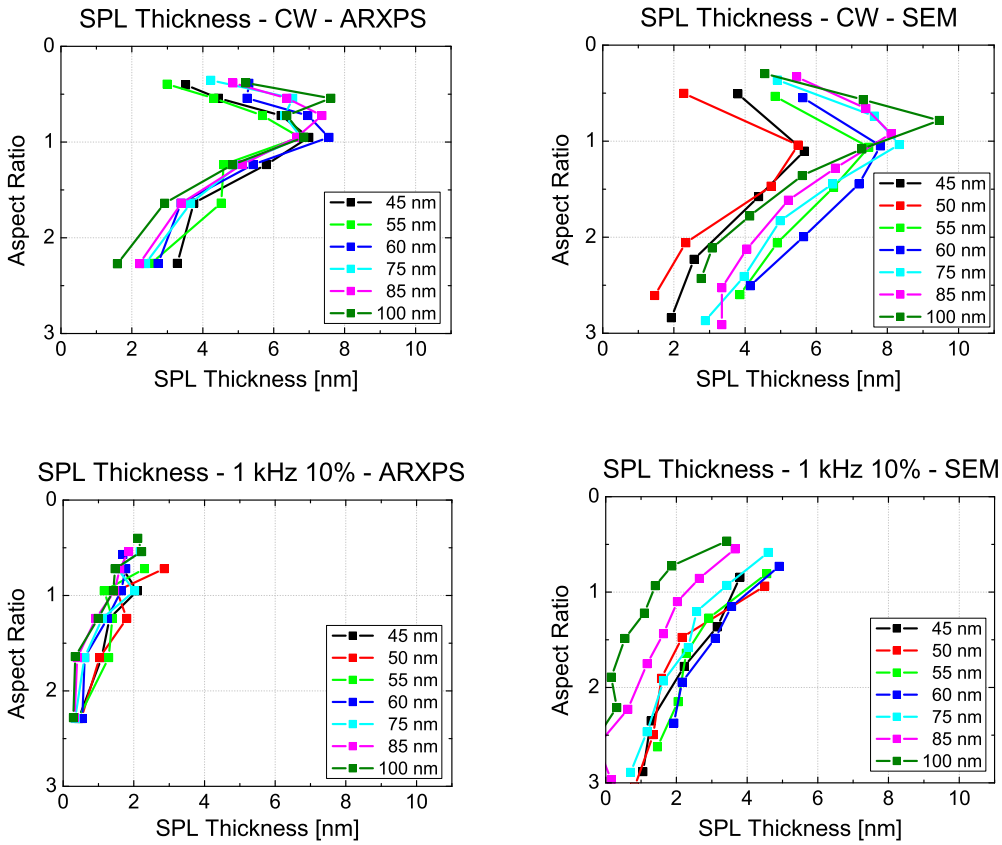

Figure 2.19.: *Results from the sidewall passivation layer analysis. Comparison between XPS and SEM for patterns from pulsed (1 kHz and 10 % duty cycle) and CW etching.*

Performance of the Technique

In order to verify the results from the ARXPS analysis, we used scanning secondary electron microscopy (SEM) to measure the SPL from cross sections of the trenches. By removing the SPL in a short bath in hydrofluoric acid (HF), the thickness can be obtained from measurements before and after HF application [141, 142].
In Fig. 2.19, the SEM and XPS thickness profiles for various trench dimensions from CW and pulsed (at 1 kHz and 10 % duty cycle) experiments are shown. The profiles will be discussed in Chap. 5.5. Here, we focus exclusively on the comparison between the XPS and SEM technique.
The performance of the SEM technique is limited since the resolution of the SEM used in this study is not better than 3 nm. Moreover, only a very limited part of the pattern can be observed with a cross section. This makes the measurement only a random sample and the real average for the whole pattern remains unknown. Still, the SEM images can give us an estimation of the absolute SPL thickness and its evolution with changing aspect ratio.

In Fig. 2.19 b the results from the SEM analysis are shown for comparison. Although the SPL thickness for a specific aspect ratio seems to depend also on the trench width, we do not observe any definite trend (e. g. thinner SPL thickness in thinner trenches). Thus, we attribute this variation to the large error in the SEM analysis technique. Nevertheless, the absolute values of the SPL thickness and the thickness profile are in very good agreement, validating the parameters used to calculate the attenuation length and R_0.
The results for the thickness measurements by XPS and SEM for a pulsed condition at 1 kHz and 10 % duty cycle are presented in Fig. 2.19 c and d for comparison. The XPS analysis indicates an SPL thickness of less than 2 nm for most of the probed area that is inside the resolution limit of the SEM. This could explain the offset to slightly larger values for the SEM measurements. Still, both results are in good agreement, considering the large error for the SEM data. For a concluding evaluation of the XPS results, a comparison to a more accurate technique like TEM would be necessary.

2.7. Spectroscopic Ellipsometry

Basic Concept

The basic principle of ellipsometric measurements is the change of phase, polarization and intensity of linearly polarized light after reflection on a flat surface. Part of the incoming electromagnetic wave at angle Φ_i is transmitted into the surface at angle Φ_t, part of it is reflected at angle $\Phi_r = \Phi_i$. A sketch of this process is shown in Fig. 2.20. The electromagnetic field $\vec{E}_i$ of the incoming wave can be split into one field parallel to the surface ($\vec{E}_{p,i}$) and one perpendicular to the surface ($\vec{E}_{s,i}$). The modification of the two components after reflection can be described by the complex reflection coefficients

$$r_p = \frac{E_{p,r}}{E_{p,i}} = |r_p| \exp(i\,\delta_p) \qquad \text{and} \qquad r_s = \frac{E_{s,r}}{E_{s,i}} = |r_s| \exp(i\,\delta_s). \tag{2.15}$$

The phase δ indicates the delay introduced by the reflection and the absolute value $|r|$ signifies the change of the amplitude. Hence, the relative change ρ of the amplitudes is

$$\rho = \frac{r_p}{r_s} = \tan(\Psi) \exp(i\,\Delta), \tag{2.16}$$

where $\Delta = \delta_p - \delta_s$ is the phase difference between both components. The measurement of the relative change of electromagnetic properties and not of absolute values makes ellipsometry a very robust, precise and reproducible technique that can be used, e. g., to determine layer thicknesses with up to Ångstrom resolution. By measuring Ψ and Δ the refractive index $n = n_r + ik$ of a large homogeneous sample or of an overlayer with known thickness can be determined. Vice versa, the

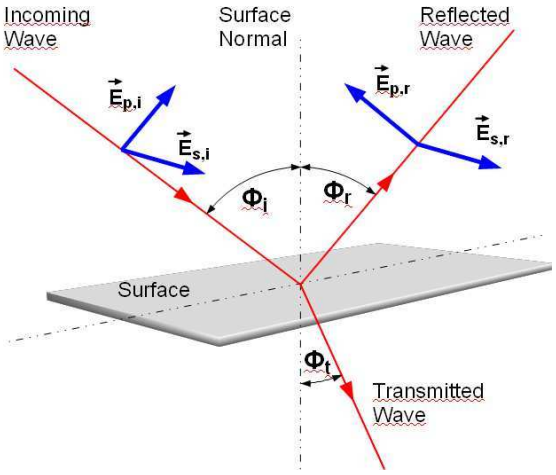

Figure 2.20.: *Sketch of a refraction process.*

thickness of a homogeneous overlayer on an opaque substrate can be determined if the optical properties of the material are known.
Some ellipsometers allow to measure Ψ and Δ at various wavelengths (spectroscopic ellipsometer) and/or at different angles. In this case it is possible to determine thicknesses and/or dielectrical properties of multi-layer systems. However, these values cannot be calculated straight forward from the measurement, but have to be fitted with a model.
The very first ellipsometers consisted of a light source, a polarizer, a compensator (e. g. a quarter wave plate) and a second polarizer (called analyzer). The electromagnetic radiation from the light source is linearly polarized, reflected from the surface where it becomes elliptically polarized and analyzed by the second polarizer. The compensator is used to introduce a known elliptic polarization before the reflection in order to achieve a linear polarization after reflection. When both compensator and analyzer are set correctly the light is totally blocked. For this reason this technique is called a nulling ellipsometry.
A more sophisticated technique is the phase modulated ellipsometry, illustrated in Fig. 2.21. Instead of a compensator, a birefringent modulator is used to introduce a periodic sinusoidal phase difference between the parallel and perpendicular component of the electromagnetic wave. The modulator is composed of a material that becomes birefringent under stress (e. g. amorphous silica) and of piezoelectric transducers with a resonance frequency of 50 kHz that apply the stress. The current collected by the photomultipliers can be analyzed using a lock-in amplifier to extract the modulated signals that carry the information of the ellipsometric parameters.

Instrumentation

In this study, two commercially available ellipsometers were used. One is the UVISEL phase modulated spectroscopic ellipsometer from HORIBA Jobin Yvon,

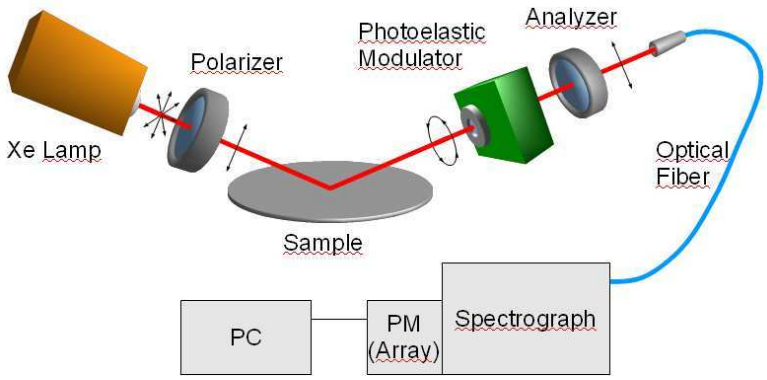

Figure 2.21.: *Sketch of a phase modulated Ellipsometer (UVISEL).*

which is directly mounted on the plasma chamber to allow *in-situ* measurements of layer thicknesses on the 300 mm wafers. The light source consists of a 75 W Xe lamp. The polarizer and analyzer are glan type devices with an extinction coefficient of 10^{-5} and an angular precision of 0.01 ° at a fixed angle. The detection system consists of 32 photomultipliers, allowing a parallel data acquisition for different wavelengths for time-resolved measurements at a frequency of about 2 Hz. The spectral resolution of the ellipsometer in the range between 190 and 880 nm is gained by a monochromator grid placed in front of the detector.
The second measurement system is a S300-Ultra from Rudolph Technologies, Inc. It is a small spot, simultaneous multi-angle, laser based, multi-wavelength ellipsometer. Four lasers at wavelengths of 458, 633, 780 and 905 nm are focused on a spot of approximately 10 µm size. The angle range for the measurement is of 30 °. The robotic wafer holder allows for a variable amount of measurement points across the wafer in order to obtain information, e. g. on the homogeneity of the measured layers.

2.8. Scanning Electron Microscopy

A commercially available JSM-7500F field emission scanning secondary electron microscope (SEM) from JEOL Ltd. is used to obtain cross section images of the etched microstructures. In theory, the maximal resolution is 1.4 nm at an acceleration voltage of 1 kV, but in praxis, the resolution is more likely to be around 3 nm.

3. HBr/O_2 Plasma Without Bias

Pulsing has been proven to be a promising approach to overcome certain limitations in current CW plasma processes [16, 41–50, 52–54]. However, the transient nature of such plasmas adds to their complexity. The more information is gained on pulsed plasmas, the easier it is to explain the impact on plasma etching and to identify potential applications. In this chapter we focus on the impact of plasma pulsing on the gas phase in an HBr/O_2 plasma without applied bias potential. Several means of diagnostic like mass spectrometry, VUV absorption spectrometry and the use of an ion flux probe help to gain insight into the basic differences compared to a CW process. The measurements are carried out in a clean plasma chamber in contrast to the real etch process, presented in Chap. 4, where etch products are re-deposited on the chamber walls. The different reactor condition might give rise to changes in recombination rates and sticking coefficients [63–70], which in turn influence the plasma composition and the species fluxes.

3.1. Neutrals

3.1.1. Mass Spectrometry

Mass spectrometry, explained in detail in Sec. 2.2, is a powerful tool to obtain a variety of information on ions and neutrals in a plasma. The focus of the experiments lies on the dependence on the duty cycle, the frequency and on the oxygen flow.

For all MS experiments it is necessary to reduce the pressure from 20 mTorr (nominal pressure of the plasma etch process) to 10 mTorr in order to ensure a low working pressure in the spectrometer. Nonetheless, the qualitative results are assumed to be similar to the conditions at 20 mTorr.

Figure 3.1 shows mass spectra from an HBr/O_2 plasma without bias. No signal is observed beyond 200 amu/e. The spectra are obtained by subtraction of a background spectrum, explained in Sec. 2.2. The peaks for HF, HCl and CO_2 do not originate from the plasma and hence, we consider them to be part of the background. The neutral species from the plasma that are observed are H_2, $OH_{0\text{-}2}$, O_2, Br, HBr and Br_2. As discussed in Sec. 2.2.4 the signal to background intensity for molecular beam mass spectrometry can be very low for light species. This was also verified experimentally for H_2O and O: in both cases the change in intensity between open and closed chopper was too small to acquire a reliable measurement. Therefore, only O_2, Br, HBr and Br_2 are studied in the following.

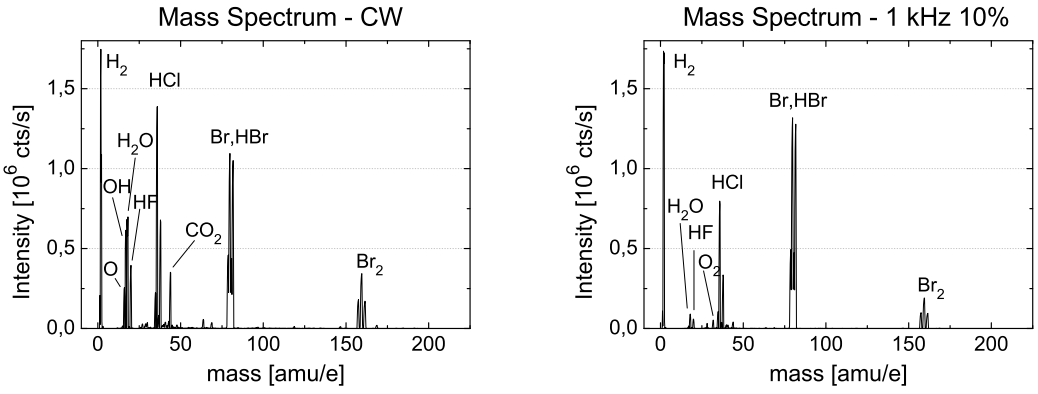

(a) **(b)**

Figure 3.1.: *Mass spectrum of HBr/O_2 (200 sccm/5 sccm, 10 mTorr, 750 W source power) with subtracted residual signal for* **(a)** *CW and* **(b)** *1 kHz, 10 % duty cycle.*

Table 3.1.: *Cross sections used for the calibration of absolute densities.*

Species	Electron Energy [eV]	Cross Section [Å^2]	Source
Br	13.2	0.11	Ali and Kim [143]
HBr	16.1	1.28	Ali and Kim [143]
Br_2	29.1	5.9	Ali and Kim [143]
$SiCl_4$	29.1	12.2	Kothari *et al.* [144]

By using reference gases with similar masses and assuming an exclusively mass dependent transmission function, we can estimate the absolute density in the reactor as described in Sec. 2.2. The O_2 and HBr neutral flux can be calibrated directly by using the same gases. The Br and Br_2 fluxes are calibrated by using HBr and $SiCl_4$ gas, respectively. For the two latter neutral species, it is necessary to know the ionization cross section from the species of interest and the reference gas. The used cross sections and electron energies for the calibration are shown in Tab. 3.1.

Impact of Pulsing

In the following, the densities of HBr, Br, Br_2, and O_2 are studied with respect to the applied duty cycles and frequencies in an HBr/O_2 plasma at 10 mTorr with a gas flow of 200 and 5 sccm, respectively. During the time of the measurements, an SiO_2 wafer was placed on the chuck for protection. Since the HBr/O_2 chemistry is known to leave SiO_2 rather unaffected for low ion energies [75, 76], we can assume that the results will reflect mainly the properties of the bulk plasma without etch products. In Fig. 3.2 the obtained density of HBr is shown.

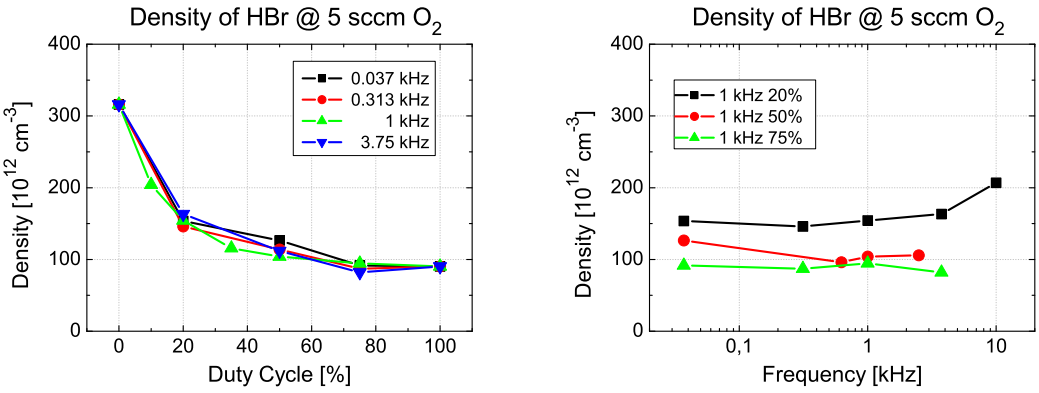

(a) (b)

Figure 3.2.: *Mass spectrometry measurement of HBr for* ***(a)*** *different frequencies and* ***(b)*** *different duty cycles in an HBr/O_2 plasma (200 sccm/5 sccm, 10 mTorr, 750 W source power).*

A duty cycle of 0 and 100 % represent the gas only (no plasma) and the CW plasma condition, respectively. With lower duty cycle, the amount of the HBr density rises by ∼100 % (from CW to 10% duty cycle). However, it increases only slightly until a duty cycle of approximately 35 % is reached; only at 20 and 10 % a significant increase is observed. The evolution with the duty cycles depends on several factors.

1. A decrease in the duty cycle leads to a reduced gas temperature compared to a CW process since the average source power is reduced. At a constant pressure, this results already in a higher gas density without considering any other changes in the plasma.
2. The reactor wall surfaces might be covered by different molecules, changing the sticking coefficients of the plasma species and leading to different recombination coefficients [63–70]. This affects the chemical composition of the plasma and in turn also the ion flux.
3. During the plasma off-time the dissociation becomes negligible compared to the on-time and recombination processes are dominant. From a time averaged view, this results in a reduced dissociation at lower duty cycles, which would increase the density of HBr.

In contrast to the duty cycle, the frequency has almost no influence on the density. The only exception to this rule can be found by going to very high frequencies at a duty cycle of 20 % and it is observed for all neutral species that we studied. The character of the change is similar to a decrease in duty cycle at a given frequency. This effect will be discussed in Sec. 5.4.

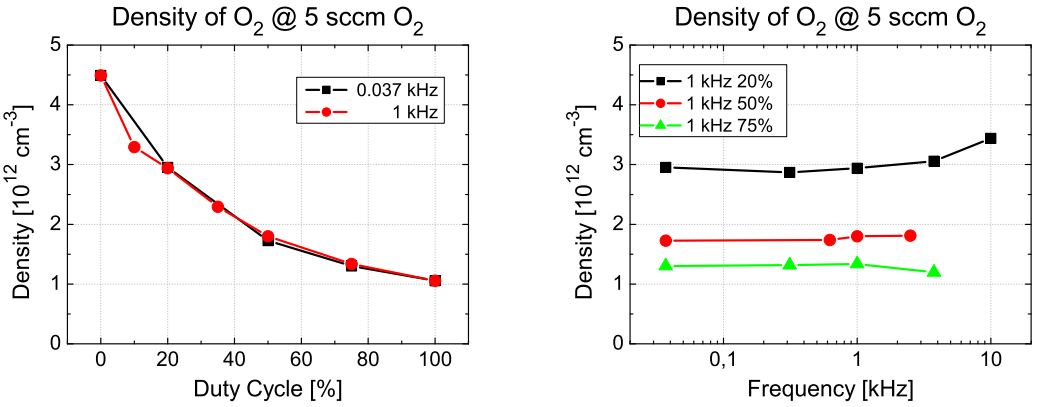

(a) **(b)**

Figure 3.3.: *Mass spectrometry measurement of O_2 for* ***(a)*** *different frequencies and* ***(b)*** *different duty cycles in an HBr/O_2 plasma (200 sccm/5 sccm, 10 mTorr, 750 W source power).*

Similar to the MS experiments close to the reactor wall, VUV absorption spectrometry (see Sec. 2.3) in the bulk plasma proves a similar dependence of the HBr density on the duty cycle.
The density of O_2, presented in Fig. 3.3, follows the same trend: it is independent of the frequency (with the same exception as for HBr) and at low duty cycle, the density is higher than under CW conditions. The only remarkable difference with respect to HBr is the continuous increase from CW to pulsing conditions. As explained above, the exact evolution with the duty cycle is linked to several factors at the same time, complicating the explanation of the small differences between O_2 and HBr.
Figure 3.4 shows the Br density with respect to the duty cycle. As opposed to HBr and O_2, the Br radical is produced by dissociation of a parent molecule in the bulk plasma and follows an different trend compared to HBr and O_2. With decreasing duty cycle, the amount of Br remains constant, only at a duty cycle of 10 % it starts to change significantly. In the absence of a plasma no Br is produced. Again, the density is independent of the frequency with the same exception as for the previous species.

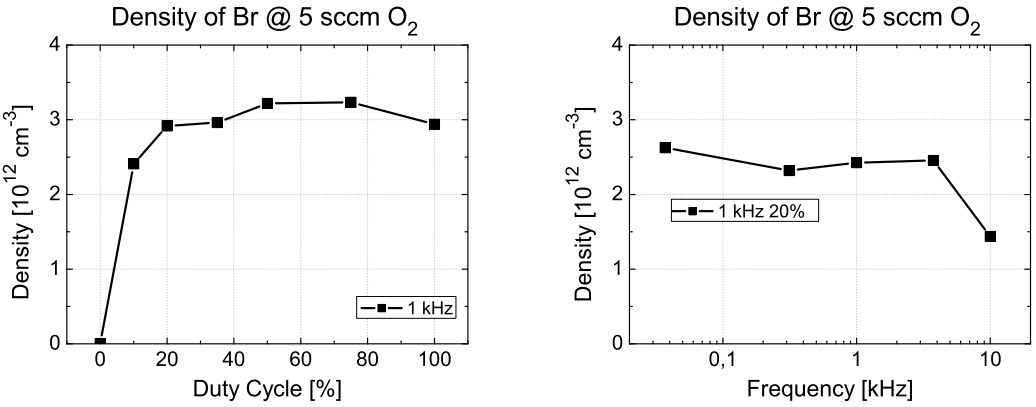

(a) (b)

Figure 3.4.: *Mass spectrometry measurement of Br for* **(a)** *different frequencies and* **(b)** *different duty cycles in an HBr/O_2 plasma (200 sccm/5 sccm, 10 mTorr, 750 W source power).*

The density measurements of Br_2, presented in Fig. 3.5, show very similar results, which is not surprising since the Br_2 molecules are produced by recombination of Br radicals. If the production of Br by dissociation of HBr is strongly reduced, significantly fewer radicals are available to form Br_2. One should also note that the Br density is ten times smaller than the Br_2 density, indicating an effective recombination of Br.

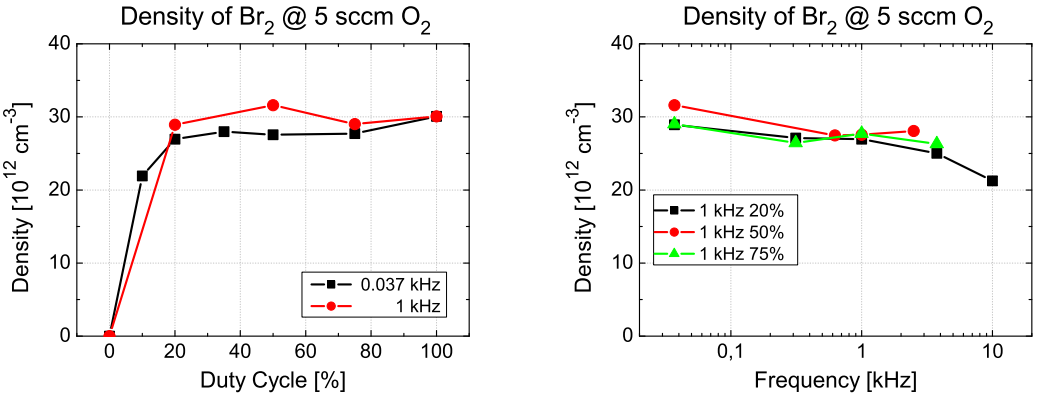

(a) (b)

Figure 3.5.: *Mass spectrometry measurement of Br_2 for* **(a)** *different frequencies and* **(b)** *different duty cycles in an HBr/O_2 plasma (200 sccm/5 sccm, 10 mTorr, 750 W source power).*

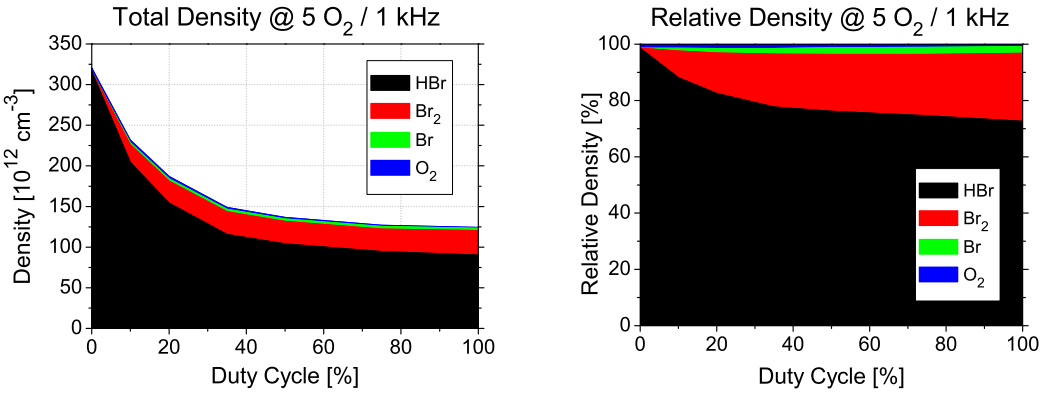

(a) **(b)**

Figure 3.6.: *Sum of all measured neutral species densities* ***(a)*** *in absolute (estimated) and* ***(b)*** *relative units.*

Figure 3.6 shows the combined estimated density of all measured neutral species in absolute and relative units. The neutral flux, from which the plasma density is estimated, is largely dominated by HBr. Only Br_2 also contributes significantly to the total flux. However, due to the very low signal to background ratio for species with low masses and the low transmission of very light species, H_x or OH_x could not be measured and are missing in this graph. It is possible that these species contribute also considerably to the total neutral flux.
With lower duty cycle, the total flux increases. One possible explanation is the reduced contribution of H and H_2 (not measured) at lower duty cycles due to a reduced dissociation of HBr. Also, the probable change in gas temperature certainly plays a major role in the evolution of the total density. Cunge *et al.* [145] measured the mean gas temperature via laser absorption in an HBr plasma for various powers and pressures and report the decrease of the plasma temperature due to a power reduction. A decrease in the duty cycle of a pulsed plasma reduces the averaged power and consequently also the temperature. For similar CW conditions but in a smaller reactor (10 mTorr, 750 W), the data from Cunge *et al.* suggest a mean gas temperature of approximately 750 K and a gas temperature close to the walls of 550 K. If we consider the temperature difference as the only reason for the change in neutral flux, we can calculate the corresponding gas temperature in CW mode based on the density change at a constant pressure. By taking into account only the measured species a temperature of 825 K can be estimated. Assuming that an equivalent amount of H and H_2 exists in the plasma compared to Br and Br_2, respectively, the resulting CW gas temperature can be calculated to 650 K, which seems more reasonable.
In summary, one of the main reasons for the increase of the total neutral flux (and density) with lower duty cycle is the change in temperature. However, realistic

temperatures are only estimated if we assume a significant amount of not measured neutrals like H and H_2.
The composition of the neutral flux indicates that with lower duty cycle HBr and O_2 become less dissociated and the relative amounts of Br and Br_2 decrease.

Impact of Oxygen Flux

All the results presented above were acquired in the same plasma chemistry, only the frequency and the duty cycle were varied. In Fig. 3.7 the dependence of the neutral flux density on the injected oxygen flux is presented. A difference in the chemical composition of the plasma is expected to change the plasma-wall interaction, leading to modified sticking coefficients of radicals on the chamber walls and, therefore, also to changed recombination rates.

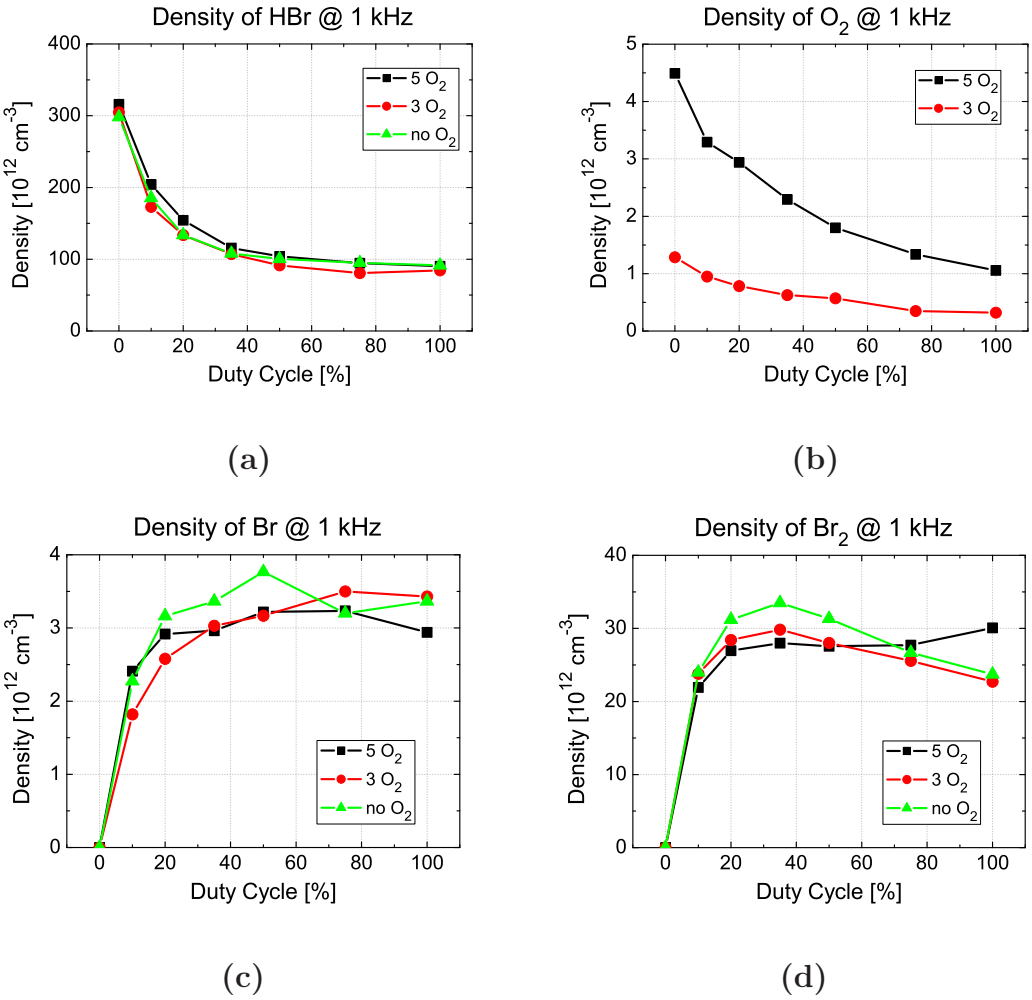

Figure 3.7.: *Dependence on the oxygen flow of the densities of* ***(a)*** *HBr,* ***(b)*** O_2, ***(c)*** *Br and* ***(d)*** Br_2.

While the measured oxygen density is overall strongly reduced, its **evolution** with the duty cycle does not change significantly. The HBr and Br densities on the other hand seem to be independent of the oxygen flux. The only species that might show a small change in the density evolution is Br_2. If only little or no O_2 is used, the Br_2 density increases at first by going to lower duty cycles. After a duty cycle of 35 % is reached, the density starts to decrease strongly. Cunge *et al.* [109] observed a similar behavior of HBr and Br_2 from absorption studies by decreasing the plasma source power from 1000 to 0 W. By reducing the duty cycle, the time averaged power input is likewise reduced. In both cases the averaged dissociation rate is reduced while the recombination rate is likely to remain unchanged. Since the densities of HBr, Br and Br_2 are governed by a complex balance of dissociation and recombination rates,

$$\mathrm{HBr} \rightleftharpoons \mathrm{Br} \rightleftharpoons \mathrm{Br_2}, \tag{3.1}$$

and the influence of the changed chemistry on the recombination rates at the reactor walls is difficult to estimate, an explanation of the observed change cannot be given.
However, the ratio of the densities of Br_2 and Br is approximately ten, regardless of the injected oxygen flux. Therefore, Br seems to be effectively recombined in all cases and the additional oxygen does not seem to influence significantly this process.

Discussion on the Oxygen Radical

Unfortunately, the signal of the oxygen radical was under our detection limit and we cannot assume that O behaves in the same way as Br. Depending on the nature of the reactor wall surfaces, the sticking coefficient and the recombination rate might be very different. For the case without applied bias power, we have observed an unchanged recombination of Br to Br_2, regardless of the amount of injected oxygen. This leads to the conclusion that in the present case the oxygen radical plays only a minor role. More interesting is the case of silicon etching **with applied bias power** in an HBr/O_2 chemistry, during which the reactor walls are covered by a layer of Si, H, Br and O, similar to the formation of a sidewall passivation layer in pattern etching [126]. It is known that oxygen radicals can further oxidize this layer to produce in the extreme case SiO_2 like layers. During this process, oxygen radicals are consumed, while Br and H radicals are reintroduced in the gas phase. Considering such a deposited layer on the surface, we can assume that a large portion of the oxygen radicals from the gas phase will be captured by the surfaces. In contrast, the Br radicals will still have a considerable density. Therefore, compared to Br, the oxygen radical density might be reduced faster with decreasing duty cycle.

Note on Hydrogen

Almost no information could be obtained on hydrogen species by mass spectrometry experiments. Nevertheless, with a decreased dissociation of HBr, e. g. at lower duty cycles, less hydrogen is certainly available to participate in chemical reactions or in the etching.

3.1.2. Summary of Results - Neutrals

Using mass spectrometry, an HBr/O_2 plasma without applied bias power was studied by carrying out density measurements for the neutrals HBr, Br, Br_2 and O_2. H_x, O and OH_x could not be measured. Among the measured species, HBr dominates by far and only Br_2 contributes also in a significant amount. With lower duty cycle, the total density increases, which is mainly attributed to the decrease in gas temperature in pulsed plasmas. A comparison with temperature measurements via laser absorption [145] indicates that other, not measured neutral species, e. g. H_2, also contribute in a significant amount to the total density.
Furthermore, the results show a decreased dissociation of the source molecules HBr and O_2 with lower duty cycle due to the lower time averaged plasma power and the reduced periods where dissociation occurs (on-time of each pulse). The Br density remains rather constant for high duty cycles and starts to drop at around 20 %. The density of the O radical, which was below our detection limit, might decrease faster with the duty cycle than the Br density; at least in real etch conditions. The Br_2 density evolves in a similar manner as Br, but is ten times higher regardless of the injected O_2 flux. This indicates that almost all Br is recombined and that the recombination is unaffected by the amount of available oxygen radicals in the range of the experimental conditions.
In contrast to the duty cycle, the frequency has little impact on the densities. Only at a low duty cycle (20 %) at a very high frequency ($\gtrsim 5\,\mathrm{kHz}$) an impact is observable, which is comparable in all cases to a further decrease in the duty cycle. This effect will be discussed in Sec. 5.4.
A reduced oxygen flux has not shown a significant influence on the density of HBr and Br, only Br_2 shows some minor differences, which remain difficult to explain.

3.2. Ions

3.2.1. Mass Spectrometry

Mass spectra of ions for an HBr and an HBr/O_2 CW plasma without bias are presented in Fig. 3.8. Both graphs show the same four peaks: H_3O^+, $H_{0-2}Br^+$, $H_{0-1}Br_2{}^+$ and Br_3^+. $H_x{}^+$ cannot be detected by the quadrupole analyzer and it is not excluded that a significant amount of protons is present.
The large amount of hydrogen rich species indicates that proton attachment plays a major role. Cunge *et al.* [63] observed a similar significance of proton attachment

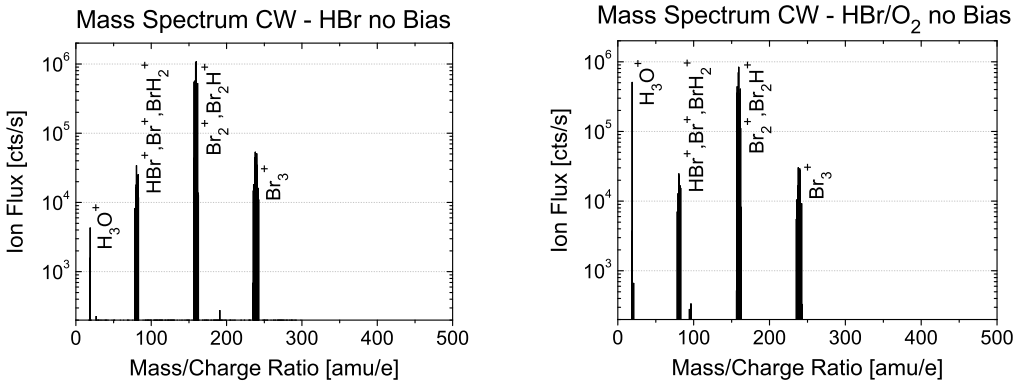

(a) (b)

Figure 3.8.: *Ion mass spectra in CW mode for an* ***(a)*** *HBr and* ***(b)*** *HBr/O_2 plasma (200 sccm/5 sccm, 10 mTorr, 750 W source power).*

in an HBr/Cl_2/O_2 with respect to the production of H_2Cl^+ ions. They expect the reaction to have a very large cross section due to the high polarizability of HCl molecules. Possibly, the cross section for proton attachment might likewise be very high for the case of HBr or H_2O.
The only major difference between both spectra seems to be the intensity of H_3O^+, which is two orders of magnitude higher if oxygen is added. The reason why H_3O^+ is detected even in the absence of oxygen in the plasma is probably linked to oxygen and H_2O residuals in the chamber and to the presence of the SiO_2 wafer.

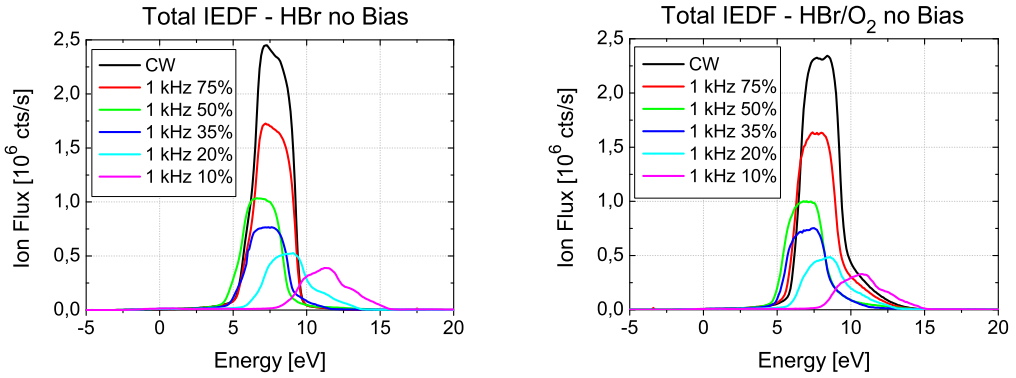

(a) (b)

Figure 3.9.: *Total IEDF for all measured ions in an* ***(a)*** *HBr and* ***(b)*** *HBr/O_2 plasma (200 sccm/5 sccm, 10 mTorr, 750 W source power).*

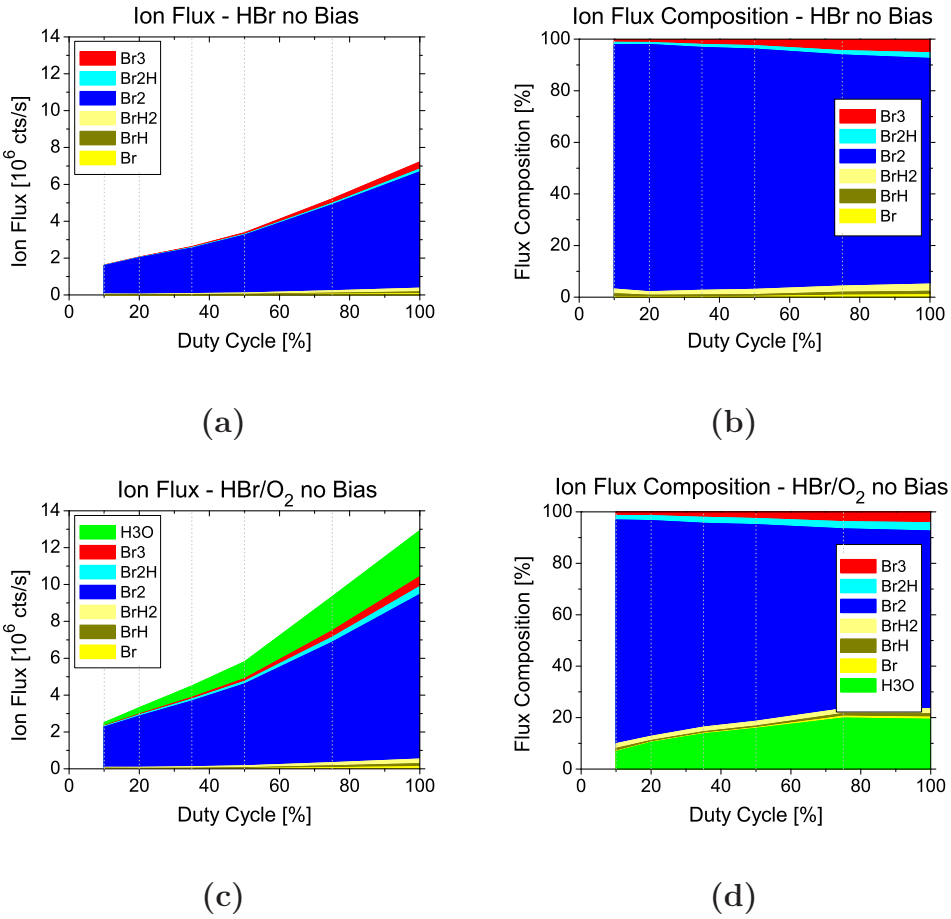

Figure 3.10.: *Total ion flux (**(a),(c)**) and ion flux composition (**(b),(d)**) for HBr and HBr/O_2, respectively (200 sccm/5 sccm, 10 mTorr, 750 W source power).*

In order to compare the ion fluxes for different process parameters, it is necessary to measure the IEDF from each species separately for each condition. From there, the total IEDF can be summed up, shown in Fig 3.9 with respect to the duty cycle. Both conditions show a very similar behavior. By reducing the duty cycle, the peak intensity decreases because ions are only produced during the decreasing on-time, while they are lost permanently, leading to a reduced time averaged ion density. As discussed in Sec. 2.2, the confidence in the energy value of the peak position is very limited and consequently, the shift in energy will not be discussed.
In Fig. 3.10 the ion flux for each species is shown in a stack diagram (left column) together with the corresponding flux composition in percent (right column) for a pure HBr and for the HBr/O_2 process. For both plasmas, the composition and its evolution are very similar. With almost the same absolute values, Br_2^+ is the main component in the ion flux in both cases, although HBr is by far the major neutral species. The only difference between both processes is the significant **additional** H_3O^+ ion flux in the HBr/O_2 case.

Table 3.2.: *Ionization E_I and bond energies E_B for various plasma species.*

Species	E_I [eV]	Source	E_B [eV]	Source
HBr	11.7	NIST [148]	3.7	Smolin *et al.* [149]
Br	11.8	NIST [148]	–	–
Br_2	10.5	NIST [148]	2.0	Ebbing and Gammon [150]
H_2	15.4	NIST [148]	4.5	Ebbing and Gammon [150]
H	13.6	NIST [148]	–	–
O_2	12.1	NIST [148]	5.1	Itikawa *et al.* [151]
O	13.6	NIST [148]	–	–
H_3O	4.3	NIST [148]*	0.2-0.3	Poterya *et al.* [152]

* for D_3O

In general, the charge from ionization will eventually be transferred to the species with the lowest ionization energies by direct ionization, charge transfer or other ion-neutral reactions [63, 81, 146]. Also, since the plasma electron energy distribution has its maximum at a rather low energy ($\sim$ 3-5 eV), more electrons are available to ionize a molecule with lower ionization threshold. The ionization and bond energies of the most important plasma species are listed in Tab. 3.2.
In the absence of oxygen, the species with the lowest ionization energy is Br_2. In addition, Br_2 has also a larger ionization cross section than HBr or Br [143]. Hence, it is understandable that most of the ion flux consist of $Br_2{}^+$.
If oxygen is added, we observe a significant contribution of H_3O^+ ions, although the oxygen inflow is very small compared to HBr and H_3O has a ten times smaller ionization cross section than Br_2 [147]. However, it has by far the lowest ionization energy, close to the maximum of the electron energy distribution function. Therefore, the large number of electrons that contribute to the ionization outweighs the small cross section. Hence, even a small amount of neutral H_xO could result in a significant H_3O^+ ion flux.
By reducing the duty cycle, the total ion flux decreases due to the lower ionization rate. At the same time, the fraction of $Br_2{}^+$ ions increases, while the percentage of all other ions in the flux composition decreases. This could be linked to the reduced dissociation of HBr, Br_2 and O_2, the augmented off-time during which only recombination dominates and the increased time to transfer the charges to the ion with lowest ionization energy. The reduction of the percentage of H_3O^+ is probably due to the reduced dissociation of O_2 and HBr.

Summary

Mass spectrometry measurements have been carried out to study the ion composition of the HBr/O_2 plasma and its dependence on the oxygen flow. The only ions that are detectable are H_3O^+, $BrH_{0\text{-}2}{}^+$, $Br_2H_{0,1}{}^+$ and $Br_3{}^+$. The major contribution originates from $Br_2{}^+$ and H_3O^+, although HBr represents by far the most

common neutral molecule in the plasma. The large amount of Br_2^+ can be attributed to its low ionization energy and high ionization cross section compared to other Br containing species. When oxygen is added, H_3O^+ contributes significantly to the ion flux, although its ionization cross section is very small. This fact is outweighed by the large number of electrons that have energies above the low ionization threshold energy.
By reducing the duty cycle, the total ion flux decreases and the percentage of Br_2^+ in the ion flux increases.

3.2.2. Ion Flux Probe

The ion flux is an important parameter in etch processes, which influences, e. g., the etch rate strongly. With mass spectrometry it is difficult to obtain the correct ion flux, as explained in Sec. 2.2. Instead, we use a capacitive ion flux probe, which is mounted to the reactor sidewall just above the wafer (see Sec. 2.4) at the same position as the mass spectrometer.

Influence of the Reactor Surface on the Ion Flux

Since the IFP is unaffected by a thin deposited layer on its surface, it is well suited to investigate the influence of different wall surfaces on the ion flux. During etch conditions, a layer consisting of Si, Br, O, and H is deposited on the reactor wall. Before each etch process the reactor is coated ("seasoned") with a layer of SiO_2, which is described in detail in Sec. 5.1. In order to investigate if the nature of the reactor walls affect the ion flux, the latter was measured for a CW HBr and HBr/O_2 plasma at 20 mTorr and 750 W source power in seasoned (SiO_2 layer) and clean conditions. The cleaning is done by an SF_6/O_2 plasma. Figure 3.11 shows the obtained ion fluxes in clean and seasoned chamber wall conditions.
The differences in the ion flux are significant between chamber conditions. Moreover, the behavior of both chemistries is opposite. While for clean conditions the ion flux in the HBr/O_2 plasma is larger than the one in the HBr plasma, the opposite is observable for seasoned conditions. The measurements for the ion flux in clean conditions is supported by the mass spectrometry measurements in Sec. 3.2.1. Since a change in the nature of the reactor walls can modify the plasma composition in terms of neutrals, it is not surprising that this will affect also the ion flux.

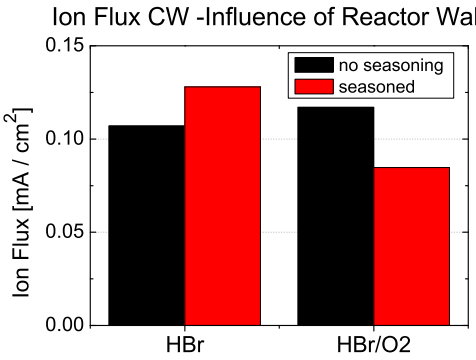

Figure 3.11.: *Influence of the nature of the reactor walls on the ion flux in an HBr and an HBr/O_2 CW plasma (200 sccm/5 sccm, 20 mTorr, 750 W source power). The seasoning consists of a thin layer of SiO_2 on the walls in contrast to a "clean" chamber in which deposited layers have been removed by an SF_6/O_2 plasma.*

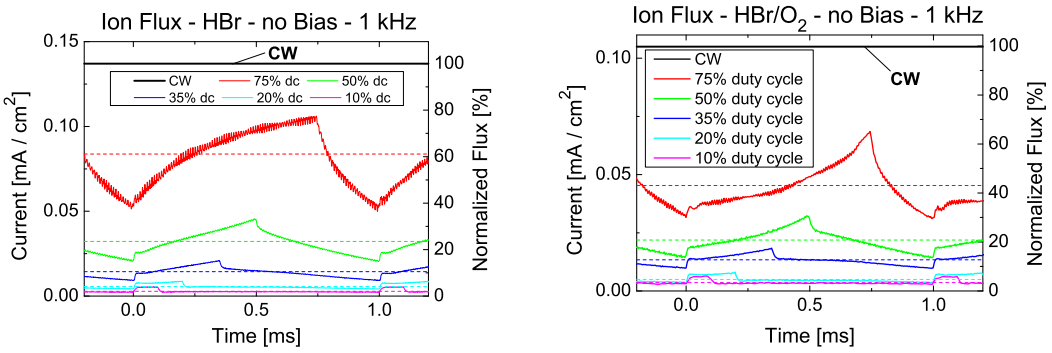

(a) **(b)**

Figure 3.12.: *Ion flux from capacitive probe (IFP) measurements in pulsed* ***(a)*** *HBr and* ***(b)*** *HBr/O_2 plasmas (200 sccm/5 sccm, 20 mTorr, 750 W source power) at a frequency of 1 kHz.*

Ion Flux in Pulsed Plasmas

In Fig. 3.12 the measured ion flux in an HBr and an HBr/O_2 plasma at 20 mTorr and 750 W source power is shown for different duty cycles at a frequency of 1 kHz. When the source power is switched on, the ion flux increases continuously until the power is switched off. Compared to the constant flux in a CW plasma, the ion flux in the HBr pulsed plasma never reaches a steady state. In the afterglow, the flux decreases at a rather slow rate, similar to the increase before. While the

Table 3.3.: *Measured (rounded) ion fluxes in HBr and HBr/O_2 plasmas (200 sccm/5 sccm, 20 mTorr, 750 W source power) at 1 kHz.*

HBr Duty Cycle	Mean Flux µA/cm^{-2}	Mean Flux % CW	Flux On-Time % Mean Flux	Flux On-Time % Mean CW Flux
100	137	100	100	100
75	84	61	79	48
50	32	24	54	13
35	14	10	41	4.2
20	6	4.1	28	1.1
10	3	2.0	18	0.4

HBr/O_2 Duty Cycle	Mean Flux µA/cm^{-2}	Mean Flux % CW	Flux On-Time % Mean Flux	Flux On-Time % Mean CW Flux
100	107	100	100	100
75	45	42	76	32
50	22	20	54	11
35	13	13	40	5.0
20	5	4.6	29	1.3
10	4	3.3	16	0.5

decrease of the ion flux is very similar for both plasmas, the evolution during the on-time is quite different. In the pure HBr plasma the ion flux rises strongly at first and then slows down. In contrast, the ion flux in the HBr/O_2 plasma starts out with a slow increase that accelerates later during the on-time of the pulse. The differences might be due to the additional H_3O^+ in the ion composition of the HBr/O_2 plasma.

Both plasmas show an almost instantaneous jump of the ion flux when the power is switched on or off. This behavior is not fully understood. However, a possible explanation might be linked to a fast change of the electron temperature at the beginning and the end of each pulse since the positive ion flux in an electronegative plasma is essentially described by $n_i \cdot v_B = n_i \cdot \sqrt{k_B T_e (1+\alpha_s)/m_i (1+\alpha_s \eta}$, where $\alpha_s = n_{i,-}/n_e$ is the ratio of negative ions to electrons and $\eta = T_e/T_{i,-}$ is the ratio of negative ion temperature to electron temperature [55]. The slow evolution during the on-time is attributed to a change in ion density.

Another explication for the observed jumps might be the photoeffect. During the on-time, UV photons can remove electrons from the surface, which are measured like incoming ions. However, this effect is thought to be of minor importance.

The mean values for the ion fluxes are given in Tab. 3.3. They follow similar trends in both plasma conditions:

1. The mean flux decreases more than proportional with the duty cycle.

2. The percentage of the flux from only the on-time of the plasma (high energy ions) decreases also, almost proportional with the duty cycle.

The second point is very important since it means that in a pulsed HBr/O_2 plasma, the relative amount of high energy ions can be drastically reduced compared to the ion flux with very low energy. This might be a way to reduce surface damage from energetic ions (see Chap. 1).
By combining both observations, we can also state that in pulsed conditions, the ion flux from only the on-time of the plasma decreases by more than the square of the duty cycle compared to CW mode. This can be understood considering a simple model in which the ion flux evolves linearly during the pulse period. In this case, the mean ion flux from the on-time is the same as from the off-time. Hence, the relative amount of the ion flux from the on-time with respect to the total flux is equal to the duty cycle. Since the time of production (on-time) is reduced (= duty cycle), the average ion flux is also reduced (almost) linearly, leading to the observed roughly quadratic dependence on the duty cycle.

Summary

Depending on the nature of the reactor wall and the gas composition of the plasma, the ion flux varies strongly. This is certainly liked to the changed reaction coefficients on the chamber walls that affect significantly the plasma composition.
The evolution of the ion flux during one pulse depends also on the plasma chemistry: while it rises strongly at first and then slows down in a pure HBr plasma, the opposite is observed for the HBr/O_2 plasma. The jump at the beginning and the end of each pulse is attributed to the fast change of the electron temperature. By reducing the duty cycle, the average ion flux and the percentage of the ion flux that originates from the on-time of the plasma decrease approximately linearly. Hence, the average ion flux from only the on-time of the plasma decreases by roughly the square of the duty cycle.
The reduction of the relative contribution of high energy ions to the total flux might be useful to reduce damages from energetic ions.

3.2.3. Summary of Results - Ions

Mass spectrometry measurements have been carried out to study the ion flux composition of the HBr/O_2 plasma and its dependence on the oxygen flow. The only ions that are detectable are H_3O^+, $BrH_{0\text{-}2}{}^+$, $Br_2H_{0,1}{}^+$ and $Br_3{}^+$, among which $Br_2{}^+$ and H_3O^+ are dominating, although HBr represents by far the most common neutral molecule in the plasma. The large amount of $Br_2{}^+$ can be attributed to its low ionization energy and high ionization cross section compared to other Br containing species. When oxygen is added, H_3O^+ contributes significantly to the ion flux, although its ionization cross section is very small. This fact is outweighed by the large number of electrons that have energies above the low

ionization threshold energy.
A decrease of the duty cycle leads to an increased percentage of Br_2^+ in the ion flux and to a drop of the average total ion flux. Moreover, the average ion flux from only the **on-time** of the plasma decreases even by roughly the square of the duty cycle, indicating that the amount of energetic ions per on-time of the plasma can be decreased in pulsed plasmas. This offers a way to reduce plasma induced damage due to high energy ions.
Finally, the nature of the reactor wall does not only have an influence on the composition of the neutral species in the plasma, but also on the ion flux and its evolution during a pulse.

3.3. General Summary

Mass spectrometry and ion flux measurements were carried out to study an HBr/O_2 plasma without applied bias.
The neutral densities of HBr, Br, Br_2 and O_2 were measured. H_2 also seems to be largely present, but the signal to background ratio was too small for a valid measurement, similar as for OH_x species. HBr dominates all other species, only Br_2 contributes also in a significant amount to the neutral plasma composition. With lower duty cycle, the total density increases, which is mainly attributed to the decrease in gas temperature in pulsed plasmas, but also other, not measured species might play a role. In general, the degree of dissociation of the source molecules HBr and O_2 decreases due to the lower time-averaged plasma power and the reduced time for dissociation during a pulse. While the Br density remains nevertheless rather constant for high duty cycles ($\gtrsim 20\,\%$) the density of the O radical, which was below our detection limit, might decrease faster, at least in real etch conditions. The Br_2 density evolves in a similar manner as Br. In contrast to the duty cycle, the frequency has little impact on the neutral densities.
The only detectable ions are H_3O^+, $BrH_{0\text{-}2}{}^+$, $Br_2H_{0,1}{}^+$ and $Br_3{}^+$. Although HBr represents by far the most common neutral molecule in the plasma, $Br_2{}^+$ and H_3O^+ dominate the ion flux, probably due to their low ionization energy and to the high ionization cross section of $Br_2{}^+$.
The percentage of $Br_2{}^+$ in the ion flux increases with lower duty cycle while the average total flux decreases. The average ion flux from only the **on-time** of the plasma decreases even by roughly the square of the duty cycle. Since the amount of energetic ions per on-time can thereby be decreased, plasma pulsing offers a possibility to reduce plasma induced damage.
Finally, the nature of the reactor wall does not only have an influence on the composition of the neutral species in the plasma, but also on the ion flux and its evolution during a pulse.

4. HBr/O_2 Plasma With Bias - Silicon Etching

In the previous chapter, the plasma pulsing was investigated without applied bias power. If the bias power is applied, the HBr/O_2 plasma changes significantly: the silicon species that are etched during the process become part of the gas phase and contribute considerably to the composition of neutrals and ions in the plasma. At the same time, the reactor walls are coated by a layer of previously etched and re-deposited material that can also change the plasma composition. In the following chapter this case is studied by various means of diagnostic for the gas phase and the etched surface.
Unfortunately, the experimental time for diagnostics is more limited compared to the plasma without bias due to the following:

1. On a blanket wafer, the etch process starts to form micro-masking after a certain amount of time, which absorbs effectively visible light ("black silicon"). In the extreme case, the wafer cannot be detected by the light sensors of the mainframe and the latter has to be opened to remove the wafer.
2. The micro-masking also partly protects the silicon from etching, reducing the amount of etched silicon in the plasma and changing thereby the plasma composition.
3. After one wafer is used to the maximum, a time intensive cleaning and seasoning process has to be carried out in order to prepare the next experiment.

4.1. Neutrals

4.1.1. Mass Spectrometry

Since the experimental time is limited, only qualitative studies were carried out concerning the neutral composition, opposed to the ion analysis that can be carried out faster.
For a qualitative study, mass spectra from the CW and a pulsed condition (1 kHz, 10 % duty cycle) are acquired, starting at 4 amu (since we cannot measure hydrogen species accurately). Again, a background spectrum needs to be acquired in order to remove the signals from residual species since the chopper is not used. By adjusting the residual spectrum by a constant factor (0.2 and 0.66 for CW and pulsing, respectively) the contribution from the background is mostly subtracted. The resulting spectra are shown in Fig. 4.1.

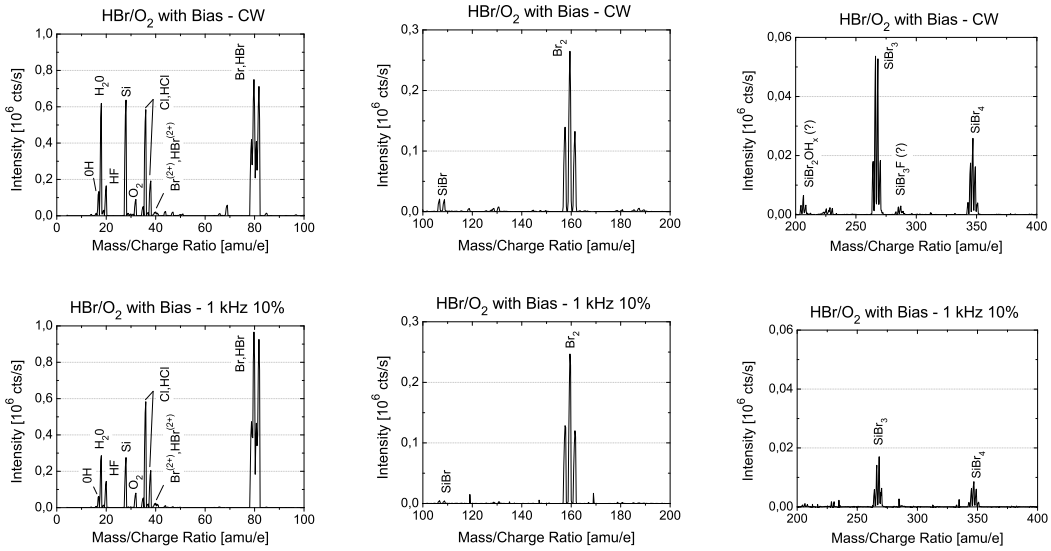

Figure 4.1.: *Mass Spectra from CW and pulsed (1 kHz, 10 % duty cycle) silicon etching (200 sccm/5 sccm, 10 mTorr, 750 W source power, 200 W bias power). Background is subtracted.*

In addition to the peaks observed in the case without bias (Br, HBr, Br_2, O, O_2), several species are detected that correspond to etch products (Si, $SiBr_x$). We also notice peaks in the background that correspond to a contamination of (H)F at 20 amu and (H)Cl at 35-38 amu.
Adequate reference gases are not available to calibrate the MS signals for all species. Therefore, we can only compare the signal of one species that cannot be produced by dissociative ionization between different process conditions (see Sec. 2.2). The intensity change of the different species are presented in Fig. 4.2, normalized to the highest peak (HBr in the pulsed plasma).
Following the considerations above, the only species that we use for comparison are H_2O, O_2, HBr, Br_2 and $SiBr_4$. For the pulsed process, the amount of HBr is increased, while the peak intensities of H_2O, Br_2 and $SiBr_4$ are decreased. This can be explained by the decreased dissociation of the parent molecules HBr and O_2 in the pulsed plasma and by a decreased plasma temperature (see Sec. 3.1.1). Another reason is the reduced time-averaged Si etch rate. In an HBr/O_2 plasma almost no spontaneous etching of silicon occurs so that the lower averaged ion flux induces also a lower etch rate. In turn, this leads probably to a reduced overall presence of Si species (like $SiBr_4$) in the plasma.

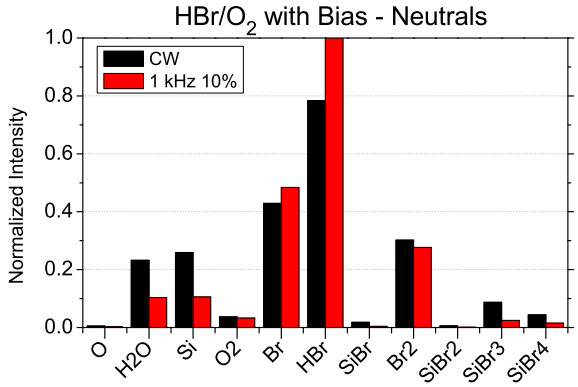

Figure 4.2.: *Silicon etching with applied bias: CW vs. pulsed mode (1 kHz, 10 % duty cycle).*

Summary

In comparison to the case without bias power the spectrum of detected species is enlarged by etch by-products like atomic Si or molecular $SiBr_x$ that contribute considerably to the composition of neutral species in the plasma. The differences in the mass spectra of CW and pulsed etching can be explained by the reduced dissociation and etch rate in a pulsed plasma.

4.1.2. UV Absorption of SiBr

In contrast to the other neutral etch products detected by MS, SiBr has a well known and good absorbance in the UV region. At the same time, its density is possibly the lowest. The time-resolved and time-averaged evolution of the absorption of SiBr during pulsing at different frequencies is shown in Fig. 4.3.
The absorption is proportional to the density, but due to the lack of the adequate cross section, we can only speak of relative density. For low frequencies the density varies strongly between the plasma on-time and off-time. For higher frequencies the modulation becomes less distinct since the pulse frequencies probably approach the characteristic time constants for loss and formation of SiBr. Above around 1 kHz the variation is small enough to use the time-averaged values for comparison between different plasma processes. As seen in Fig. 4.3 b, the absorption of SiBr is constant with changing frequencies in the margin of error. By decreasing the duty cycle we can observe a decrease in the absorption starting at around 50 %, which is probably linked to the reduced average etch rate and the greater availability of Br to form more volatile molecules.

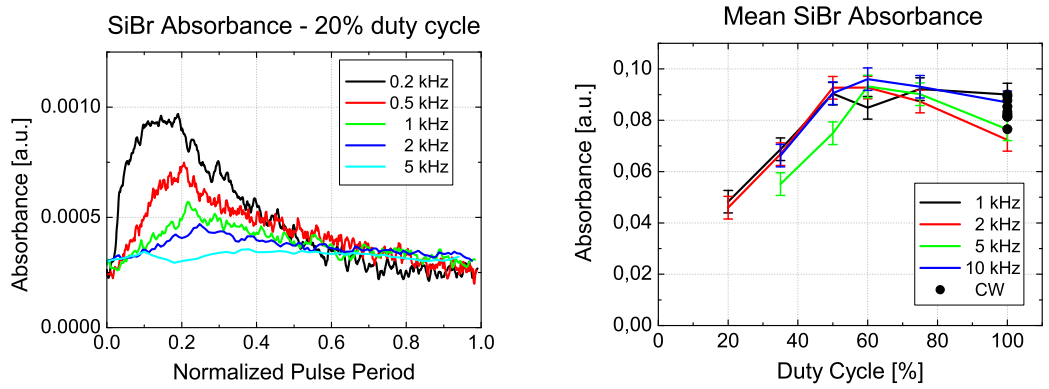

(a) (b)

Figure 4.3.: ***(a)*** *Time-resolved SiBr absorption measurements for different frequencies at a duty cycle of 20% and* ***(b)*** *time-averaged absorption for different duty cycles at various frequencies above 1 kHz (HBr/O_2, 200 sccm/5 sccm, 20 mTorr, 750 W source power, 200 W bias power).*

4.1.3. Summary - Neutrals

Mass spectrometry experiments were carried out to study the neutral composition of an etch plasma with applied bias power. In contrast to the case without bias power, etch products like atomic silicon or molecular $SiBr_x$ contribute considerably to the composition of neutral species in the plasma. For a reduced duty cycle, more HBr is found, but less other molecules, which can be explained by a reduced degree of dissociation and a reduced time-averaged etch rate. SiBr, one of the detected etch products, was additionally studied by UV absorption in the bulk plasma. For frequencies above approximately 1 kHz the modulation in the density during a pulse becomes small enough to compare time-averaged values. While the averaged SiBr density is independent of the frequency, it is reduced with a decreasing duty cycle, starting at around 35 to 50 %.

4.2. Ions

4.2.1. Mass Spectrometry

Compared to the case without bias power, additional silicon containing ion species are detected in the real etch conditions. A mass spectra of the ion composition is presented in Fig. 4.4.
A great variety of atomic and molecular ions is detected, many of whom are very large, e. g., $Si_2Br_5O^+$. Compared to the ion spectrum without bias power no Br_3^+ is detected any more. Unfortunately, the mass scan is limited to 500 amu/e and

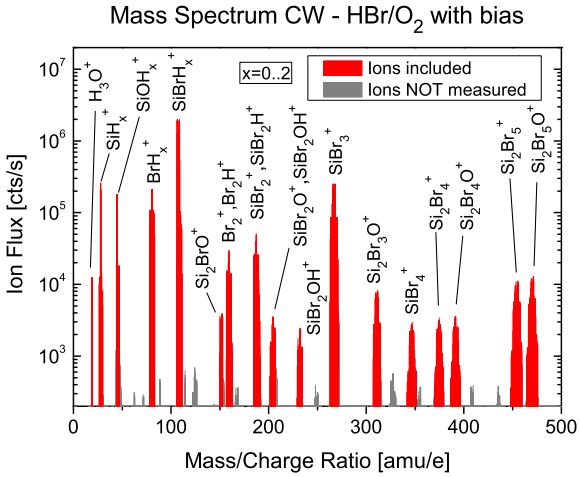

Figure 4.4.: *Ion mass spectra in CW mode for an HBr/O_2 plasma (200 sccm/5 sccm, 10 mTorr, 750 W source power, 200 W bias power).*

we cannot exclude the existence of even heavier ions. Also, as for the case without bias, protons might be present in a significant number but cannot be detected by the spectrometer. Since the IEDF from each species has to be acquired in order to gain information on the ion flux and since the experimental time is limited, only the strongest peaks in the spectrum are studied, here indicated in red. The other peaks (grey) are neglected.
A drawback in the experiments was a distortion of the spectrometer signal by the applied bias power near a duty cycle of 50 % (at 1 kHz). The farther away the pulse parameters are set from this duty cycle, the smaller the distortion gets. However, even at a duty cycle of 75 % we cannot exclude a small influence. Thus, the interpretation of the measurement at 1 kHz 75 % should be handled with caution.
In Fig. 4.5 the ion flux for each species is shown in a stack diagram (left column) together with the corresponding flux composition in percent (right column).
Compared to the plasma without bias, the ion flux is now dominated by etch products, especially SiBr, and the contribution of Br_2 is reduced to an almost negligible value. The largest contribution to the total flux from species without incorporated Si comes from BrH_{0-2}. In contrast to the clean reactor walls during unbiased conditions the reactor is now coated with a mixed layer of Si, Br, O and H that might change the recombination rate considerably for various species like Br and Br_2, as explained in Sec. 3.2.2, leading to the observed significant contribution to the ion flux. Moreover, large silicon containing etch products that leave the wafer can easily be ionized and dissociated due to the low energy thresholds for these processes, contributing also to the observed presence of Si containing species. For lower duty cycles, the total ion flux decreases and the relative composition changes. The decrease of the total ion flux is linked to the increased off-time

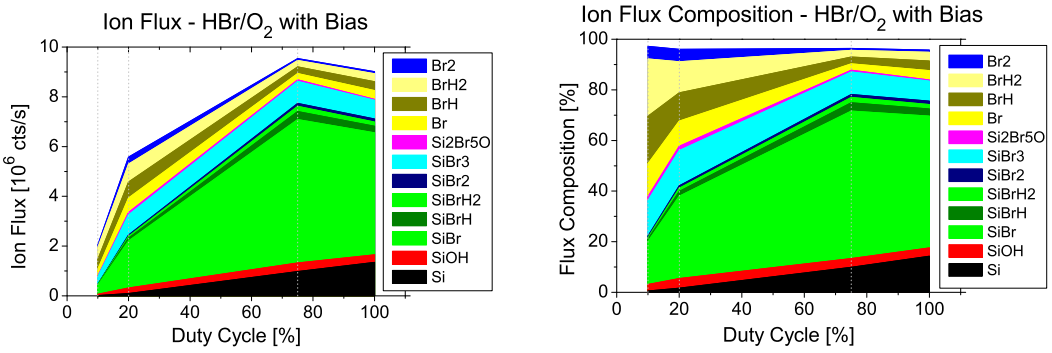

(a) **(b)**

Figure 4.5.: ***(a)*** *Total ion flux and* ***(b)*** *relative ion flux composition for HBr/O_2 (200 sccm/5 sccm, 10 mTorr, 750 W source power, 200 W bias power).*

(only ion loss) and the decreased on-time (production of ions) of the plasma. The percentage of all ionized etch products decrease with a lower duty cycle, while the relative BrH_x and Br_2 signals increase. The overall reduction of Si species in the plasma is probably linked to the lower averaged etch rate. Especially the contribution of atomic Si is reduced to a very small percentage at low duty cycles, indicating that most of the etched silicon is incorporated in larger and more volatile molecules.

Summary

Compared to a plasma without bias, the composition of the ion flux in the etch conditions shows many additional ions that include at least one Si atom. Br_3^+, on the other hand, is not detected any more and the percentage of Br_2^+ is almost negligible. The main contribution of the total ion flux comes from Si^+, $SiBr^+$, $SiBr_3^+$ and BrH_{0-2}^+. Large silicon containing etch products that leave the wafer can easily be ionized and dissociated due to the low energy thresholds for these processes, leading to the observed significant contribution to the ion flux. In addition, the nature of the reactor walls change compared to no-bias conditions, influencing the recombination rates and, hence, also the reaction balance between all species.
A decrease in the duty cycle leads to a drop of the total ion flux, which is in good agreement with the ion flux probe measurements in Sec. 3.2.2. At the same time the percentage of BrH_{0-2}^+ increases. One should also note that almost no Si^+ can be detected at a very low duty cycle. This might indicate that almost all silicon is incorporated in larger, more volatile molecules probably due to a better chemical reactivity of pulsed discharges. Finally, the lower etch rate of the Si wafer reduces the overall silicon presence in the plasma.

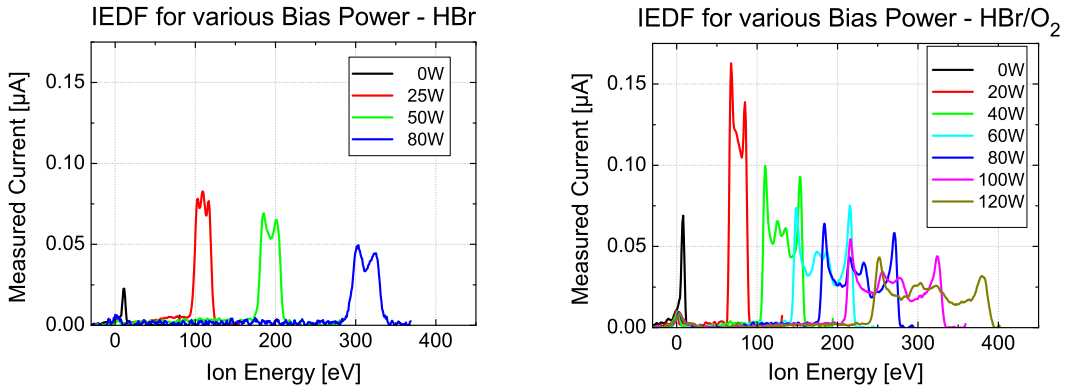

(a) **(b)**

Figure 4.6.: *IEDFs from CW mode of* ***(a)*** *an HBr and* ***(b)*** *an HBr/O_2 plasma (200 sccm/5 sccm, 20 mTorr, 750 W source power, 200 W bias power).*

4.2.2. Ion Energy and Flux Probes

The mass spectrometry results indicate a large difference in the composition of the ion flux due to the additional etch products if the bias power is applied. The retarding field analyzer and the capacitively coupled ion flux probe can give accurate information on the IEDF/ion flux on the wafer and on the sidewall close to the wafer.

CW Plasma

In Fig. 4.6 the IEDFs for an HBr/O_2 and HBr plasma are shown at different bias power in CW mode. When no bias is applied, the IEDF consists of a single peak at rather low energy (plasma potential minus floating potential). In biased conditions the distribution changes to a bimodal (HBr) or double-bimodal (HBr/O_2) function that originates from the oscillating RF sheath above the electrode [153, 154]. For the HBr/O_2 plasma, two bimodal functions overlap each other. Each one can be attributed to a major ion with a different mass, where the heavier species is also observed in the plasma without oxygen. Several authors have investigated the dependence of the width ΔE of the bimodal IEDF [155–157] and find an analytical expression that is in good agreement with experimental results:

$$\Delta E = \frac{8e\tilde{V}_s}{3\bar{s}\omega}\left(\frac{2e\bar{V}_s}{m}\right)^{1/2}, \tag{4.1}$$

where $V_s(t) = \bar{V}_s + \tilde{V}_s \sin(\omega t)$ is the (assumed) sinusoidal sheath voltage, $\bar{s}$ the (assumed) constant sheath width and m the ion mass. Although this equation is based on several approximations, it is found to be accurate enough to roughly

mass resolve the IEDF [158–160].

Discussion on Major Ion Species

In a simple approximation, it is possible to estimate the absolute masses of both major ions. Following Eq. 4.1, we assume a sheath width of 1 cm (high RF bias power) and a mean sheath voltage $\bar{V}_s$ equivalent to the mean ion energy. At one point during the RF period the sheath voltage breaks almost down, so that the electrons can reach the electrode and neutralize the accumulated ion flux. Hence, we approximate the amplitude of the RF sheath voltage by the magnitude of the mean sheath voltage ($\tilde{V}_s \approx \bar{V}_s$). The calculated masses are approximately 3 and 80 amu. Since the error in this approximation is quite large, the result needs to be treated with caution.
A more reliable information is the mass ratio, which can be calculated without usage of the unknown plasma parameters. From the different widths of the presented double-bimodal distribution, an average mass ratio of 27 can be calculated for the two ion species.
Mass spectrometry measurements from Sec. 3.2.1 indicate a large variety of ion species, dominated by $SiBrH_{0-2}{}^+$. The lightest measured ion is H_3O^+, but possibly H^+ also might be present, which could not be detected. Four arguments support the assumption that the additional peak in the HBr/O_2 plasma could be attributed to H^+.

1. The calculated mass that corresponds to the broad peak is below 6 amu, even if the parameters of the calculations are extensively changed. No ions with masses smaller than 16 amu were detected and hence we have to assume that undetectable protons are the origin of the additional bimodal distribution function.
2. The mass spectrometry measurement shows only a very insignificant contribution of H_3O^+ to the total ion flux.
3. If H_3O^+ actually **was** the light ion species, the bimodal peak of the heavy species would correspond to a mass of $\sim$ 500 amu, assuming the calculated mass ratio is correct. In the case without oxygen, no contribution of ions with a lower mass are observed in the IEDF. This scenario seems improbable since we also expect lighter silicon species to contribute to the ion flux in an HBr etch plasma.
4. Finally, if H^+ is considered to be the dominating light ion species, the second major ion peak can be attributed to $SiH_x{}^+$. This is strongly supported by the mass spectrometry data, showing that Si^+ is the lightest detected ion with a significant contribution.

Summarized, we assume that by adding oxygen to the HBr etch plasma, a large part of the ion flux onto the wafer originates from protons, which cannot be detected by the mass spectrometer.
This implicates that in an HBr/O_2 plasma one of the major ions that contributes

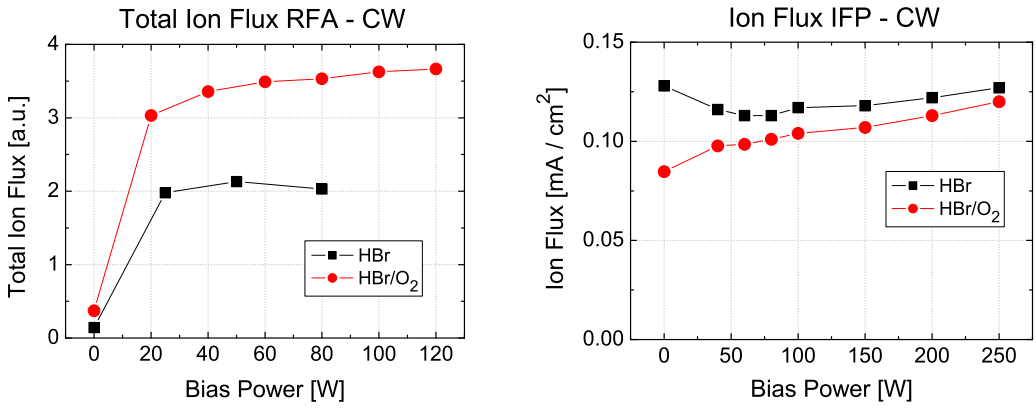

(a) (b)

Figure 4.7.: *Total ion flux for different bias powers in CW mode at 20 mTorr and 750 W source power (HBr flow at 200 sccm, O_2 flow at 5 sccm).* ***(a)*** *RFA and* ***(b)*** *IFP data.*

to the silicon etching is H^+. By reducing the duty cycle, less HBr is dissociated and the contribution from the protons might be reduced. Since hydrogen might penetrate deeply into the surface due to its low mass, a reduction of the duty cycle might help to decrease the plasma induced damage on surfaces.
In the above discussion, we assumed an equal magnitude and composition of the ion flux on the wafer and the chamber wall. However, the conditions on the wafer (high voltage sheath, highly energetic ions and secondary electrons) are quite different compared to the reactor wall (low voltage sheath), which could give rise to a modified ion flux. Consequently, other light species, e. g. $H_2{}^+$, might cause the broad bimodal distribution if they contribute **only** to the ion flux on the wafer. Still, the last of the arguments that supports the H^+ hypothesis still holds and we will assume this case in the following.

Discussion on Ion Flux and Energy

Figure 4.7 shows the total ion flux with respect to the bias power for the HBr and HBr/O_2 plasma, obtained from the IEDFs from Fig. 4.6 and from IFP measurements. For all data points from the RFA the ion flux of the pure HBr plasma is lower than the flux in the HBr/O_2 plasma. The opposite is the case for the IFP measurements where the HBr/O_2 plasma produces a lower flux. The differences are probably linked to the different positions of the probes: while the IFP probe is situated in plane with the reactor sidewall, the RFA probe lies on a dummy silicon wafer. Moreover, the RFA data indicates that H^+ contributes significantly to the total ion flux in the HBr/O_2 plasma, but not in a pure HBr plasma. The difference in the ion fluxes could be explained if we assumed a local production of protons

close to the wafer in the oxygen containing plasma. In this case, the ion flux in the HBr/O_2 plasma would be increased by the additional protons above the wafer, but not close to the chamber wall. A possible mechanism might be proton detachment due to high energy secondary electrons that are produced by ion bombardment on the wafer and in turn accelerated by the strong sheath potential drop. In order to explain the absence of H^+ in a pure HBr plasma, we have to assume that certain species in the HBr/O_2 plasma that do not exist in the pure HBr plasma, e. g. H_xO, are susceptible to this kind of proton production.
Another possibility to explain the observations might be linked to the changed reactor wall conditions. During silicon etching in an HBr/O_2 plasma, an oxygen rich Si-Br layer is formed on the chamber walls, which might prevent H radicals to recombine. The increased amount of H radicals might be ionized locally above the wafer. However, atomic hydrogen has a very high ionization energy and a very low electron impact ionization cross section and therefore, this hypothesis seems to be improbable. Since the only evidence of the H^+ presence comes from the RFA measurement in the HBr/O_2 CW plasma, this observation should be validated by other experiments.
The evolution of the ion flux from the IFP data shows differences depending on the used plasma chemistry. From theoretical considerations, the ion flux should not change much with different bias conditions since the plasma density is expected to be controlled mainly by the ICP source power, which remains constant. Only for the case without bias, where the silicon is not etched and the plasma composition changes significantly due to the absence of etch products, a slight difference would be expected.
For the HBr case, the ion flux decreases slightly with higher bias power at first and starts to increase gradually afterwards. In the HBr/O_2 case, the flux is constantly increasing. For higher bias powers, both fluxes approach each other. The differences between both chemistries are attributed to the different composition of the plasma, as explained above.
The ion flux from the RFA data is very low without applied bias, increases drastically when it is switched on, and increases only slightly thereafter. The abnormal value of the ion flux at 0 W bias power is not expected in an ICP and might be linked to the ceramic shield that prevents the metallic body from being sputtered. Since it is dielectric, it might be charged differently compared to the wafer and the RFA body itself. For low ion energies, this difference might be sufficient to deflect ions and to reduce thereby the number of ions that reach the detector. Another possible reason might be linked to the very thin plasma sheath in the case without bias. If the sheath is thin enough, the plasma might be able to extend to some degree into the holes of the dielectric shield [161]. Since the ion trajectory runs perpendicular to the sheath, the distortion in the proximity of the holes could make some ions hit the ceramic hole sidewalls instead of entering into the RFA. Hence, the ion flux at 0 W bias might be underestimated for the RFA measurements.
Comparing the RFA data for both plasma conditions, two features can be ob-

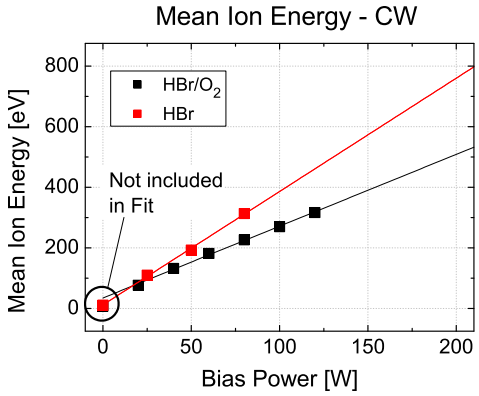

Figure 4.8.: *RFA measurements of the mean ion energy in CW mode at 20 mTorr and 750 W source power (HBr flow at 200 sccm, O_2 flow at 5 sccm).*

served: the total ion flux is increased when oxygen is added and at the same time, the mean ion energy is decreased. Both parameters are correlated via the bias power. In a rough approximation, the bias power is proportional to the product of the ion flux Γ_i and the sheath voltage $\bar{V}_s$ ($\approx$ ion energy E_i) [55] if collisional losses (e. g. ionization) are neglected. In other words, the applied bias power is mainly consumed by accelerating the ions. In this case, the product of the ion flux and ion energy is proportional to the bias power (see Eq. 1.4). If the ion density and, consequently, also the ion flux increase, the mean ion energy decreases for a constant bias power. In the case of added oxygen, the total ion flux is increased, considering the RFA measurements. Therefore, the mean ion energy of the IEDF decreases. In both plasmas the ion flux is almost constant with changing bias power. Hence, an increase in bias power leads to the linear increase in mean ion energy, as observed in Fig. 4.8.
Since the voltages applied to the RFA are limited to a maximum of 400 V, the IEDF for the process plasma with 200 W bias power could not be measured. However, based on the linear approximation of the ion energy we can estimate for this case a mean energy of approximately 500 and 750 eV for the HBr/O_2 and the HBr plasma, respectively.

Pulsed Plasma

As we have seen in Sec. 3.2.2 for the case without bias, the ion flux decreases with lower duty cycle since the average ion production rate in the plasma is reduced. This evolution is unchanged if bias power is applied. During the on-time of the plasma, the instantaneous bias power is the same as for CW, only the ion flux will be significantly lower, leading to a very much increased ion energy compared to CW mode (considering Eq. 1.4). Figure 4.9 a shows the time-averaged IEDF for a pulsed HBr plasma at different duty cycles, as well as the corresponding ion

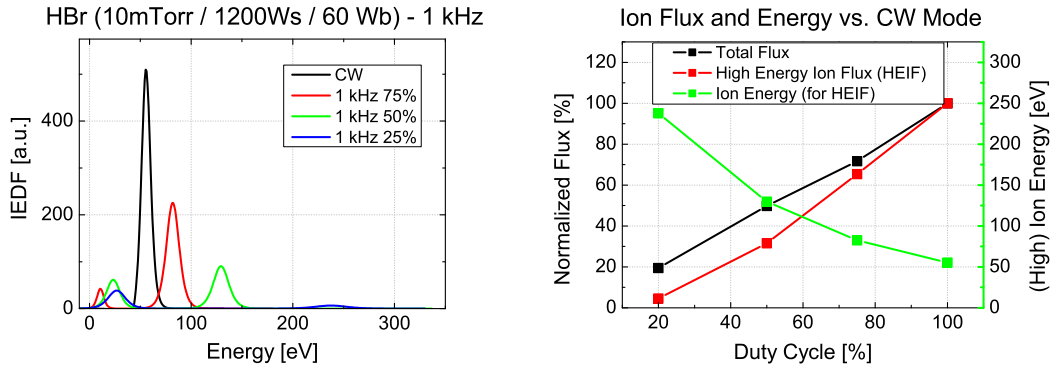

(a) **(b)**

Figure 4.9.: ***(a)*** *IEDFs of a pulsed HBr plasma (200 sccm, 10 mTorr, 1200 W source power, 60 W bias power) at 1 kHz with bias.* ***(b)*** *Total ion flux, high energy ion flux (HEIF) and mean energy of the latter.*

flux. The plasma conditions are very much altered compared to the standard etch process (20 mTorr, 750 W source power, 200 W bias power) in order to obtain a signal that is strong enough to be analyzed (10 mTorr, 1200 W source power, 60 W bias power). Also, a different dielectric shield for the RFA was used (Al_2O_3 instead of ceramic).
In CW mode only a single peak is visible. We do not observe a bimodal distribution in this case, probably due to the changed plasma conditions and possibly also to the different analyzer that was used. If the plasma is pulsed a low energy (LE) peak from the afterglow appears in addition to the high energy (HE) peak from the active source and bias power. For the low energy peak, we would expect an energy of just a few eV, corresponding to a vanishing sheath voltage. The rather high measured energy and its slight evolution might be linked to the poor measurement accuracy for the RFA floating potential that is used to calibrate the IEDF. This increases the possible error to several tens of eV. Also, for low energy ions, charge effects that falsify the IEDF measurement might play a role, as explained above in this section. Therefore, the energy from the LE peak will not be discussed. However, the measured ion flux of both peaks and the very large energy shift for the HE peak are assumed to be correct.
For decreasing duty cycles, the high energy peak shifts to very large values since the ion flux decreases. The ratio between high and low energy flux is decreasing until the high energy flux becomes almost insignificant, shown in Fig. 4.9 b. This is in good agreement with the time-resolved measurement of the ion flux in no-bias conditions in Sec. 3.2.2 and might open the possibility to reduce surface damage due to high energy electrons.
With increasing frequency the IEDF also changes, but only slightly. Unfortunately, the ion current measurement data is very noisy for high frequencies and hence it is

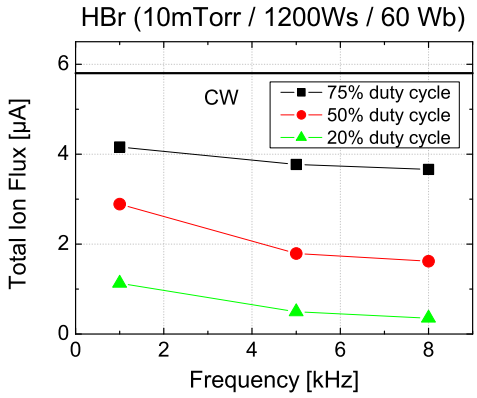

Figure 4.10.: *Total ion flux for pulsed HBr plasma conditions (200 sccm, 10 mTorr, 1200 W source power, 60 W bias power) from RFA measurements.*

difficult to derive a meaningful IEDF from it. However, it is quite straightforward to extract the total ion flux. Figure 4.10 shows the total ion flux for several duty cycles and frequencies.
For all duty cycles, the ion flux decreases if the frequency is increased, comparable to a further reduction of the duty cycle. The relative reduction of the ion flux becomes stronger for lower duty cycle. Whether the reduced ion flux also induces a higher ion energy, could not be determined. The mass spectrometry measurements in Sec. 3.1.1 show a similar behavior of the neutral density evolution, where for high frequencies is equivalent to a further reduction of the duty cycle. In addition, the MS data shows that the influence of the frequency becomes more important at very low duty cycles. The general impact of the frequency will be discussed in Sec. 5.4.

Summary

The ion energy distribution and the ion flux were studied in CW and pulsed modes with applied bias (200 W). The results indicate mean ion energies of approximately 500 and 750 eV in etch process conditions for the HBr/O_2 and the HBr plasma, respectively. In a pure HBr plasma the ion energy distribution shows the characteristic bimodal function originating from the oscillating RF potential of the wafer. In an HBr/O_2 plasma it becomes a double bimodal function, which indicates an additional major ion species with a lighter mass. It seems probable that the additional ion is H^+. The next lightest ion that governs the maximum width of the IEDF in a pure HBr plasma might be $SiH_x{}^+$.
The ion flux increases slightly with higher bias power. This behavior is only changed close to the case without bias due to the absence of etch products that alter the plasma composition and chemistry or due to charge effects at the probe. Directly on the wafer, the ion flux from an HBr/O_2 plasma is higher than in the

pure HBr chemistry. The opposite is observed with the IFP at the reactor sidewall. It is not fully understood where the difference comes from. One hypothesis is an additional production of the light ion observed with the RFA (H^+) close to the wafer from oxygen containing species due to energetic secondary electrons.
For pulsed mode the IEDF shows a high and a low energy peak, which correspond to the ions from the on- and the off-time of the plasma, respectively. If the duty cycle is reduced, the total ion flux, measured by the RFA on the wafer, decreases linearly and the high energy peak shifts to even higher energies. The relative contribution from the high energy peak to the total ion flux is also reduced with the duty cycle. These results are in good agreement with the IFP measurements in unbiased conditions in Sec. 3.2.2.
Similar to a decrease in duty cycle also an increase in frequency, especially for low duty cycles, results in a further reduction of the total ion flux.

4.2.3. Summary - Ions

Compared to a plasma without bias, the composition of the ion flux shows many additional ions that incorporate at least one Si atom. $Br_3{}^+$, on the other hand, is not detected any more and also the percentage of $Br_2{}^+$ is close to being negligible. The main contribution of the total ion flux comes from Si^+, $SiBr^+$, $SiBr_3{}^+$ and $BrH_{0-2}{}^+$. Large silicon containing etch products that leave the wafer can easily be ionized and dissociated due to the low energy thresholds for these processes, leading to the observed significant contribution to the ion flux. In addition, the nature of the reactor walls changes compared to no-bias conditions, influencing the recombination rates and, hence, also the reaction balance between all species. The double bimodal IEDF in the HBr/O_2 plasma, measured with an RFA, suggests also a significant amount of H^+, which cannot be detected by mass spectrometry. In a pure HBr plasma, no H^+ can be observed. The reason for the (dis-)appearance of H^+ remains unclear.
In CW mode, the ion flux is almost independent from the bias power. It is only reduced for the case without bias where the absence of etch products change the whole plasma chemistry. While the total ion flux at the reactor sidewall is larger in a pure HBr plasma (IFP) compared to an HBr/O_2 plasma, the opposite is the case close to the wafer (RFA). One hypothesis to explain this phenomenon could be the additional production of H^+ from oxygen containing species close to the wafer due to energetic secondary electrons.
By extrapolating the RFA data, mean ion energies of approximately 500 eV in the HBr/O_2 and 750 eV in the HBr plasma can be estimated for the CW etch process with 200 W bias power.
For pulsed mode, the IEDF shows a high and a low energy peak, which correspond to the ions from the on- and the off-time of the plasma, respectively. If the duty cycle is reduced, the total ion flux decreases almost linearly and the high energy peak shifts to even higher energies. In addition, the relative contribution from the high energy ions to the total ion flux is reduced, which is in good agreement with

the IFP measurements in unbiased conditions in Sec. 3.2.2.
With lower duty cycle, the relative contribution of $BrH_{0-2}{}^{+}$ to the total ion flux increases. One should also note that almost no Si^{+} can be detected at a very low duty cycle. This might indicate that almost all silicon is incorporated in larger molecules probably due to a better chemical reactivity of pulsed discharges. In addition, the lower averaged etch rate of Si reduces the overall presence of silicon containing species in the plasma.
Although the change in frequency did not affect the UV absorption of SiBr, the ion flux **does** shows a slight dependency on this parameter: an increase in frequency (>1 kHz), especially for low duty cycles, results in a reduction of the total ion flux, similar to a further slight decrease in duty cycle.

4.3. Reactive Etch Layer

The interaction of the plasma process with the wafer is analyzed via X-ray photoelectron spectroscopy. The immediate impact of the plasma etching can be observed in the reactive etch layer (REL) that is formed on the silicon surface due to ion enhanced etching reactions of the modified silicon surface. Depending on the ion energies, the disturbed layer can have thicknesses up to several nm [80,162,163]. It is heterogeneous with a continuous change in chemical composition. Hence, it is not possible to calculate an accurate layer thickness based on XPS data, as shown in Sec. 2.6. Still, information on the relative thickness can be obtained from the measured percentage of the bulk material: the greater the amount of undisturbed bulk silicon, the thinner should the reactive etch layer be. Figure 4.11 shows the chemical composition of the XPS signal at an angle of $46.25° \pm 3.75°$ from the REL for various pulse conditions.
The contribution of the bulk silicon increases significantly for duty cycles lower than approximately 50 % at a constant frequency, indicating a decrease of the REL thickness. Only insignificant differences are observable with increasing frequency at a constant low duty cycle of 20 %. It is difficult to give significant tendencies for the rest of the elements in the chemical composition since the percentages and their variations are too small.
Mass spectrometry and ion flux data indicate that the ratio between neutral and ion flux is largely increased for low duty cycles. During the on-time, high energy ions hit the surface where they break molecular bonds (amorphization) and chemically sputter atoms and molecules. The ion flux from the on-time decreases strongly with lower duty cycle compared to the total averaged flux, but the ion energy increases at the same time. The bromine that is available on the surface combines with silicon to form volatile species, which can desorb into the gas phase. If more bromine is available, more silicon atoms can be removed by this process. The thickness of the REL can be described by a balance between additional destruction of Si-Si bonds and the removal of available Si via Br radicals. It should also be noted that for a thick REL less ions reach the remaining bulk lattice and

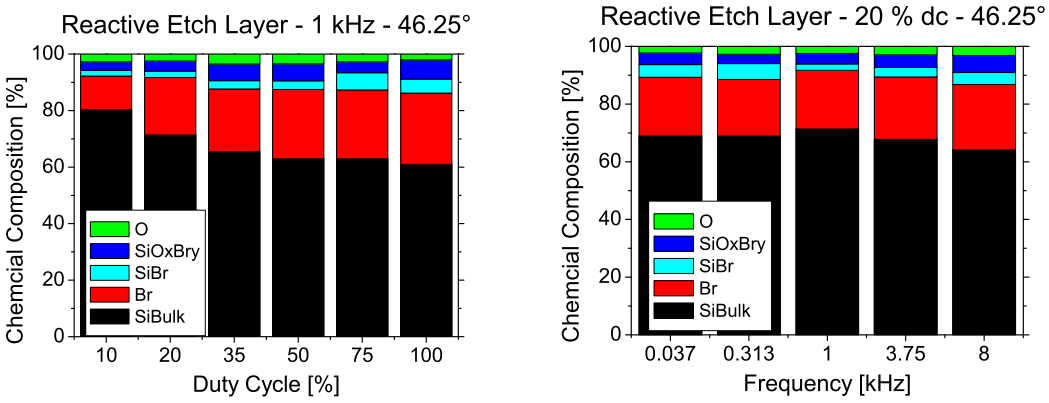

(a) **(b)**

Figure 4.11.: ***(a)*** *Chemical composition of the XPS signal (at 46.25°) from the reactive etch layer for different duty cycles (at 1 kHz) and* ***(b)*** *frequencies (at 20 % duty cycle). Standard plasma etch conditions (200 sccm HBr/5 sccm O_2, 20 mTorr, 750 W source power, 200 W bias power).*

introduce additional Si to the REL. This leads to two scenarios:

1. An increase in ion energy (or to some point also in ion flux) would increase the REL thickness since the penetration depth and the amorphization would increase.
2. An increase in the ratio of neutral to ion flux at constant ion energy would reduce the REL thickness: The removal rate is increased, reducing the REL thickness. A thinner REL can be traversed by ions more easily, increasing the amorphization rate until a new balance between both processes is found.

In the presented case, the neutral to ion flux ratio increases with lower duty cycle, leading to a more efficient Si removal. Although the ions from the on-time have higher energies than in CW mode, the relative contribution of the high energy ion flux to the total ion flux decreases. At low duty cycle, the bulk of the ion flux is composed of ions with low energies (plasma off-time). Together, the mean ion energy is reduced and consequently, the REL thickness decreases.

Summary

The reactive etch layer that is formed on the surface of the bulk material during etching was studied by XPS. With lower duty cycle the REL thickness decreases due to an increased availability of radicals and a decreased mean ion energy. The frequency does not have a significant influence on the REL thickness.

4.4. General Summary

Mass spectrometry, UV-absorption, ion flux and XPS measurements were carried out to study the impact of pulsed plasma etching on the gas phase and the plasma-surface interaction.
The spectrum of neutrals detected by mass spectrometry is enlarged by etch products compared to the case without bias power. For a reduced duty cycle, more HBr is found, but less other molecules, which can be explained by a reduced degree of dissociation and a reduced etch rate. For frequencies above approximately 1 kHz the modulation in the neutral density during a pulse becomes small enough to compare time-averaged values as shown for the case of SiBr.
Compared to a plasma without bias, the composition of the ion flux, dominated by Si^+, $SiBr^+$, $SiBr_3{}^+$ and $BrH_{0-2}{}^+$, shows many additional ions that incorporate silicon. $Br_3{}^+$, on the other hand, is not detected any more and also the percentage of $Br_2{}^+$ is almost negligible. Large silicon containing etch products that leave the wafer can easily be ionized and dissociated due to the low energy thresholds for these processes, leading to the observed significant contribution to the ion flux. In addition, the nature of the reactor walls changes compared to no-bias conditions, influencing the recombination rates and, hence, also the reaction balance between all species. The double bimodal IEDF in the HBr/O_2 plasma, measured with an RFA, suggests a significant amount of H^+, which cannot be detected by mass spectrometry. In a pure HBr plasma no H^+ can be observed. At low duty cycles the relative contribution of $BrH_{0-2}{}^+$ to the total ion flux increases. Also, almost no Si^+ can be detected any more, indicating that almost all silicon is incorporated in larger molecules probably due to a better chemical reactivity of pulsed discharges. In addition, the lower averaged etch rate of Si reduces the overall presence of silicon containing species in the plasma.
By extrapolating the RFA data, mean ion energies of approximately 500 and 750 eV in the HBr/O_2 and the HBr plasma can be estimated for the CW etch process with 200 W bias power.
For pulsed mode the IEDF shows a high and a low energy peak, which correspond to the ions from the on- and the off-time of the plasma, respectively. Similar to the case without bias, the total ion flux decreases linearly with the duty cycle and the high energy peak shifts to higher energies. Since at the same time the contribution of the high energy ions to the total flux is strongly reduced, the mean ion energy is also decreased at low duty cycles.
An increase in frequency (>1 kHz), especially for low duty cycles, results in a reduction of the total ion flux, similar to a further slight decrease in duty cycle.
The relative increase of the Br radical flux and the decrease of the mean energy of the ions at lower duty cycle lead to a decrease of the REL thickness on the silicon wafer surface (measured by XPS) for low duty cycles. The frequency does not have a significant influence on the REL thickness.

5. Pulsed Plasma Silicon Etching

In Chap. 3 and 4 the impact on the gas phase and the plasma-surface interaction from pulsing an HBr/O_2 etch plasma was studied by multiple diagnostic systems. The results give already large insight in the fundamental differences between CW and pulsed mode. In this chapter, the etching of silicon patterns by pulsed plasmas will be discussed. At first, the reactor conditioning prior to all experiments is presented. Then, experiments on blanket wafers are studied, followed by a discussion on the profile etching with two different masks. The observed features are compared to the CW mode and will be explained based on the results from the previous chapters.

5.1. Reactor Seasoning

The condition of the reactor walls can have a strong influence on the plasma process and the etch result since it may change the sticking and recombination coefficients of the plasma species [66, 68, 69]. Such a difference can lead to a significant change in the plasma chemistry and the ion flux (see Chap. 3 and 4) which in turn influences the etching. Therefore, before the etch experiments were performed, a cleaning and seasoning procedure was carried out to set the reactor into a well defined condition. At first, an SF_6/O_2 plasma without bias is generated to etch silicon oxide layers or similar materials that remain from previous processes from the alumina reactor walls. Subsequently, a two step seasoning process deposits a SiO_2 layer on the clean reactor walls. The first step consists of a $SiCl_4/O_2$ plasma process which deposits chlorine rich SiOCl on the walls. A further oxidation in a pure O_2 plasma produces SiO_2(Cl) layers with a very low percentage of chlorine. During both steps, a Si or SiO_2 wafer is placed on the wafer holder for protection. It is important that some of the deposited layer remains until the end of the final etch step of the pattern etching. In order to verify this requirement, the wafer with the deposited layer was exposed to all etch process steps without bias power to simulate the evolution of the wall surface after a standard seasoning procedure. The steps consist of consecutive etching of SiO_2, amorphous Carbon, and SiN layers, as well as the final silicon bulk etching. Although the plasma process without bias is quite different compared to the real process, in the latter the etch products are often re-deposited on the reactor walls, **increasing** the deposited layer even more. Hence, without bias power we can obtain a lower limit of the remaining protective layer. Between each etch step, ellipsometric measurements were acquired to follow the evolution of the layer on the wafer. In Fig. 5.1 the measurement for a

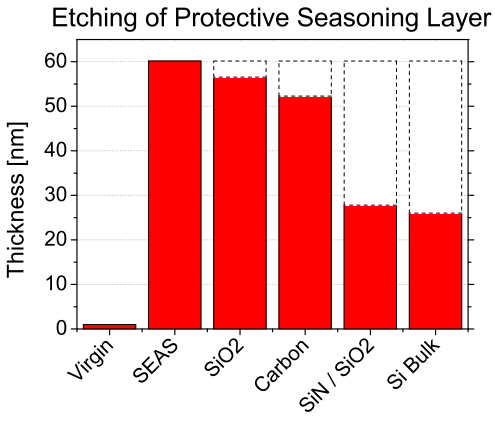

Figure 5.1.: *Reactor wall seasoning layer thickness on a sample wafer for all process steps without bias power.*

standard etch process is shown. From the initial thickness after seasoning of 60 nm 50 % still remain after the final etch process. Not surprisingly, the layer is mostly consumed during the SiO_2 and Si_3N_4 etching.

5.2. Etch Rates and Selectivities between Materials

Blanket wafer studies were carried out in order to study etch rates and etch selectivities between silicon and the different etch mask materials. An *ex-situ* multi-point automatic ellipsometer is available to give accurate measurements of the amount of etched material. It also gives an estimate of the homogeneity of the etch process across the wafer since it measures between 9 and 49 points across the wafer. The homogeneity of the etch rate is indicated in the graphs in terms of the standard deviation σ from the mean value (in %).
By reducing the duty cycle, the process etch rate will be decreased since both the radical and ion flux are reduced. In order to compare etch rates and etched patterns, two concepts can be used. The first one is to compare etch processes with the same amount of total plasma on-time, here called time compensation (TC). Compared to the process time in CW mode t_{CW}, the pulsed process time t_p is extended proportionally with the duty cycle dc to $t_p = t_{CW}/dc$. This way the instantaneous and the total used plasma power remain the same compared to the CW case. The second concept is called power compensation (PC). In this case the source power is increased according to the duty cycle to achieve the same average power input as in CW mode in order to compensate the reduced ion and radical fluxes. Similar to the TC concept, the power in pulsed conditions is therefore $P_p = P_{CW}/dc$. This leaves the process time constant, but the plasma itself is changed quite strongly between different pulse conditions. Even if the ion flux

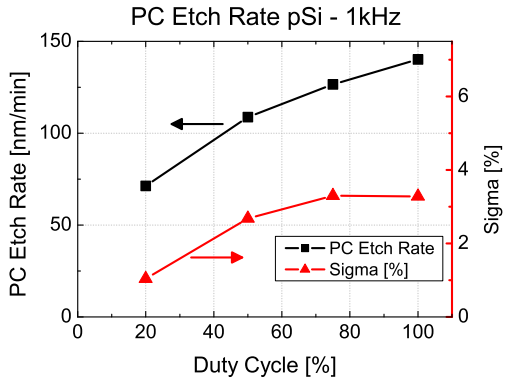

Figure 5.2.: *Power compensated etch rates of polycrystalline silicon from blanket wafer experiments ($P_{CW} = 500\,W$).*

was increased linearly with the source power, the change in ion density would also influence the sheath dynamics close to the target wafer, leading to a decrease in the ion energy [55, 62]. Also, a higher source power increases the degree of dissociation, the plasma temperature and the relative mixture of plasma species. In summary, PC changes several parameters at the same time, so that it is difficult to explain differences in the process. A further compensation of the bias power (not tested here) would lead to an increase in the ion energy.
Figure 5.2 shows the PC etch rate for polycrystalline silicon (pSi) for various duty cycles and the averaged relative standard deviation for all 25 measurement points. Clearly, the etch rate cannot be sustained by compensating just the source power. Nevertheless, an increase in source power could be potentially used to reduce the process time for future pulsed plasma processes.
With lower duty cycle the homogeneity of the etching is improved, which will be discussed in the next section.
In the following, only TC etch rates (TCER) will be discussed.

5.2.1. Silicon Etching

Etch Regime

Silicon is thought to be etched by physical/chemical sputtering and by the formation of volatile $SiBr_xH_y$ species, triggered by energetic ions that supply the needed activation energy and destroy Si-Si bonds [76, 81]. Hence, the silicon etching can be limited by either the radical flux and surface coverage (Br, H), or the ion flux and energy. Figure 5.3 shows the etch rate in CW mode for different bias powers. Each bias power corresponds to a mean ion energy, obtained from the ion energy and flux measurements in Sec. 4.2.2.

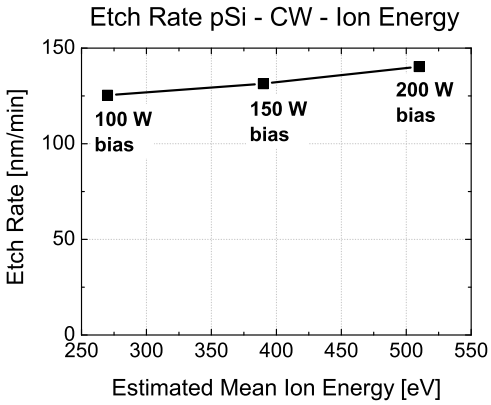

Figure 5.3.: *Etch rate of poly-silicon in a CW process with various bias powers (from blanket wafer experiments).*

The ion flux, as seen in Fig. 4.7, hardly evolves. Even if the ion energy is cut in half (at a constant ion flux), the etch rate decreases only by 11 %. This suggests that in the etch conditions at 200 W bias, more energy is available than radicals to form volatile products: the silicon etching is rather radical limited. This assumption is supported by experiments from Vitale *et al.* [81] who investigated the temperature dependent etch rate of silicon in an HBr plasma and found that for higher temperature (lower sticking coefficient) the etch rate decreases. The authors give two possible explanations. Either the coverage of radicals on the surface is reduced or the ratio between H and Br radicals on the surface is changed. Both explanations also indicate a radical limited etch regime.

TCER Evolution with the Duty Cycle

The TCER of polycrystalline silicon is shown in Fig. 5.4 a for various duty cycles, including the relative standard deviation σ for 25 measurement points across the wafer. Figure 5.4 b shows the evolution of the time compensated and normalized Br radical flux from the mass spectrometry measurements (without bias power) in Sec. 3.1.1. Although the plasma conditions were not the same, the **evolution** of the flux is assumed to be similar, regardless of the applied bias power and the reactor wall conditions.
The TCER of pSi increases with lower duty cycles up to 60 %. Since in our conditions the etching seems to be radical limited, this is probably linked to an increase of the availability of radicals on the Si surface. Assuming that during the off-time of the plasma radicals can accumulate on the surface, the surface coverage with radicals is increased with respect to the on-time of the plasma. Its evolution resembles the increase in TCER of Si.
The homogeneity of the etching follows the same trend. The relative standard deviation decreases with lower duty cycle, indicating a more homogeneous etch-

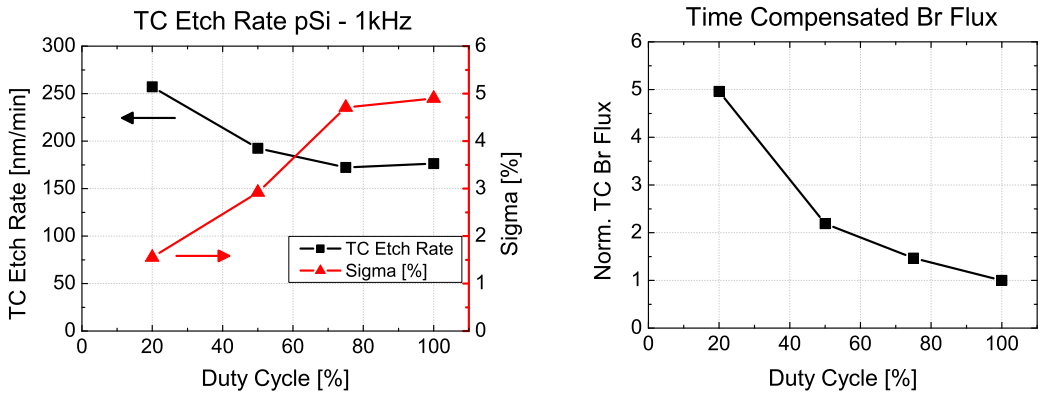

(a) (b)

Figure 5.4.: *(a) TCER of poly-silicon from blanket wafer experiments for various duty cycles and (b) time compensated normalized Br radical flux.*

ing. An explanation might also be linked to the increased off-time between the plasma pulses where radicals accumulate on the surface. If the surface coverage of Br becomes more saturated and therefore homogeneous, a similar amount of silicon can be etched everywhere on the wafer, even if the ion flux is distributed inhomogeneously, as long as the etching remains radical limited.

TCER Evolution with the Frequency

Figure 5.5 shows the TCER of pSi for various frequencies and the relative standard deviation σ from the mean value of all 25 measurements points across the wafer. With increasing frequency the etch rate also increases. Moreover, the lower the duty cycle is, the more pronounced is the gain. At the same time no significant impact on σ is observed. The same evolution will be shown for actual pattern etching, where possible reasons will be discussed.

5.2.2. SiO_2 Etching

While the silicon etching was found to be radical limited, the etching of SiO_2 in a HBr/O_2 plasma depends almost exclusively on the ions since the main etch mechanism is physical sputtering [75,76]. Figure 5.6 shows the dependence of the TCER of SiO_2 on the duty cycle and the resulting selectivity towards pSi.
In comparison with Si, the TCER of SiO_2 is already very low in CW mode. By reducing the duty cycle, it first increases slightly and is then significantly reduced. Consequently, the selectivity increases drastically with lower duty cycles up to around 800. The opposite trends in the etch rate can be attributed to the important differences in the etch mechanisms of silicon (radical limited) and SiO_2 (ion driven) in an HBr/O_2 plasma.

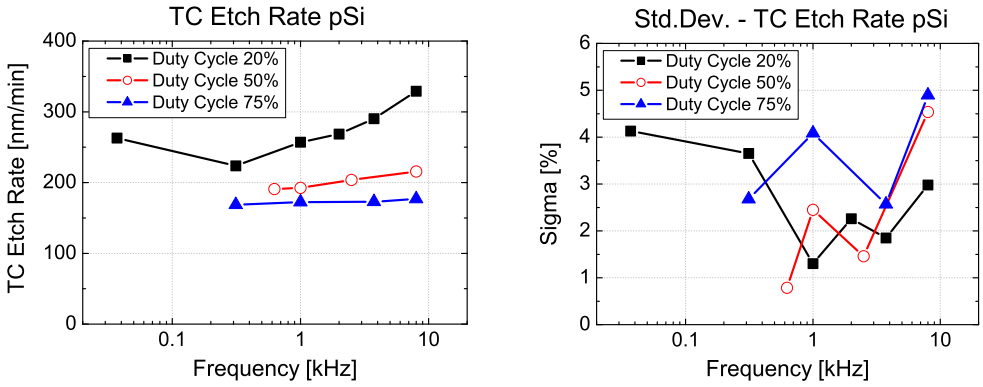

(a) (b)

Figure 5.5.: ***(a)*** *TCER of poly-silicon from blanket wafer experiments for various frequencies and* ***(b)*** *the corresponding relative standard deviation across the wafer from the mean value.*

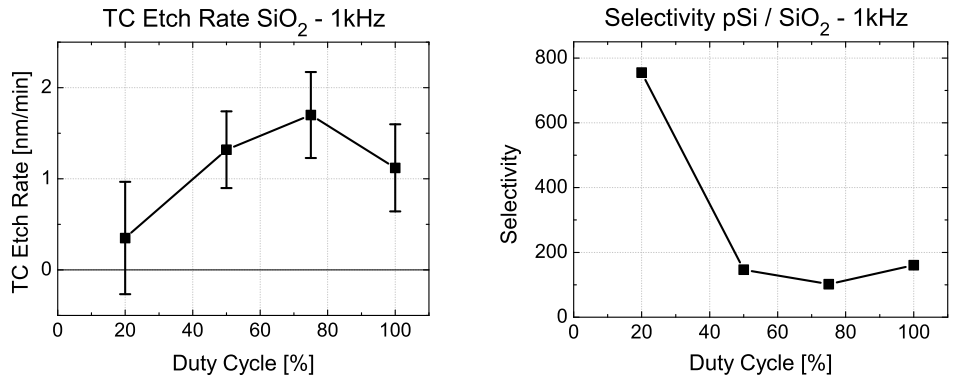

(a) (b)

Figure 5.6.: *Etch rate and selectivity of SiO_2 (mask material) with respect to pSi from blanket wafer experiments.*

The evolution in the SiO_2 TCER can be understood by modeling the evolution of the time compensated sputter yield. The results from the ion flux and energy measurements in Sec. 3.2.2 for an HBr plasma indicate that most of the ions have a low energy which might not be sufficient to etch SiO_2 in a significant amount [75]. The flux of highly energetic ions decreases more than proportional compared to the duty cycle, but at the same time its mean energy increases significantly. The sputter (etch) yield is directly proportional to the number of incoming ions, but depends only on the square root of the ion energy [164–168]. Assuming that only the high energy component of the flux contributes to the sputtering of SiO_2 and the

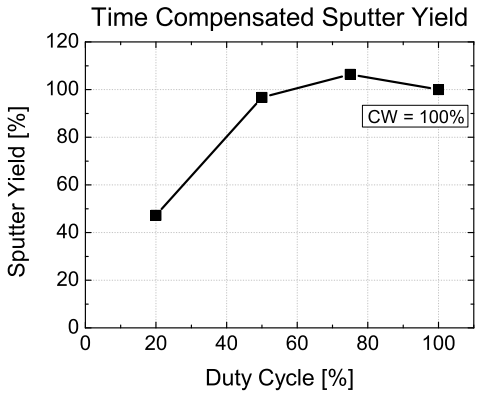

Figure 5.7.: *Approximated sputter yield evolution compared to CW (100 %) based on the change of high energy ion flux and its mean energy. The data is taken from the RFA measurements at 10 mTorr, 1200 W source power and 60 W bias power.*

threshold energy is negligible ($E_{Th} \ll E$), we can calculate the change in TCER at a specific duty cycle *dc* based on the data from Sec. 4.2.2 for the ion flux Γ and energy E via

$$\frac{\mathrm{TCER}_p}{\mathrm{ER}_{CW}} = \frac{1}{dc} \cdot \frac{\Gamma_p}{\Gamma_{CW}} \sqrt{\frac{E_p}{E_{CW}}}. \tag{5.1}$$

The resulting evolution is shown in Fig. 5.7 with $\mathrm{ER}_{CW} = 100\,\%$.
The approximated evolution of the sputter yield agrees very nicely with the observed TCER for the SiO_2 etching in Fig. 5.6 a although the plasma conditions are very different (RFA measurements at 10 mTorr, 1200 W source power and 60 W bias power). This shows that for our experiments the impact of high energy ions and their ability to induce damage can be reduced if the duty cycle is decreased.

5.2.3. Amorphous Carbon Etching

Amorphous carbon (αC), the second mask material used in the pattern etching, is not only etched by physical sputtering, but also by ion assisted chemical etching, mainly with the help of H and O radicals. It is not exactly clear if O or O_2 is the more important species for the ion assisted chemical etching of αC [169]. However, in a purely chemical sense, oxygen radicals are reported to be more reactive than O_2 and hydrogen atoms [170].
In Fig. 5.8 the TCER of αC is shown, including the standard deviation for a nine measurement points across the wafer. The deduced selectivities towards pSi for the CW mode and pulsing at 1 kHz 20 % are also presented.
In pulsed condition the TCER is slightly increased. In contrast to the silicon etching, the pulsing reduces the homogeneity of the etching. Since the TCER of silicon is strongly increased, the resulting selectivity between both materials is

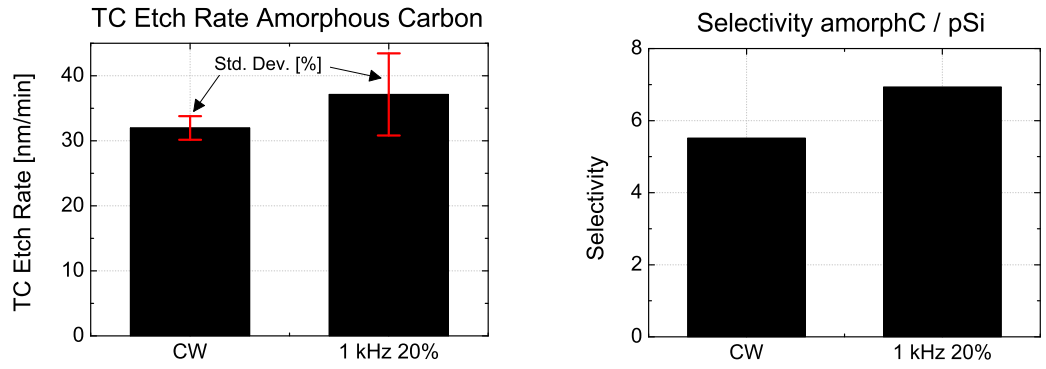

(a) (b)

Figure 5.8.: *Etch rate and selectivity of amorphous carbon (mask material) with respect to poly-silicon from blanket wafer experiments. The relative standard deviation across the wafer is indicated in red.*

also improved. In comparison to the etching of Si and SiO_2, the observed features are more difficult to explain. On the one hand the contribution of the physical sputtering is reduced, but on the other hand the time to accumulate O (and H) on the surface is increased. Therefore, the dependence of the etch rate on the duty cycle is thought to be in between the evolution of Si and SiO_2. Since the TCER increases we suppose that the increase of the chemical component is more important than the decrease of the physical component.

5.2.4. Summary - Etch Rates

Blanket wafers of different materials were etched to study the evolution of the etch rate and selectivity with respect to changing pulse conditions.
As the power compensated experiments have shown, the use of pulsed plasmas is not equal to a simple reduction of the average plasma power.
A decrease in duty cycle leads to opposite evolutions of the TCER of Si and SiO_2. The results for silicon etching indicate a radical limited etch regime. An increase in the ratio of radical flux to ion flux leads to a net increase of the availability of radicals during the etching, which explains in turn the increase in silicon TCER for lower duty cycles. Both the silicon TCER and the time compensated Br radical flux follow a similar evolution. In addition, the homogeneity of the etch rate across the wafer is improved for decreasing duty cycle.
The etching of SiO_2 is mainly initiated by physical sputtering. It increases slightly for a duty cycle of 75 % and decreases afterwards. As a result, the selectivity between Si and SiO_2 is strongly enhanced. An approximation of the sputtering yield based on measurements from Sec. 4.2.2 is in very good agreement with the observed behavior.

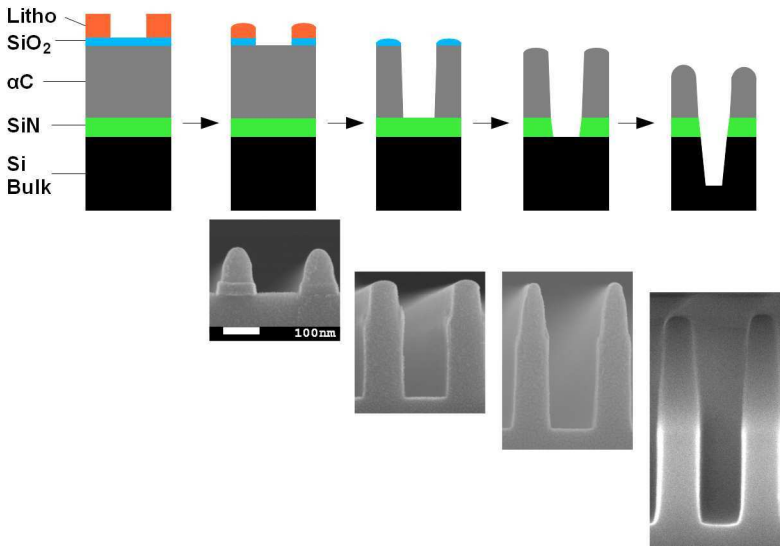

Figure 5.9.: *Sketch of the etch steps and corresponding SEM images of a 120 nm line-equal-space pattern.*

The TCER of αC is also slightly increased, probably for the same reason as for silicon (increased O and H radical availability). This gain is lower than for silicon, leading to an overall increase in selectivity between both materials.

5.3. Si Etching with a Carbon Mask

5.3.1. Reference Process in CW Mode

Following the approach of the process for shallow trench isolation etching, provided by Applied Materials Inc., we started out by studying silicon bulk etching with a hard mask of amorphous carbon (αC). In Fig. 5.9 the used stack and SEM images after each etch step are shown to illustrate the process flow. In order to etch the silicon bulk, several preliminary etch steps need to be carried out to open the hard mask. An overview of all process steps is given in Tab. 5.1.
In order to study the impact of plasma pulsing on the etch process, a reference etch profile in a continuous wave (CW) process needs to be obtained. In Fig. 5.10 the etch result from the initial process ($HBr/O_2/CF_4$) is shown.
The most obvious observation is the formation of a thick passivation layer that depends on the neutral species collection angle (aspect ratio). While dense profiles are rather straight, the etch slope becomes far from vertical for isolated lines.

Table 5.1.: *Plasma etch processes for Si etching with a carbon mask.*

Material	Layer [nm]	Gases [sccm]	Pressure [mTorr]	Source [W]	Bias [W]	End-point
SiO_2	30	200 Ar/80 CF_4/50 CHF_3	7	200	250	O/R*
αC	300	80 HBr/36 O_2/80 Ar	4	350	120	O/R*
SiN	80	100 CF_4	4	1200	100	O/R*
Si (bulk)		200 HBr/8 O_2/12 CF_4	20	750	200	timed
		200 HBr/5 O_2	20	750	200	timed

* optical emission spectrometry / reflectometry

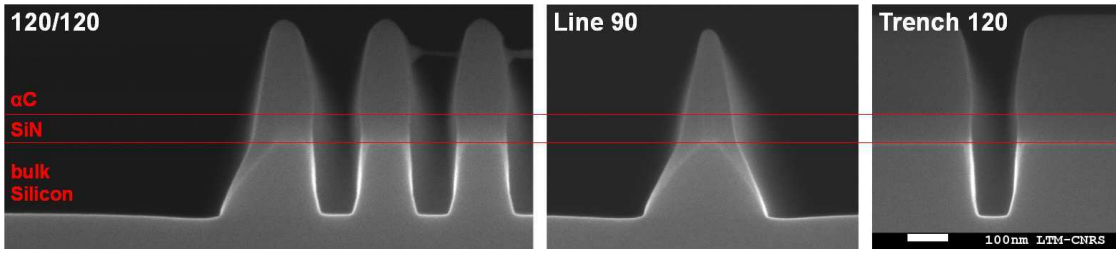

Figure 5.10.: *Pattern etched using the CW recipe from Applied Materials, Inc. ($HBr/O_2/CF_4$).*

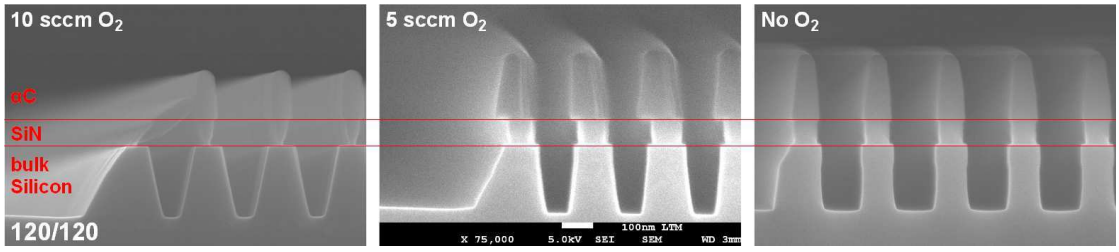

Figure 5.11.: *Dependence of the pattern etching on the oxygen flow in CW mode.*

To reduce the complexity of the chemistry, CF_4 is removed from the process. Subsequently, the process was re-developed in order to give comparable results. The easiest way to do so is to vary the oxygen flow and to study its impact on the etching. In Fig. 5.11 etched profiles (CW mode) are shown for different flows of O_2 at a constant flow of HBr. The passivation layer is removed by exposure to an HF bath (1 %) in order to make the differences in etching more visible.
By reducing the oxygen flow, the etching becomes more vertical. This is due to a decreased formation of the sidewall passivation layer (SPL) that is formed by non-volatile etch products, e. g., Si, C, N, O, Br. Oxygen plays a major role to form, harden and to protect this layer from subsequent re-etch [75, 124, 126, 127]. Without external oxygen flow, the only oxygen sources are the SiO_2 covered reactor

walls and possible contaminations in the wafer layers. This seems to be insufficient to protect the sidewalls from lateral etching as manifested by the slight bow in the trenches. A more detailed study on the sidewall passivation layer will be given at the end of this chapter.
Another important feature is the decreased consumption of the carbon hard mask with lower oxygen flow. This supports the assumption made for the blanket wafer experiments that the oxygen flow is a key parameter for the ion assisted chemical etching of carbon in our conditions.
Based on these results, an intermediate gas flow of 5 sccm is used for the future CW reference etch process.

5.3.2. Impact of Plasma Pulsing on the Etched Profiles

The pulsed plasma etching is studied based on the exact same process conditions. The only difference is the synchronous pulsing of both RF generators (source and bias) and the changes in the automatic matching network. To facilitate the comparison between profiles from different pulse conditions, the concept of time compensation is used. For the CW mode the etch time was set to 64 seconds, the pulsed experiments were timed accordingly (e. g. 320 seconds for a duty cycle of 20 %).
Figure 5.12 shows profiles from pulsed plasma etching at a frequency of 1 kHz and various duty cycles. Obviously, the duty cycle has a large influence on the pattern etching. Each feature will be discussed individually in the following.

Etch Rate

By reducing the duty cycle, the time compensated etch rate (TCER) is increased, similar to the observation on blanket wafers. Again, this can be explained by the increased availability of radicals on the surface.

Faceting and Consumption of Hard Mask

In general, with lower duty cycle, the carbon hard mask is less faceted, especially at 20 %. The decrease in the faceting leads to a lower carbon mask consumption and could be linked to the reduced physical sputtering at low duty cycles. The slightly increased TCER of αC in the blanket wafer experiments cannot be observed and is probably outweighed by the change in faceting. Also, compared to blanket wafer etching, silicon containing etch products can be re-deposited on the mask, which reduces its etch rate.

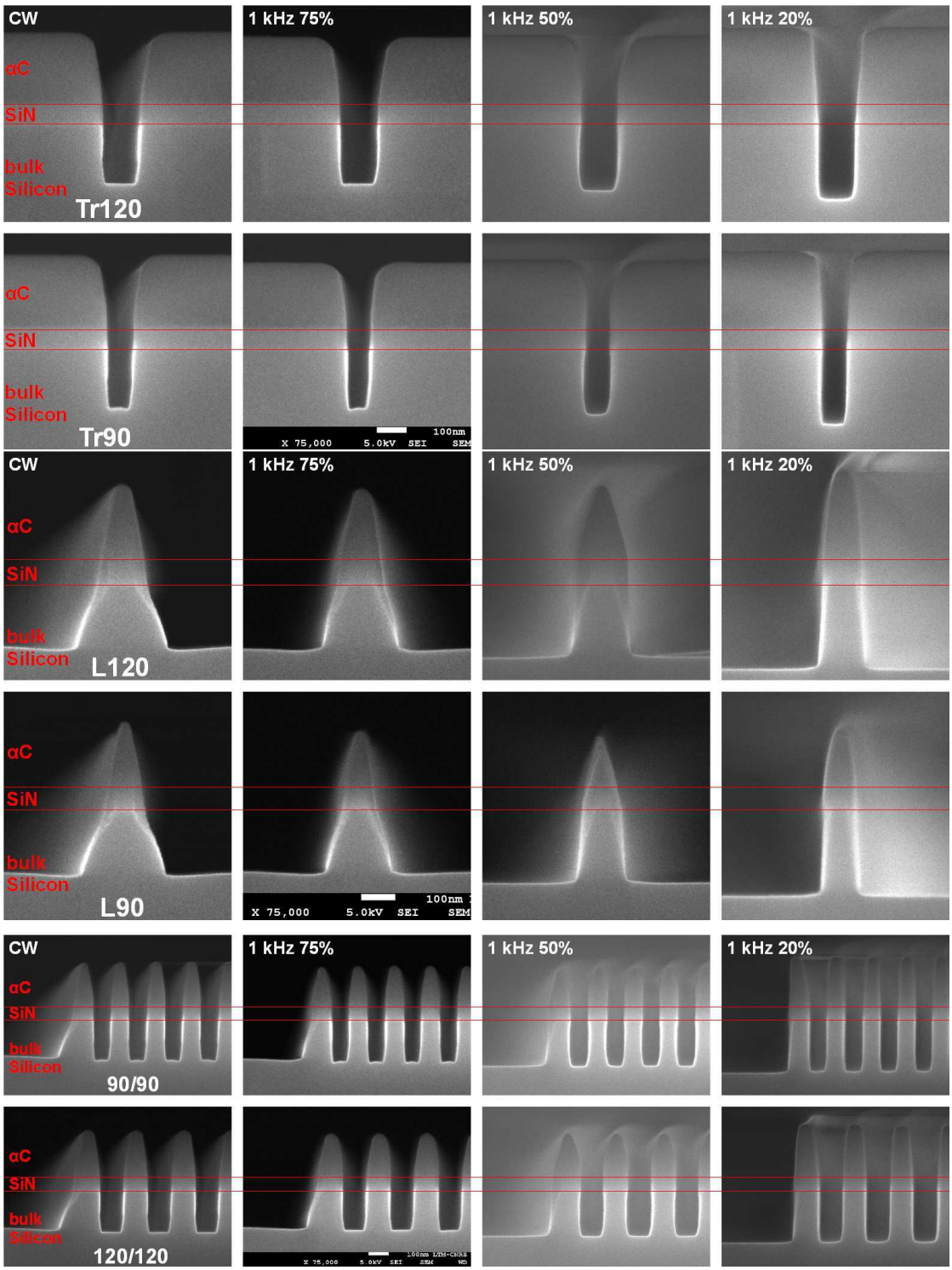

Figure 5.12.: *Dependence of the etched patterns on the duty cycle.*

Slope of the Etched Profile

By decreasing the duty cycle, the etch slope of the profiles becomes more and more vertical. This is certainly due to a reduced formation of the sidewall passivation layer that is observed on the etched isolated lines. The SPL is built up by non-volatile Si species that adsorb on the sidewalls and combine with additional oxygen to form stable SiO_2 like layers [124,126,127,171]. For a low duty cycle, less oxygen radicals are available to combine on the sidewall surface. Moreover, the increased availability of etch radicals might lead to more volatile etch products that have a lower sticking coefficient, so that the formation of the SPL is reduced. In addition, these etch products are less re-dissociated and thus, also less re-deposited in pulsed plasmas. More details on the formation of the SPL will be given in Sec. 5.5.

Profile Difference Open/Dense Patterns

In CW mode, a large difference between open and dense profiles can be observed. The larger collection angle for neutral species from the gas phase can increase the amount of deposited material on open (exposed) sidewalls. By decreasing the duty cycle, this effect of aspect ratio dependent etching (ARDE) is reduced. At 1 kHz 20 % open and dense profiles become close to being identical. The change in the formation of the SPL is thought to play a crucial role. Since the SPL thickness is reduced everywhere, as explained above, the absolute differences between open and dense pattern structures are also reduced, even if the relative difference might still be the same. Moreover, during the additional off-time between pulses, the coverage of oxygen radicals might saturate on the sidewalls of both dense and isolated structures, leading to a more homogeneous growth of the SPL. More details on the formation of the SPL are given in Sec. 5.5.

Micro Trenching

Two types of micro trenching can be observed: a very broad micro trenching close to isolated patterns and a localized one, especially visible in narrow trenches.
The very broad trenching disappears for lower duty cycles and might be linked to the collection angle for species from the gas phase, which increases with larger distances to adjacent lines. Since oxygen radicals can oxidize the reactive etch layer and inhibit thereby the etching of silicon [75,76,78,79] the differences in etch rate might be attributed to a reduced oxygen radical flux (see end of Sec. 3.1.1) at lower duty cycles, making the etching more homogeneous.
Another explanation for the broad micro trenching might be a re-deposition from the gas phase. For low duty cycles the ratio of Br radical to ion flux is increased, leading to a great availability of Br radicals to form volatile etch products like $SiBr_4$. Also the reduced average power leads to a lower amount of re-dissociated molecules that can stick to the surface. Hence, the re-deposition from the gas phase is reduced for lower duty cycles, possibly leading to the disappearance of the broad micro trenching.

The localized micro trenching could be explained by the following: in a purely geometrical view, more vertical sidewalls, seen at lower duty cycles, lead to a focus of scattered ions close to the sidewall. In addition, the radical (Br) to ion flux ratio increases, leading to conditions in which the etching becomes more limited by the ion flux and energy. In this case, the etch rate might be more susceptible to a local change in the ion flux (where ions are focused). Finally, charging effects, which are known to be reduced in pulsed plasmas [41–46], might also play a role concerning the micro trenching [8, 11]

5.3.3. Summary

The silicon pattern etching in an HBr/O_2 plasma can be significantly altered by using synchronized pulsing of source and bias power. The original process from Applied Materials Inc. uses CF_4 in the reactive gas mixture, which was neglected to reduce the complexity of the process. A new reference CW process was developed and the influence of the oxygen flow has been shown: a reduction in the oxygen flow leads to a modification in the sidewall slope, probably due to a reduced formation of the sidewall passivation layer. Based on the new CW etch process, the impact of the duty cycle at a frequency of 1 kHz was investigated. By reducing the duty cycle, the following profile evolution can be observed and explained:

1. The time compensated etch rate is increased due to an increased availability of etch radicals.
2. The faceting of the carbon hard mask is reduced. This leads to a reduced mask consumption, which outweighs the increased TCER of αC that was observed in the blanket wafer experiments. Also, compared to blanket wafer etching, silicon containing etch products can be re-deposited on the mask, further reducing its etch rate.
3. The slope of the etched profile becomes more vertical. Similar to a reduction of the oxygen flow, the formation of the sidewall passivation layer is reduced since less oxygen radicals and non-volatile etch products are available.
4. The difference between dense and isolated profiles is reduced. This might also be linked to a reduced formation of the SPL, but also to a more homogeneous distribution of neutral species, e. g., O.
5. The broad trenches at high duty cycles (75 %) and in the CW mode might be linked to the difference in the collection angle for depositing or oxidizing (etch inhibiting) species from the gas phase. By reducing the duty cycle, less species are deposited and the broad micro trenching disappears. The appearance of localized micro trenching in dense patterns, especially at lower duty cycles ($\lesssim 20\,\%$), could be explained by a focusing of scattered ions at vertical sidewalls, observed at low duty cycles, which increases locally the ion flux. Thus, the etch rate also rises since it is more susceptible to a change of ion flux due to the great availability of Br radicals. Reduced charging effects in pulsed processes might also play a role.

5.4. Si Etching with an Oxide Mask

One inconvenience for a detailed study on the etch process with an αC hard mask is the large amount of different species that are involved, namely Si, O, N, C, Br and H. To further simplify the etch chemistry, we changed the stack slightly (SiO_2 instead of SiN) and removed the carbon mask with an oxygen strip plasma before the main silicon etch. Subsequently, the thin layer of oxidized bulk silicon needs to be removed to expose the underlaying bulk Si to the etch plasma. The remaining silicon oxide from the last stack layer is used as the new mask. Thus, we are able to remove most of the nitrogen and carbon from the etch chemistry. At the same time we re-developed the carbon etch for a better profile control. Figure 5.13 shows the new stack and SEM images after each etch step. The modified process flow is presented in Tab. 5.2.

Table 5.2.: *Plasma etch processes for Si etching with a SiO_2 mask.*

Material	Layer [nm]	Gases [sccm]	Pressure [mTorr]	Source [W]	Bias [W]	End-point
SiO_2	30	200 Ar/80 CF_4/50 CHF_3	7	200	250	O/R*
αC	300	80 HBr/34 O_2/80 Ar	4	350	100	O/R*
SiO_2	80	50 CF_4/50 CHF_3	4	1200	100	O/R*
rem. αC		50 O_2	4	800	10	O/R*
oxid. Si		100 CF_4	4	1200	100	3 sec
Si (bulk)		200 HBr/5 O_2	20	750	200	timed

* optical emission spectrometry / reflectometry

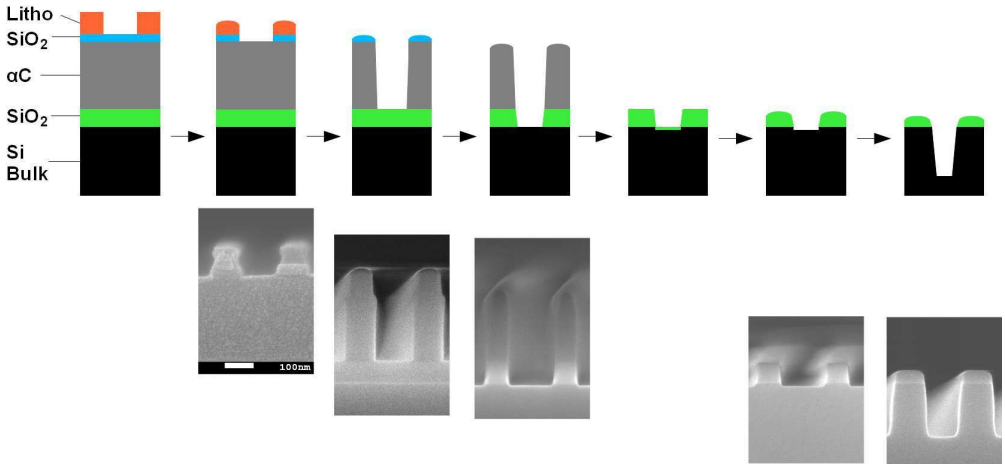

Figure 5.13.: *Sketch of the etch steps and corresponding SEM images of a 120 nm line-equal-space pattern.*

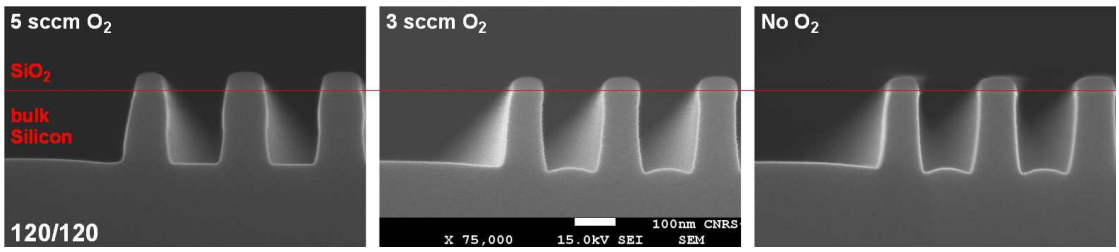

Figure 5.14.: *Dependence of the etched patterns on the oxygen flow in CW mode.*

5.4.1. Dependence on the Oxygen Flow

In the same manner as for the carbon mask etching, the impact of the oxygen flux on the etching of the bulk silicon in CW mode is investigated. The resulting etch profiles, patterns with dimensions of 120 nm for the lines and spaces, are presented in Fig. 5.14.
By reducing the oxygen flow, a bow in the sidewalls can be observed, indicating an increased erosion rate of silicon. This can be explained once more by the decreased formation of the sidewall passivation layer, which is due to a decreased amount of oxygen radicals [127].
Another aspect is the increased consumption of the oxide mask for lower oxygen fluxes. If more oxygen is available, it is more likely that the surface is re-oxidized and SiO_2 bonds are rebuilt before volatile $SiBr_x$ species are created.
Last but not least, the different geometry and a lower oxidation of the silicon REL in combination with the increased ion energy might lead to the emerging micro trenching.

5.4.2. Dependence on the Duty Cycle

For the modified etch process, the duty cycle is also expected to have a rather large influence on the profiles. In Fig. 5.15, three different patterns are presented that were etched at a frequency of 1 kHz and various duty cycles. In addition, some of the profiles are also shown after an HF bath that removes the remaining oxide mask and the passivation layer.
In general, the observation is very similar to the case with a carbon hard mask. With a lower duty cycle the time compensated etch rate is increased, the faceting and consumption of the mask is reduced (except for 10 %), the etch slope is more vertical and local micro trenching on the outer trench bottoms starts to appear.

Etch Rate

The increase in time compensated etch rate of silicon is again due to the increased availability of etch radicals.

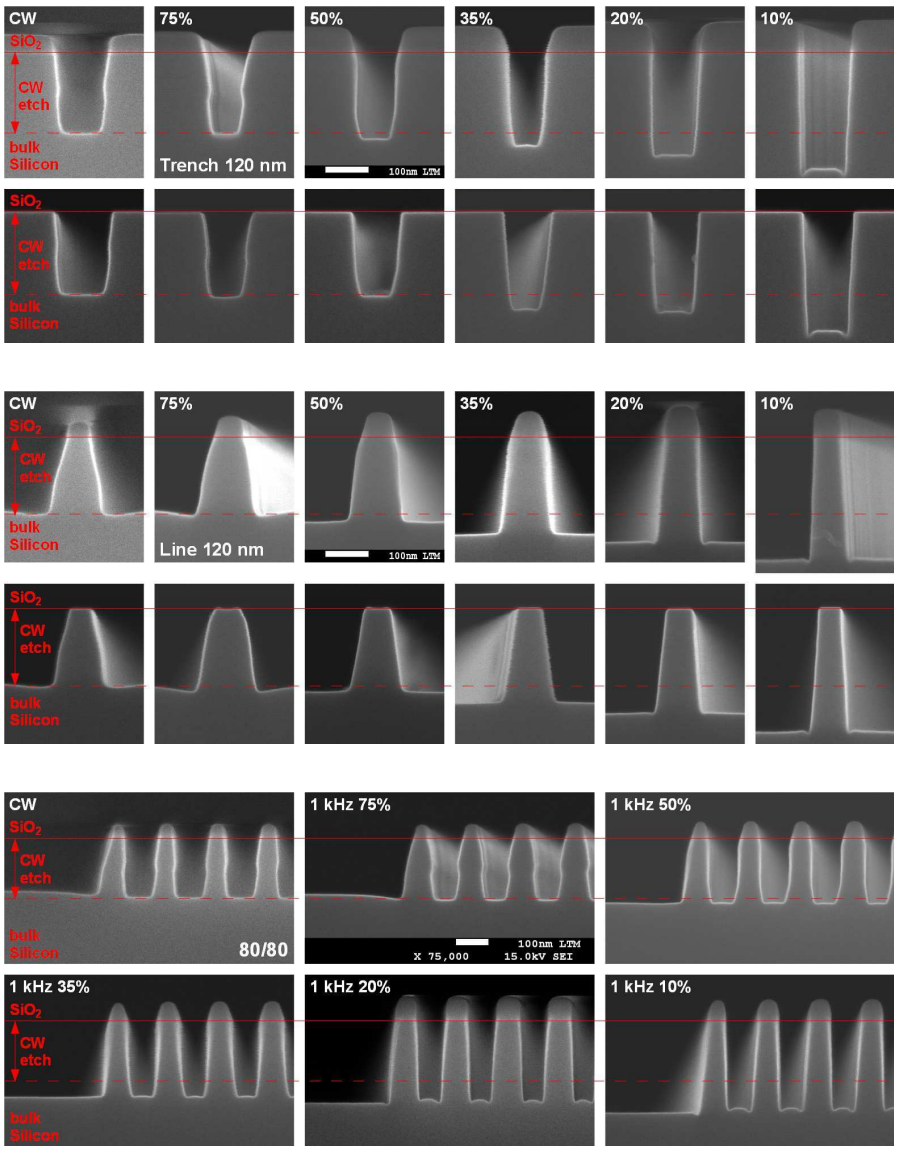

Figure 5.15.: *Dependence of the etched patterns on the duty cycle.*

Faceting and Consumption of Hard Mask

Compared to the observations for the carbon mask etching, the low consumption and the reduced mask faceting of the oxide hard mask can be explained more easily. It is directly linked to the decreased physical sputtering at low duty cycles, which was discussed in detail for the blanket wafer experiments in the previous section.

Slope of the Etched Profile

By decreasing the duty cycle, the etch slope of the profiles becomes more vertical. Just as for the carbon mask, this is probably due to a reduced formation of the sidewall passivation layer.

Profile Difference Open/Dense Patterns

The explanation for the reduced difference between open and dense profiles is the same as for the carbon hard mask.

Micro Trenching

Again, two different types of micro trenching can be observed. For the CW mode and at 75 % duty cycle a very broad micro trenching is found, which disappears for decreasing duty cycle until a very localized micro trenching appears at 20 and 10 %. The mechanisms of formation of the two different types of micro trenching are assumed to be the same as for the etching with the carbon mask.

Only the profiles obtained at 1 kHz 10 % do not fit into the overall evolution. Compared to a duty cycle of 20 % the mask is more consumed and facetted, indicating an increase in physical sputtering. A similar effect can also be seen by going to high frequencies, which will be discussed in the following.

5.4.3. Dependence on the Frequency

The plasma diagnostic data indicates an influence of the frequency at low duty cycles. In Fig. 5.16 the impact of the frequency is shown for etch processes at duty cycles of 75, 50 and 20 %, up to a frequency of 8 kHz.
The impact of the frequency can clearly be seen on the three series of SEM images. By increasing the frequency up to a certain limit that is dependent on the duty cycle, no significant change in the etched profiles is observable. For higher frequencies beyond this limit, the etch rate starts to increase for silicon, but also for the oxide mask. Moreover, an increased faceting of the hard mask can be observed.
For a lower duty cycle, the limiting frequency decreases. It is possible that the pulsed etching at 1 kHz 10 % is already in this limit, which could explain the differences to the general evolution with respect to a decreasing duty cycle.
If the frequency is increased, the number of transitions per second between on and off increases and the pulse period could become so small that it approaches the characteristic time constants for dissociation, recombination and ionization. Since we have no time resolved information on the transitions at high frequencies, the analysis remains highly speculative.
The increased etch rates of both Si and SiO_2, as well as the faceting indicate that the physical part of the etching becomes more important. The RFA data in Sec. 4.2.2 shows a reduced ion flux for increased frequency, with an increased

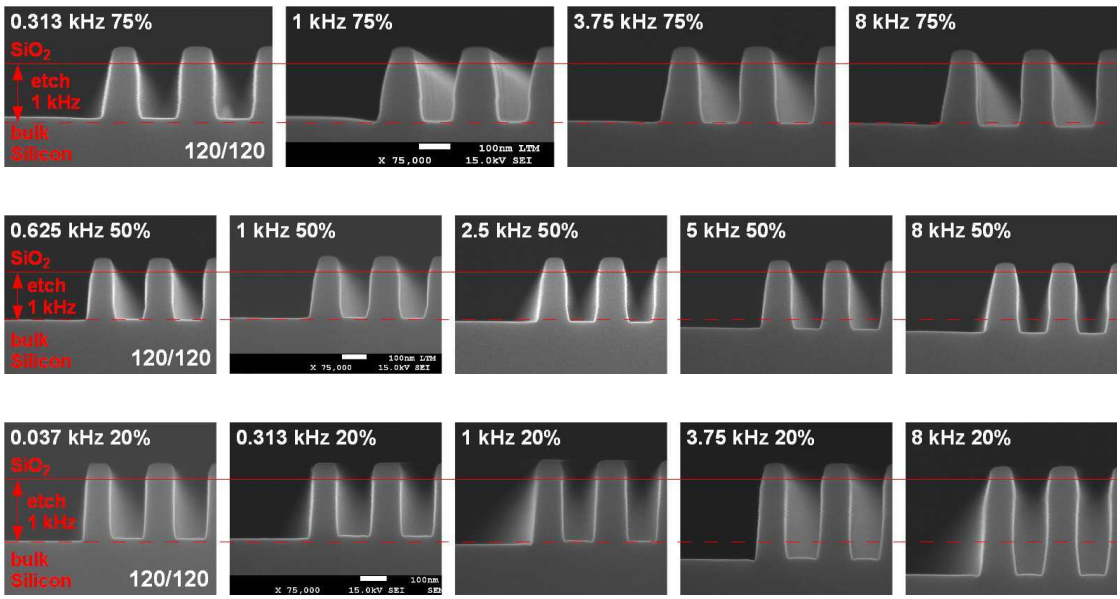

Figure 5.16.: *Dependence of the etched patterns on the frequency.*

effect for low duty cycles. The evolution could be correlated to the observed profile features. However, since the ion flux decreases, but an increased physical etching is observed, we have to assume a strongly increased ion energy that more than compensates the reduced ion flux. One possible explanation for the increased ion energy might be the overshoot of T_e at the beginning of each pulse. For high frequencies this overshoot happens more often, which might influence the average ion energy.
Mass spectrometry data shows an increased HBr density and decreased densities of Br and Br_2, indicating a reduced dissociation of the plasma. Probably this indicates also a reduced ionization and hence, a reduced ion density that can explain the lower ion flux. This would lead to an increased ion energy for a constant bias power. However, overall this would lead to a reduced physical sputtering.
Moreover, while all diagnostic data show a similarity between the frequency effect and the decrease of the duty cycle, they affect the pattern etching differently.
For a detailed analysis beyond this discussion the transient character of the plasma at high frequencies needs to be investigated, especially concerning the bias power and the impedance matching of the power generators.

5.4.4. Comparison to smaller profiles

In the previously presented experiments, etch results for rather large patterns are examined. In the following, these results are compared to profiles with smaller dimensions, down to a trench width of 45 nm. The stack materials and the process flow are the same as for the oxide mask experiments. However, the thickness of each layer was reduced in order to be sure that the thinner lines are stable enough

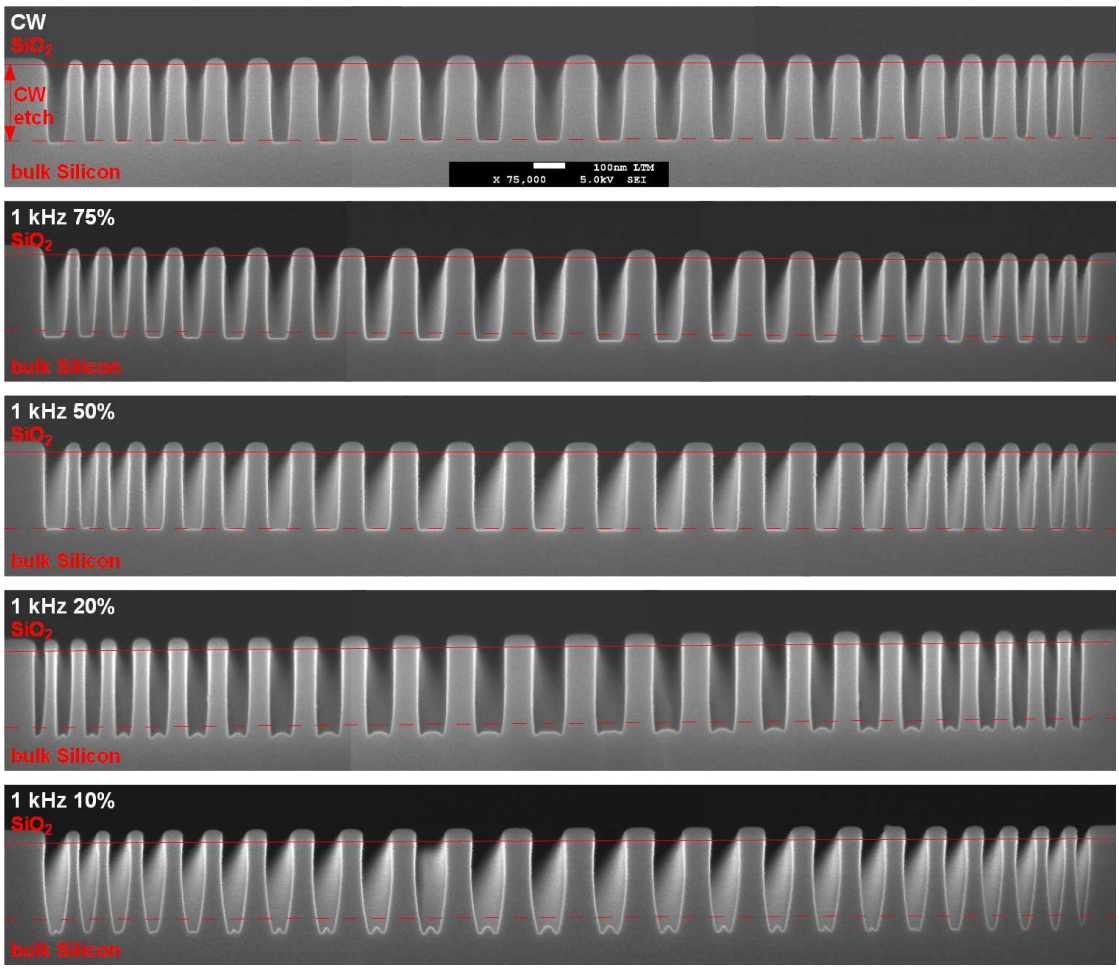

Figure 5.17.: *Etched Si patterns with changing trench dimensions from 45 nm on the outside to 100 nm in the middle with a step size of 5 nm for CW and pulsed conditions.*

and do not collapse. The stack consists now of

1. 20 nm of silicon oxide (SiO_2)(anti-reflective layer)
2. 100 nm of amorphous carbon (αC)
3. 50 nm of silicon oxide (SiO_2)
4. bulk silicon

In order to achieve such small structures, it was necessary to use electron beam lithography. In Fig. 5.17, etched lines and trenches are shown with changing dimensions from 45 nm on the outside to 100 nm in the middle for CW and pulsed conditions. Neighboring trench and line dimensions differ by 5 nm, so that possible ARDE effects, e. g.etch rates that depend on the aspect ratio ("RIE lag"), can easily be observed.
The only differences compared to the previous stack and pattern are the extremely

strong micro trenching and the bowed sidewalls at a duty cycle of 10 %. Even at 20 % the micro trenching and a very light bow are observable. The general trends, however, are the same as before: with a lower duty cycle the TCER is increased, the faceting and consumption of the mask is reduced (except for 10 %), micro trenching appears and the etch slope is changed due to a reduced formation of the SPL. The discrepancy to the larger patterns might be due to the different mask coverage and to the different amounts of previously etched layer materials that could influence the reactor wall coating.
In all cases no RIE lag is observed.

5.4.5. Summary

The profiles etched with a mask of SiO_2 showed the same evolution with decreasing duty cycle as observed for the carbon mask: increased TCER, less faceting and consumption of the mask, more vertical profiles and less differences between open and dense patterns. The reduced consumption of the hard mask can be explained more easily compared to the carbon mask since SiO_2 is etched mostly by physical sputtering. As shown before, the etching becomes more chemical while the physical sputtering is reduced if the duty cycle is lowered.
Two types of micro trenching can be observed, similar to the etching with the carbon mask. Broad trenches are observable for high duty cycles (75 %) and the CW mode, which might be linked to the difference in the collection angle for depositing species from the gas phase. By reducing the duty cycle, less species from the gas phase can oxidize the reactive etch layer or can form a deposition, leading to the disappearance of the broad micro trenching. At low duty cycles ($\lesssim$ 20 %) a localized micro trenching appears during the etch, which could be due to the increased etch yield per ion (ion limited versus radical limited etching), the more vertical sidewalls that focus reflected ions on a very small area, and reduced charging effects.
By studying high frequencies at low duty cycles, an impact of the frequency can be observed. By increasing the frequency above a certain limit that depends on the applied duty cycle, the etch rate increases for both the silicon and the oxide hard mask. This might be linked to an increase in the ion energy. The reason for this effect remains unclear.
A comparison with profiles of smaller dimension shows the same evolution with changing duty cycle. However, the etch result at 1 kHz 10 % shows a stronger micro trenching and a significantly bowed sidewall. The discrepancy is attributed to the change in the mask layout and coverage, and to the different amounts of previously etched layer materials that could influence the reactor wall coating.

5.5. Sidewall Passivation Layer Analysis

One of the most important changes in the profiles that are observed in pulsed conditions is the profile evolution that can be attributed to a changed sidewall passivation layer formation. Oehrlein *et al.* [126] proposed a model of the formation of the sidewall passivation layer. At first, species from the silicon surface that are sputtered at off-normal angles reach the pattern sidewalls in the same state as when they left the etched surface (line-of-sight deposition). Often, these sputtered species are non-volatile, e. g. atomic Si or $SiBr_x$, and they should, therefore, have a high sticking probability. Since the ion bombardment is very limited at the sidewalls, these species remain adsorbed for a relatively long time. Similar species could also be deposited from the gas phase after dissociation of volatile etch products. Reactive oxygen species in the plasma interact with the adsorbed molecules and form oxide rich silicon compounds (formation of SiO_2 is thermodynamically favored). Based on this model, the formation of the SPL can be either limited by the oxygen flux from the gas phase, or by the deposition of non-volatile silicon species. The neutral flux from the gas phase is correlated to the aspect ratio of the pattern (collection angle). The line-of-sight deposition is linked to the sputter angle distribution and the width of the etch surface (trench bottom).
In order to study quasi *in-situ* the chemical composition and the thickness of the SPL, an XPS technique, described in Sec. 2.6.3, was developed in the framework of this Ph.D. thesis [137]. For this purpose, a special pattern with equal line and space width is needed. The pattern from the previous section that was realized by electron beam lithography complies with all necessary requirements.
A quasi *in-situ* analysis is important since bromine could be exchanged by oxygen in the SPL if exposed to the atmosphere [65, 75, 79] or to low pressure conditions where oxygen is present.

5.5.1. Thickness Profiles

The thickness profiles from the SPL analysis are shown in Fig. 5.18 for various trench dimensions in different pulsed (1 kHz, 10 % duty cycle) conditions. In general, the SPL thickness decreases with a larger aspect ratio. It seems **only** to depend on the aspect ratio, but neither on the probed trench depth, nor on the trench width. This also means that it does not (strongly) depend on the exposure time to the plasma. Based on these results, the thickness profiles are considered to be independent of the trench dimensions in the margin of error and averaged profiles are used for comparison between different plasma etch processes.
As explained above, the model given by Oehrlein *et al.* [126] suggests two mechanisms that lead alone or in combination to the formation of the SPL. The flux from the gas phase (radicals or etch products) and a line-of-sight deposition of strongly sticking, non-volatile sputtered species.
Hübner [172] developed an analytical model to describe the deposition on the sidewalls by both processes. In Fig. 5.19 the resulting sidewall passivation thicknesses

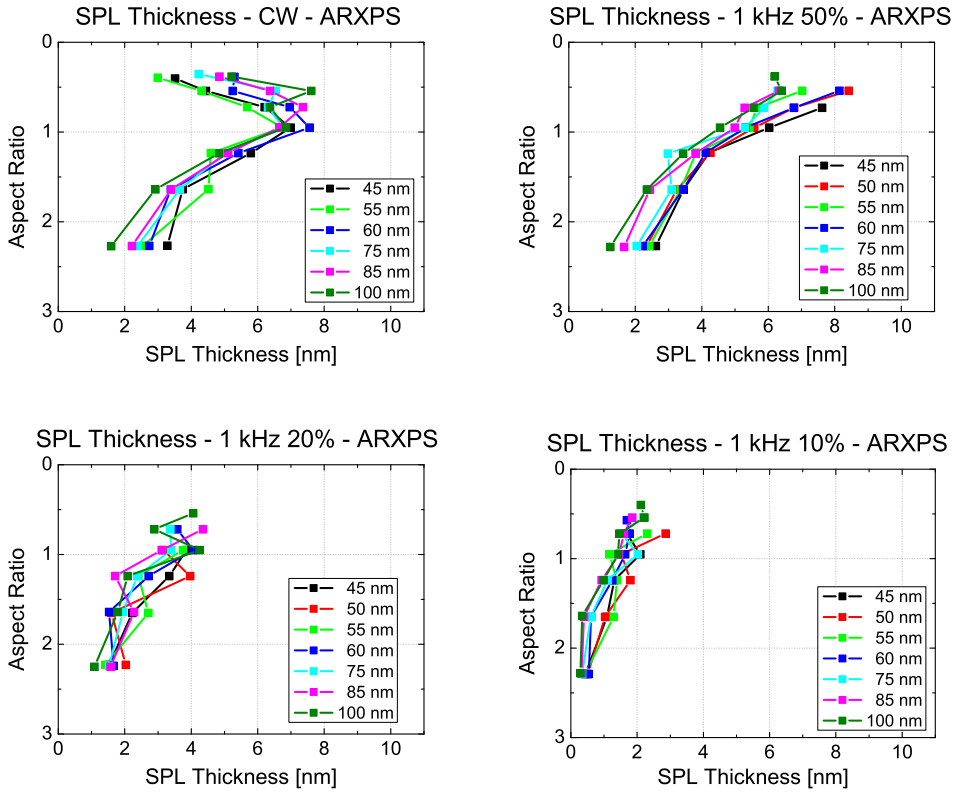

Figure 5.18.: *Sidewall passivation layer analysis: XPS results for pulsed etching.*

are shown for either **only** gas phase deposition or **only** line-of-sight deposition of sputtered etch products. The obtained profiles are very different. For the gas phase deposition, the aspect ratio is the main factor, but a small dependence on the trench width is also visible. The wider the trench is, the thinner is the SPL at a constant aspect ratio since the exposure time to the plasma is reduced in this case. The direct deposition of sputtered species, on the other hand, depends strongly on the trench width. In this case, the SPL thickness is increasing for wider trenches at constant **depth** since more material is removed from the trench bottom and deposited on the sidewalls, seen for small aspect ratios. This deposition mechanism is strongly dependent on the exposure time to the plasma and, therefore, the thickness order of different trench widths inverses by going to higher aspect ratios (= deeper in the trench for large trench dimensions).
While the model for the line-of-sight deposition is very different to the experimental results, the gas phase deposition model resembles the observed thickness profiles to some extend. Therefore, we assume that the formation of the SPL in our conditions is due to a combination of both mechanisms, as it was also proposed by Oehrlein *et al.* [126]: unsaturated, strongly sticking, silicon containing etch products adsorb on the sidewalls and are transformed into a protective layer **only** if they are oxidized by O radicals from the gas phase.

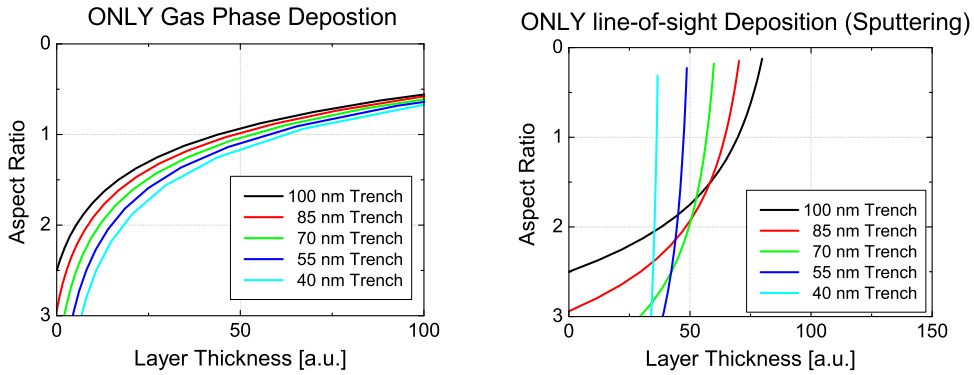

(a) (b)

Figure 5.19.: *Passivation layer thicknesses from model calculations [172] for* ***(a)*** *only gas phase deposition and* ***(b)*** *only line-of-sight re-deposition of sputtered etch products. Trench dimensions are chosen close to reality (depth of 240 nm, different trench widths).*

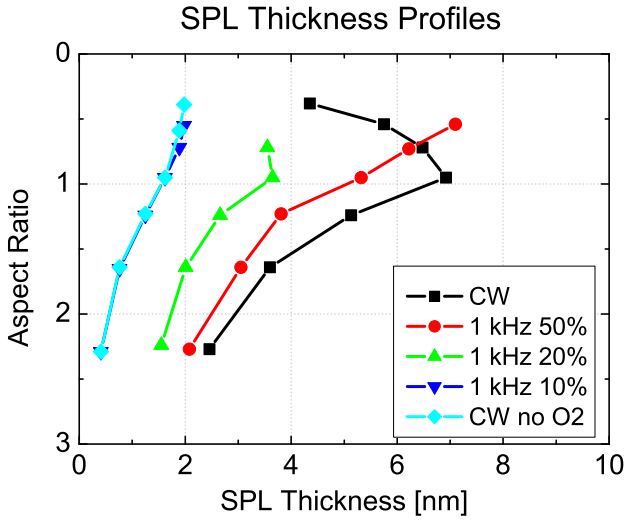

Figure 5.20.: *Average thickness of sidewall passivation layer for different duty cycles and CW mode, with and without O_2.*

Figure 5.20 shows the average SPL thickness profile for various pulsed conditions and for the CW mode with two oxygen flows. For a better visualization, the theoretical error of up to 30 % is not included. With decreasing duty cycle at a constant frequency of 1 kHz, the overall thickness of the sidewall passivation layer decreases significantly. The reduced SPL thickness explains the more vertical etch

profiles and partly the reduced differences between dense and open patterns, as noted in Sec. 5.3. The decrease of the SPL thickness for small aspect ratios (top of the trenches) in CW mode is due to strong mask faceting, leaving the top of the sidewalls less protected by the mask (see Fig. 5.17). Consequently, the top of the SPL is partly eroded, leading to a thinner layer. A similar profile was also found by Detter *et al.* [142]. The SPL for all other profiles decreases continuously towards larger aspect ratios (also 1 kHz 20 %, within the error).
The reduced thickness of the SPL with lower duty cycles could be linked to either a lower time compensated flux of highly sticking silicon species, or to a reduced TC flow of oxygen radicals (or a combination of both). At a lower duty cycle, the TC flux of Br is increased, so that more Br is available on the surface to form volatile etch products. Probably, this reduces the amount of non-volatile etch species in the plasma. In addition, since the overall dissociation in the plasma is reduced, also less etch products are re-dissociated into non-volatile species that can be deposited. Therefore, we suppose that the time compensated flux of highly sticking species will be reduced, even though the TCER is increased.
As explained in Sec. 3.1.1, we expect to see a fast decrease in the O radical density at reduced duty cycles since the $SiBr_xH_y$ layer that forms on the reactor walls could scavenge the radicals from the gas phase. If the production of O is very low, the reduced flux into the pattern is likely to limit the SPL formation. Moreover, the thickness profiles from CW without oxygen and from the pulsed experiment at 1 kHz 10 % are almost identical. This also supports the assumption that oxygen plays a major role in the formation of the SPL in our conditions [127] and that the SPL thickness is limited by gas phase oxidation. A similar result was found for the pattern comparison with different oxygen flows in Sec. 5.3 and 5.4, where the passivation layer was significantly reduced at lower oxygen fluxes.
The evolution of the flux of highly sticking silicon species and the flow of oxygen radicals lead to a decrease in the SPL thickness. However, the reduced oxygen flux probably plays a more important role.

5.5.2. Chemical Composition Profiles

In addition to the SPL thickness, its chemical composition is also analyzed. In Fig. 5.21 the atomic percentage of oxygen in the SPL is shown with respect to the aspect ratio for pulsed etching at 1 kHz 10 %. The amount of oxygen is clearly dependent on the aspect ratio, but the variation is too large to identify any dependence on the trench dimension, similar to the thickness profiles. This is also true for the other elements present in the SPL, namely silicon and bromine, supporting the assumed formation mechanism.
For a comparison between etch conditions, the chemical composition for each aspect ratio is averaged over the range of different trench dimensions. In Fig. 5.22 the mean chemical composition of the SPL is presented without the contribution of the bulk silicon versus the probed aspect ratio. In all conditions a decreasing amount of oxygen and a greater amount of bromine and silicon is observed for an

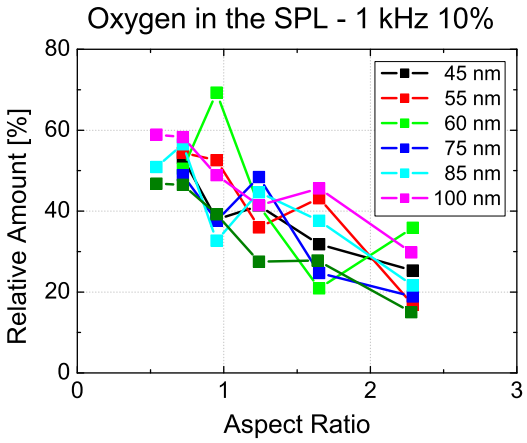

Figure 5.21.: *Percentage of oxygen in the SPL for various trench CDs and aspect ratios for pulsed etching at 1 kHz, 10 % duty cycle.*

increasing aspect ratio. In CW mode without oxygen and at very low duty cycle, this feature is especially pronounced. If no oxygen is added to the gas mixture, oxygen atoms can still be sputtered from the reactor wall (deposited protective layer) or the oxide mask. Nevertheless, the oxygen density is certainly reduced.
For all aspect ratios and in all conditions, the ratio of Si to Br in the SPL is approximately 1, only at a duty cycle of 50 % this ratio is slightly increased. For pulsing at 1 kHz 10 % and for CW mode without O_2 the evolution of the oxygen amount with the aspect ratio is especially pronounced. While the percentage of oxygen at the top (small aspect ratio) is comparable to the other conditions, oxygen represents only 20 % of the chemical composition of the SPL at a high aspect ratio. Probably, this can be attributed to the strong reduction of the oxygen radical flux for low duty cycles. It might still be large enough to oxidize the SPL sufficiently at the top of the trenches where the collection angle is large. Yet, for higher aspect ratios, the radical flux might become very low, reducing the percentage of incorporated oxygen strongly. For higher duty cycles the radical flux could be much larger, so that even at high aspect ratios it furnishes a sufficient amount of oxygen atoms for the SPL formation.

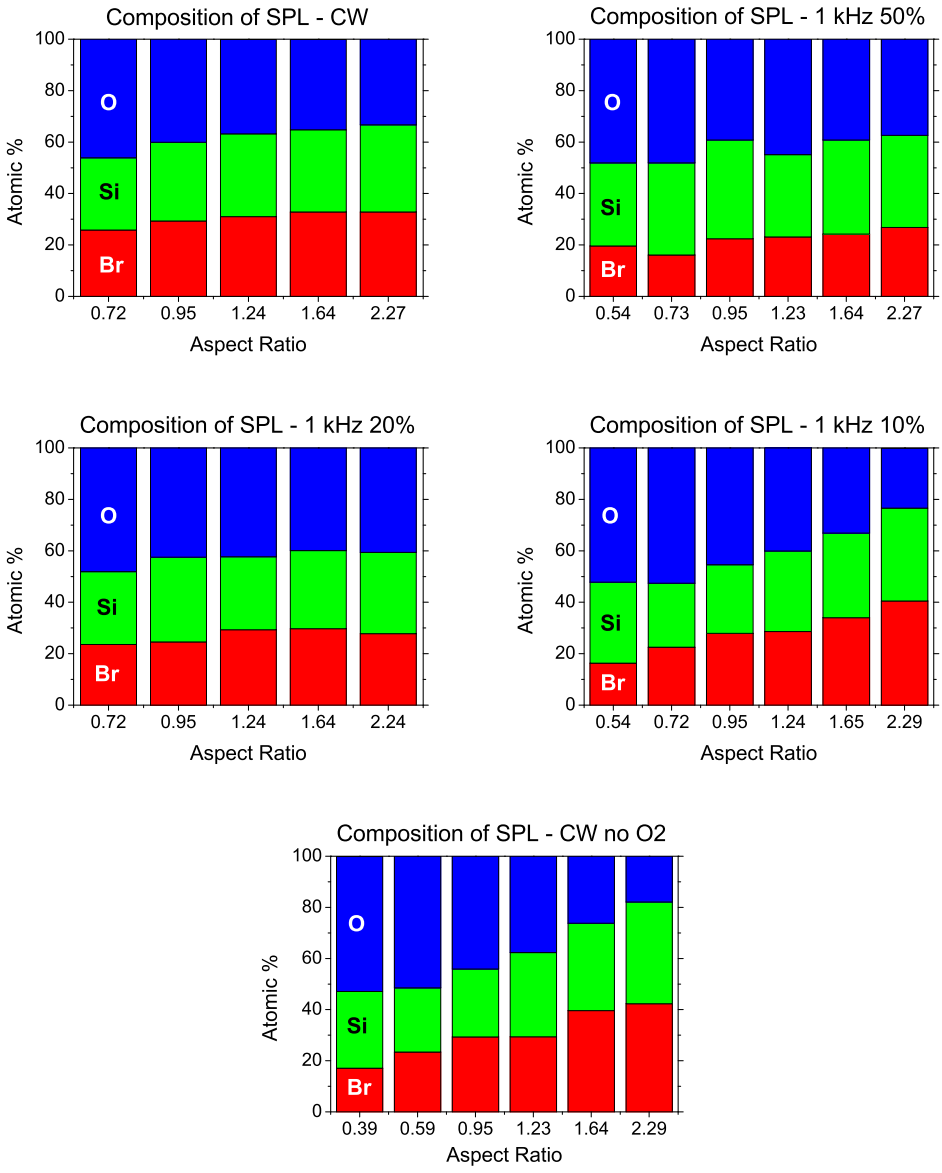

Figure 5.22.: *Sidewall passivation layer analysis - average chemical composition for different duty cycles.*

5.5.3. Summary

With a non-destructive quasi *in-situ* XPS technique, the sidewall passivation layer was studied. The SPL thickness is decreasing with larger aspect ratio. We suppose that it is formed by a combination of the deposition of highly sticking silicon etch products and by a subsequent oxidation by oxygen from the gas phase, the latter playing the limiting role. The strong influence of oxygen is supported by the thin SPL in a pure HBr plasma. By reducing the duty cycle in the HBr/O_2 plasma, a similar reduction of the SPL thickness is observed. This might be linked to a reduced availability of oxygen radicals, but also on a reduced flux of non-volatile Si species due to a greater availability of Br radicals and less re-dissociation of volatile etch products.
The chemical composition of the SPL also indicates that the formation process of the SPL is strongly influenced by the amount of oxygen. At a duty cycle of 10 % and in CW mode without oxygen, the relative amount of oxygen is strongly reduced at high aspect ratios, possibly because of a very much reduced O radical flux. The Si-Br ratio remains almost constant for all conditions.

5.6. General Summary

Pulsed plasma etching of silicon patterns with different masks were investigated with respect to changing pulse parameters. The observed features are explained based on blanket wafer etch rates and the ARXPS quasi *in-situ* analysis of the sidewall passivation layer that strongly influences the pattern profile.
The silicon pattern etching in an HBr/O_2 plasma can be significantly altered by using synchronized pulsing of source and bias power. By reducing the duty cycle, the following profile evolution can be observed and explained:

1. The time compensated etch rate is increased due to a greater availability of etch radicals. Blanket wafer experiments show opposite evolutions of the time compensated etch rates of Si and SiO_2 at a decreasing duty cycle. The results for silicon etching indicate a radical limited etch regime: an increase of the TC radical flux leads to a net increase of radicals available during the etching, explaining in turn the increase in silicon TCER for lower duty cycles.
2. The faceting of the **carbon mask** is reduced, which is probably due to a decreased physical sputtering. This leads to a reduced mask consumption, which outweighs the increased TCER of αC that was observed in the blanket wafer experiments. The lower consumption and faceting of the **oxide mask** can be explained more easily since the etching of SiO_2 is mostly triggered by physical sputtering. The TCER increases slightly for a duty cycle of 75 % and decreases strongly afterwards. As a result, the selectivity between Si and SiO_2 is strongly enhanced. An approximation of the sputtering yield

based on measurements from Sec. 4.2.2 is in very good agreement with the observed behavior.

3. The slope of the etched profile becomes more vertical because of a reduced formation of the SPL. The latter is thought to be controlled by a combination of the deposition of highly sticking silicon etch products and by a subsequent oxidation (by oxygen) from the gas phase, where the latter plays the limiting role. The strong influence of oxygen is supported by the thin SPL observed in a pure HBr plasma. By reducing the duty cycle in the HBr/O_2 plasma, a similar reduction of the SPL thickness is observed. This might be linked to a reduced availability of oxygen radicals, but also on a reduced flux of non-volatile Si species due to a greater availability of Br radicals and to less re-dissociation of volatile etch products.
   The chemical composition of the SPLs indicates that the formation process of the SPL is indeed strongly influenced by the amount of oxygen. At a duty cycle of 10 % and in CW mode without oxygen the relative amount of oxygen is strongly reduced at high aspect ratios, possibly because of a very much reduced O flux. The Si-Br ratio remains almost constant for all conditions.
4. The difference between dense and isolated profiles is reduced. This might also be linked to the reduced formation of the SPL, but also to a more homogeneous distribution of neutral species like, e. g., O.
5. The broad trenches at high duty cycles (75 %) and in the CW mode might be linked to the difference in the collection angle for depositing or oxidizing (etch inhibiting) species from the gas phase. By reducing the duty cycle less species are deposited and the broad micro trenching disappears. The appearance of localized micro trenching in dense patterns, especially at lower duty cycles ($\lesssim 20\,\%$), could be explained by a focusing of scattered ions at almost vertical sidewalls, which increases locally the ion flux. Thus, the etch rate also rises since it is more susceptible to a change of ion flux due to the great availability of Br radicals. Reduced charging effects in pulsed processes might also play a role.

For high frequencies (several kHz) at low duty cycles ($\lesssim 20\,\%$) an impact of the frequency can be observed. By increasing the frequency above a certain limit that depends on the duty cycle, the etch rate increases for both the silicon and the oxide hard mask. This indicates that the ion energy might be increased under these conditions, but the reason for this observation remains unclear.
A comparison with profiles of smaller dimension shows the same evolution with changing duty cycle. However, the etch result at 1 kHz 10 % shows a stronger micro trenching and a significantly bowed sidewall. The discrepancy is attributed to the change in the mask layout and coverage, and to the different amount of etched layers that might influence the reactor seasoning.

6. Discussion on Plasma Pulsing

The impact of plasma pulsing was studied in a model HBr/O_2 etch process of silicon by various means of plasma and surface diagnostics. The plasma itself and the resulting etch profiles are strongly altered by the pulsing. This chapter summarizes the effects of plasma pulsing on the studied process and presents characteristics that we can expect of plasma pulsing in general, including a discussion of the advantages and downsides of plasma pulsing. Finally, an outlook is given.

6.1. Pulsed HBr/O_2 Plasma Etching of Silicon

6.1.1. Impact of Plasma Pulsing on the Gas Phase

The composition of the plasma is strongly dependent on the used gas mixture, the etched surface and the reactor wall surfaces. The main difference between a HBr/O_2 plasma with bias power and a process without is linked to the etching of silicon in the first case. During the process with bias many etch products (Si species) are created that can be found as neutrals or ions in the gas phase. Many of these species are non-volatile and can be re-deposited on the reactor walls, forming a thin layer. This changes the sticking and recombination coefficients, possibly leading to a different balance between radicals and stable molecules, as well as to different ion fluxes. If conditions with and without bias power are compared, this needs to be kept in mind.

Neutrals

In case of the HBr/O_2 plasma without bias, mainly HBr, Br_2, Br and O_2 species are observed. H_2 also seems to be largely present, but the signal to background ratio was too small for a valid measurement, similar as for OH_x species. By reducing the duty cycle the HBr and O_2 densities increase while the amount of Br and Br_2 remains rather constant at first before their density decreases significantly at very low duty cycle. This leads to an increase of the time compensated Br radical flux on the wafer. The most important reason for the increase in the densities of HBr and O_2 might be the change of temperature, but a reduced dissociation also plays a significant role.
If the bias power is applied to a silicon wafer, several Si containing etch products appear in the mass spectrum, namely SiBr, $SiBr_3$ and $SiBr_4$. SiBr follows a similar trend as Br: up to a duty cycle of approximately 50% the density remains constant,

but decreases significantly thereafter. In average, less Si species are found at lower duty cycles, which can be attributed to the reduced average process etch rate and to a formation of larger and more volatile etch products.
Finally, the analysis of pattern etch experiments indicate that for lower duty cycle the amount of oxygen radicals is reduced.

Ions

If no bias is applied to the process, mainly Br_2^+ and H_3O^+, and to a small amount also BrH_{0-2}^+ and Br_3^+ are observed. For several of the observed ions, proton attachment seems to play a role.
In the process with bias power, the composition of the ion flux shows many additional ions that incorporate at least one Si atom. Br_3^+, on the other hand, is not detected any more and also the relative amount of Br_2^+ is rather small. The main contribution of the total ion flux comes from $SiBr^+$, Si^+, $SiBr_3^+$ and BrH_{0-2}^+. Large silicon containing etch products that leave the wafer can easily be ionized and dissociated due to the low energy thresholds for these processes, leading to the observed significant contribution to the ion flux. In addition, the nature of the reactor walls change compared to no-bias conditions, influencing the recombination rates and, hence, also the reaction balance between all species. With lower duty cycle, the relative contribution to the total ion flux of silicon-free ions like BrH_{0-2}^+ increases while the relative amount of silicon containing ions decreases. One should also note that almost no Si^+ can be detected at a very low duty cycle, indicating that almost all silicon is incorporated in larger molecules. In addition, the lower averaged etch rate of Si reduces its overall presence in the plasma.
The double bimodal IEDF in the HBr/O_2 plasma, measured with an RFA on the wafer surface, indicates a significant amount of H^+, which is not detected at the reactor walls. This implicates that in an HBr/O_2 plasma, one of the major ions contributing to the silicon etching is H^+. By reducing the duty cycle, less HBr is dissociated and the H^+ contribution might be reduced. Since hydrogen might penetrate deeply into the surface due to its low mass, a reduction of the duty cycle might help to decrease the plasma induced damage on surfaces. In a pure HBr plasma, no H^+ is observed. The reason for the (dis-)appearance of H^+ is probably linked to the different composition of the plasma and/or to the changed nature of the reactor walls.
For pulsed mode, the IEDFs shows a high and a low energy peak, which correspond to the ions from the on- and the off-time of the plasma, respectively. If the duty cycle is reduced the total ion flux decreases linearly and the high energy peak shifts to even higher energies. At the same time, the relative contribution from the high energy peak to the total ion flux is strongly reduced, leading to an overall decreased averaged ion energy.

6.1.2. Impact of Plasma Pulsing on Silicon Etching

Reactive Etch Layer

With decreasing duty cycle, the REL thickness is reduced, which is linked to the increased relative radical flux (compared to the ion flux) and the reduced mean ion energy: Br radicals accumulate on the etch surface, also during the off-time, and increase thereby the removal rate of amorphous silicon from the REL. The lower ion energy decreases the amorphization rate of the silicon bulk. The new balance between both processes leads to a reduced REL thickness. Therefore, by pulsing the plasma, the surface damage is reduced with a simultaneous increase of the TCER of silicon.

Etch Rates and Selectivity

The low dependence of the silicon etch rate on the ion energy (bias power) indicates a rather radical limited etch regime. The higher TC radical flux at a reduced duty cycle leads to an **increase** of the Si TCER. On the other hand, the lower sputtering ability of the ions leads to **decrease** in SiO_2 TCER. As a result, the selectivity between Si and SiO_2 is strongly enhanced. The TCER of αC is slightly increased, probably for similar reasons as for silicon. Since the Si TCER evolves faster than the αC TCER, the selectivity is also slightly increased.

Profile Etching

By reducing the duty cycle, the following profile evolution is observed:

1. The time compensated etch rate of silicon is enhanced due to an increased availability of etch radicals.
2. The faceting of the **carbon mask** is reduced, which could be attributed to the reduced physical sputtering. The lower consumption and faceting of the **oxide mask** can be explained more easily since SiO_2 is etched mostly by physical sputtering, which is reduced for lower duty cycles.
3. The slope of the etched profile becomes more vertical. Similar to a decrease of the oxygen flow, the formation of the sidewall passivation layer is minimized, as explained below.
4. The difference between dense and isolated profiles is smaller. This might also be linked to a reduced formation of the SPL, but also to a more homogeneous distribution of neutral species like, e. g., O.
5. The broad trenches at high duty cycles (75 %) and in the CW mode might be linked to the difference in the collection angle for depositing and oxidizing species from the gas phase that inhibit the silicon etching. By reducing the duty cycle less species are deposited and the O radical flux is reduced, leading to the disappearance of the broad micro trenching. At low duty cycles ($\lesssim$ 20 %) a localized micro trenching appears, which could be due to

the more vertical sidewalls that focus reflected ions on a very small area combined with the increased etch yield per ion.

Summarized, the silicon TCER, the selectivity (towards SiO_2 and αC) and the homogeneity are enhanced. Moreover, the pattern profile can be controlled via the SPL formation by the duty cycle without the drawbacks of an oxygen reduction in the gas flow.
By increasing the frequency above a certain limit that depends on the duty cycle the etch rate increases for both the silicon and the oxide hard mask, indicating that possibly the ion energy is increased under these conditions. The reason for this observation remains unclear.
A comparison with profiles of smaller dimension shows the same evolution with changing duty cycle. However, the etch result at 1 kHz and 10 % duty cycle shows a stronger micro trenching and a significantly bowed sidewall. The discrepancy is attributed to the change in the mask layout, mask coverage and to the different amounts of previously etched layer materials that could influence the reactor wall coating.

Sidewall Passivation Layer

The SPL thickness is probably controlled by a combination of line-of-sight etch product deposition and gas phase oxidation: non-volatile Si species adsorb on the sidewalls and are subsequently oxidized by O radicals. Thus, without oxygen in the gas mixture, the SPL thickness is strongly reduced due to the smaller amount of oxygen radicals that can fix the deposited species on the sidewalls to build up the SPL. By decreasing the duty cycle in an HBr/O_2 plasma, a similar evolution is observed. This might as well be linked to a reduced availability of oxygen radicals, but also on a lower amount of non-volatile Si species. The latter is assumed since more Br radicals are available during the etching to form volatile species and less re-dissociation occurs during pulsing at low duty cycles. Surprisingly, the SPL thickness almost only depends on the aspect ratio in the trenches and not significantly on the exposure time.
The chemical composition of the SPLs support the assumed formation process. At a duty cycle of 10 % and in CW mode without O_2 the relative amount of oxygen in the SPL is strongly reduced at high aspect ratios, possibly because of a very limited O flux.
Similar to the effect of pulsing, the modification of the O_2 flow in CW mode can be used to obtain a thinner SPL. However, in CW mode, this layer does not efficiently prevent lateral etch. Pulsing on the other hand can be used to obtain almost vertical profiles in a highly selective process.

6.1.3. Open Questions to be Investigated

The presented results from the investigation on pulsed HBr/O_2 plasma etching of silicon patterns have shown the impact of plasma pulsing on the gas phase and the etched surface. Although most of the observed features can be explained, some open questions remain and could be addressed in future experiments to verify the proposed hypotheses:

1. **What role does hydrogen play in the process and how does it change with respect to the pulse parameters?**
   Since the only data on hydrogen is obtained from the RFA measurements, we cannot give any definite statement on the role of hydrogen in the plasma and how its density evolves with the pulse parameters. Thus, it seems necessary to verify the experimental data and to find a way to measure the amount of hydrogen in the plasma.

2. **Is the amount of oxygen radicals in the plasma really reduced with the duty cycle?**
   Compared to hydrogen, we have even less direct information on the oxygen radical. Nevertheless, the presented results for the pattern etching indicate a decrease of its density for lower duty cycles. This needs to be verified to confirm the drawn conclusions.

3. **How can we explain the influence of the frequency?**
   The reason for the impact of the pulse frequency on the gas phase and the pattern etching remains unclear. One problem of the study of high frequencies and low duty cycles is the increased difficulty of the impedance matching that might affect the plasma properties.

6.2. General Characteristics of Pulsed Plasmas

Neutrals

By decreasing the duty cycle, the average input power is also reduced. This leads to a reduction of the gas temperature and subsequently to a rise in the neutral gas density if the pressure is held constant during the process. Consequently, the total neutral flux towards the wafer will be increased. A similar effect might be achievable by increasing the overall pressure or decreasing the source power, but in these cases, the plasma characteristics will also change significantly.
At the same time, the averaged degree of dissociation is reduced. During the on-time, the dissociation does not reach a constant value compared to the CW mode if the frequency is high enough ($\sim$ 1 kHz). During the off-time the dissociation becomes negligible and only recombination and other loss processes occur. In low pressure discharges most of the chemical reactions take place on the surface of the reactor walls. Depending on the recombination rates and the sticking coefficients

of the species on the surface, as well as on the temperature change of the plasma, the average concentration of dissociation products can evolve differently compared to the reduced duty cycle. In the present case, the Br radical density is observed to remain constant at first for decreasing duty cycles while the oxygen radical density might possibly decrease faster (in etch conditions) due to a high sticking coefficient on the reactor walls.
Above a certain frequency of approximately 1 kHz, the modulation in the density during a pulse becomes rather small for neutral species and average values can be used to describe the plasma. This does not necessarily hold for ions since their characteristic loss time is significantly smaller.

Ions

The ionization in a pulsed plasma only occurs during the on-time. Similar to the dissociation, the ion density in the plasma needs a certain time to obtain a constant value. During the off-time ions are lost to all the surfaces exposed to the plasma (mainly the chamber walls). Hence, it is not surprising that the average ion flux decreases more than proportionally to the duty cycle, as it was also found for the HBr/O_2 plasma. In this particular plasma, the ion flux at a frequency of 1 kHz does not decrease to zero, even at a duty cycle of 10 %. The relative contribution of the flux from the on-time to the total flux is also proportional to the duty cycle. Consequently, the absolute ion flux from the on-time decreases roughly by the square of the duty cycle.
During the off-time, the sheath between the wafer and the plasma collapses and following ions have strongly reduced energies. Considering a plasma process with applied bias power, the kinetic energy from ions during the on-time is increased for lower duty cycles since the ion flux is reduced (see Eq. 1.4).
Hence, compared to CW mode, the majority of the ions have much lower energies at reduced duty cycles while the few ions from the on-time have higher energies. In average, the ion energy is significantly reduced.

Combined Effects

The strong decrease of the ion flux at lower duty cycle, especially of ions with high energies, reduce the time compensated yield of physical sputtering (see Fig. 5.7). At the same time, the time compensated radical flux increases (see Fig. 5.4 b). Together, the character of the plasma etching becomes more chemical and less physical, at least in the studied range of conditions.

Depending on the used gas chemistry the consequences of pulsing for the plasma process can be different and have to be analyzed individually.

6.3. Potential of Plasma Pulsing

6.3.1. Advantages of Pulsed Plasmas

Plasma pulsing offers new ways to improve existent etch processes and opens up new domains of plasma etching. In comparison to the CW mode, pulsing (in the analyzed parameter range) introduces several features:

1. Less plasma induced damage
2. Enhanced chemical character of the plasma process
3. Reduced average degree of dissociation
4. Lower plasma (gas) temperature at similar radical densities

Reduced Plasma Induced Damage

Plasma processes always induce surface damage like amorphization due to the bombardment of ions that have energies equivalent to the floating sheath potential ($\gtrsim 15\,\mathrm{eV}$). By using pulsed plasmas the mean energy of the ions can be reduced and less damage is inflicted, especially if no bias power is applied.

Enhanced Chemical Etching

The increased chemical component of the etching offers a possibility to etch highly selectively between materials that are etched by different mechanisms, as it is the case, e. g., for Si and SiO_2 in the presented process chemistry. Moreover, since the duty cycle can control the ratio of time compensated radical to ion flux in certain processes, the change in chemical character can possibly be used to tune, e. g., the sidewall passivation layer and consequently the pattern profiles.

Reduced Average Degree of Dissociation

Since the dissociation in pulsed plasmas only occurs during the on-time of the plasma, the average dissociation is reduced in pulsed plasmas, affecting the etching in various ways. In the here presented case, the reduced dissociation and deposition can be used to control the pattern etch slope due to their influence on the thickness of the sidewall passivation layer. For other processes in which the selectivity between materials is achieved by selective deposition of radical molecules [173], a reduced deposition rate could lead to selectivity loss.

Lower Plasma Temperature

At lower duty cycle, the plasma temperature is reduced. At the same time, we have found that the average radical density does not change dramatically until a certain duty cycle is reached. For heat sensitive surfaces that need to be exposed to radical fluxes, pulsed plasmas could give an advantage, similar to plasma diffusion

chambers. Thus, plasma pulsing can be used to render a standard etch chamber to a more polyvalent tool.

6.3.2. Disadvantages of Plasma Pulsing

Several drawbacks have to be weighed against the advantages of pulsed plasmas for each process of interest. First of all, the average etch rate usually decreases, although this is not the case for **all** processes and pulse conditions [50]. Therefore, plasma pulsing mainly targets damage sensitive processes where the etch rate is only of minor importance, as it is the case, e. g., in over-etch processes.
One of the existing problems that also needs to be addressed in the future is the difficulty to achieve a decent matching between the plasma impedance and the power generator. Since the plasma has a very transient character, the impedance matching network needs to adapt very fast. Several techniques have been developed so far, including an automatic sweep of the frequency of the power supply, but nevertheless the usable duty cycles and frequencies are limited.

6.4. Outlook

This section discusses the application of the presented results in various plasma processes and gives an outlook on the possibilities to improve plasma pulsing further.

Possible Applications of Pulsed Plasmas

Based on the (dis-)advantages of plasma pulsing presented in the previous section, some processes can be identified where, e. g., plasma induced damage needs to be minimized. Petit-Etienne *et al.* [48] have demonstrated how the silicon recess during gate etching of the transistor pattern can be reduced. "Silicon recess" is the loss of silicon due to oxidation under a thin oxide etch stop layer. Another possible application of pulsed plasmas is the damage free etch stop on a graphene layer, which is of great interest for future graphene electronics.
Pulsed plasmas also offer a way to modify the chemical character of a plasma process. This could be used to modify the formation of the passivation layer in critical etch steps or to control precisely the change in pattern dimensions between etch steps.

Embedded Pulsing

One way to further improve plasma pulsing might be the concept of embedded pulsing. In this case, the bias power is applied just after the source power in each pulse. Moreover, just before the source power is switched off, the bias power is already cut off. The strong ion energy and the low ion flux from the beginning in synchronous pulsing can be removed. Possibly, this could reduce the mean ion

energy even more while the ion flux would not change considerably compared to synchronous pulsing.

7. Conclusion

This Ph.D. thesis is focused on the impact of plasma pulsing on the etching characteristics of silicon. Based on a model HBr/O_2 plasma, the evolution of the plasma properties, the plasma-surface interactions and the impact on the profile of etched silicon patterns was presented with respect to pulsing at different frequencies and duty cycles.

The characterization of plasma properties was accomplished by using various diagnostic systems, such as mass spectrometry, an ion energy probe, an ion flux probe, and UV absorption spectroscopy. A complete protocol for reliable mass spectrometry measurements of ions and neutrals was developed, including reference measurements for possible process drifts and a calibration for the mass dependent transmission function.
The plasma-surface interactions were studied by X-ray photoelectron spectroscopy (XPS). In addition to the analysis of the reactive etch layer (REL) on the wafer surface, a new technique was developed, based on angle resolved XPS, to determine the profile of the sidewall passivation layer (SPL) and its composition on silicon patterns. Depending on the detection angle, different areas of the sidewall of patterned structures can be probed. Using two consecutive angles the composition and thickness of the SPL can be calculated for the additionally probed area.

The thesis is divided into three parts. The first part is focused on the impact of the pulse parameters on an HBr/O_2 plasma without bias power (no material is etched). Mass spectrometry showed that mainly HBr and, to a small extent, also Br_2 contribute to the total neutral density. H_x and OH_x could not be measured. With lower duty cycle, the total density of neutrals increases, which is mainly attributed to the decrease in gas temperature in pulsed plasmas. Furthermore, the results indicate a decreased dissociation of the source molecules HBr and O_2 with lower duty cycle due to the lower time-averaged plasma power and the increased time for recombination. In contrast to the duty cycle, the frequency has little impact on the densities.
Mass spectrometry analysis of the ions show that the dominant ions are H_3O^+, Br_2^+, BrH_{0-2}^+, $Br_2H_{0,1}^+$ and Br_3^+ when no silicon is etched. The first two ion species dominate the rest, although neutral HBr represents by far the most common neutral molecule in the plasma. By reducing the duty cycle, the percentage of Br_2^+ in the ion flux increases while the total ion flux decreases. Moreover, the average ion flux from only the on-time of the plasma decreases even by approximately the square of the duty cycle, indicating that the amount of energetic ions

per on-time can be decreased in pulsed plasmas.

In the second part, the impact of silicon etching on the plasma characteristics is shown. The spectrum of neutrals detected by mass spectrometry is enlarged compared to the case without bias power by etch products like atomic silicon or molecular $SiBr_x$. At a low duty cycle, more HBr is found, but less other molecules, which can be explained by a reduced degree of dissociation and a lower etch rate. For frequencies above approximately 1 kHz the modulation of the neutral density during a pulse becomes small enough to compare time averaged values.
Compared to a plasma without bias, the composition of the ion flux, dominated by $SiBr^+$, Si^+, $SiBr_3{}^+$ and $BrH_{0-2}{}^+$, shows many additional species that incorporate silicon. $Br_3{}^+$, on the other hand, is not detected any more and the percentage of $Br_2{}^+$ is almost negligible. Furthermore, retarding field analyzer measurements indicate a great amount of H^+ when oxygen is added to a pure HBr plasma. With lower duty cycle the relative contribution of $BrH_{0-2}{}^+$ increases while almost no Si^+ can be detected any more, indicating that almost all silicon is incorporated in larger molecules. An increase in frequency, especially for low duty cycles, results in a reduction of the total ion flux, similar to a further (slight) decrease in duty cycle.
The IEDFs in pulsed mode show a high and a low energy peak, which correspond to the ions from the on- and the off-time of the plasma, respectively. If the duty cycle is reduced, the total ion flux decreases linearly, the high energy peak shifts to higher energies and the relative contribution from the latter to the total ion flux is reduced. This leads to a decrease of the mean ion energy, possibly reducing ion induced surface damage.
With lower duty cycle the REL thickness decreases due to an increased availability of radicals and a decreased mean ion energy. The frequency does not have a significant influence on the REL thickness.

The last part of the thesis examines the impact of HBr/O_2 plasma pulsing on silicon pattern etching, which can be significantly altered by using synchronized pulsing of source and bias power. By reducing the duty cycle, the following profile evolution can be observed and explained:

1. The radical limited, time compensated etch rate of silicon is enhanced. An increase of the time compensated radical flux leads to a net increase of radicals available during the etching.
2. The faceting and consumption of the mask is reduced due to a decreased physical sputtering.
3. The slope of the etched profile becomes more vertical due to a reduced formation of the sidewall passivation layer (SPL). Its formation is controlled by a combination of the deposition of highly sticking silicon etch products and by a subsequent oxidation by O radicals from the gas phase, where the latter plays the limiting role.

4. The difference between dense and isolated profiles is smaller. This might be linked to a reduced formation of the SPL, but also to a more homogeneous distribution of neutral species like, e. g., O.
5. The broad trenches at high duty cycles and in the CW mode decrease. In contrast, localized micro trenching in dense patterns occurs, especially at lower duty cycles, which is linked to a localized focusing of reflected ions at almost vertical sidewalls and to a higher ion sensitivity of the etch rate.

By increasing the frequency above a certain limit that depends on the duty cycle, the etch rate increases for both the silicon and the oxide hard mask, indicating that the ion energy is increased under these conditions. However, the reason for this observation remains unclear.

Based on these results, general conclusions were presented on plasma pulsing: e. g. the degree of dissociation and the mean ion energy are reduced at low duty cycles.
Characteristics that offer an application in future processes are the decrease of plasma induced damage, the enhanced chemical character, the reduced average degree of dissociation and the lower plasma temperature. Possible applications are damage sensitive processes like gate etching or the etch stop on graphene.

Conclusion en français

Dans le présent travail, nous avons étudié l'impact des plasmas pulsés sur les caractéristiques de la gravure du silicium. Le rôle de la fréquence de pulsation et du rapport cyclique sur l'évolution des propriétés du plasma, les interactions plasma-surface et l'impact sur le profil des structures gravées dans le silicium ont été présentés dans le cas d'un plasma model de HBr/O_2.

La caractérisation des propriétés du plasma a été réalisée en utilisant divers systèmes de diagnostic, tels que la spectrométrie de masse, une sonde d'énergie des ions, une sonde de flux d'ions, et la spectroscopie d'absorption UV. Un protocole complet pour des mesures fiables de spectrométrie de masse pour les ions et les neutres a été développé, comprenant des mesures de référence pour prendre en compte les dérives éventuelles des mesures et un processus d'étalonnage pour l'évaluation de la fonction de transmission qui dépend de la masse des espèces.

Les interactions plasma-surface ont été étudiées par la spectrométrie de photo électrons des rayons X (XPS). En plus de l'analyse standard de la couche réactive de la gravure sur la surface du substrat, une nouvelle technique a été développée sur la base de l'XPS résolu en angle pour déterminer le profil et la composition de la couche de passivation des flancs (SPL) des structures gravées dans le silicium. Selon l'angle de détection, différentes parties de la paroi latérale des motifs peuvent être sondées. En comparant l'analyse à deux angles consécutifs, la composition et l'épaisseur de la SPL peuvent être calculées pour la partie qui est sondée entre ces deux angles.

La thèse est divisée en trois parties. La première partie se concentre sur l'impact des paramètres de modulation sur un plasma de HBr/O_2 sans polarisation additionnelle du substrat (aucun matériau n'est gravé). La spectrométrie de masse a montré que principalement HBr et, dans une moindre mesure, également Br_2 contribuent à la densité totale des neutres. Les espèces H_x et OH_x ne peuvent pas être mesurées avec notre système du fait d'une alimentation du quadrupole inadaptée ou d'un trop faible rapport signal sur bruit. Avec un rapport cyclique bas, la densité totale des neutres augmente, ce qui est principalement attribué à la diminution de la température moyenne du plasma. En outre, les résultats indiquent que la dissociation d'HBr et O_2 diminue en raison de la puissance moyenne réduite du plasma et de l'augmentation du temps de recombinaison. Contrairement au rapport cyclique, la fréquence a peu d'impact sur la densité des espèces neutres. L'analyse par spectrométrie de masse des ions montre que les ions domi-

nant sont H_3O^+, Br_2^+, BrH_{0-2}^+, $Br_2H_{0,1}^+$ and Br_3^+ si le silicium n'est pas gravé. Les deux premières espèces dominent le reste, bien que HBr soit l'espèce neutre de loin la plus présente dans le plasma. En réduisant le rapport cyclique, le pourcentage de Br_2^+ dans le flux d'ions augmente tandis que le flux d'ions total baisse. De plus, le flux d'ions moyen provenant du temps ON diminue comme le carré du rapport cyclique, ce qui indique que la quantité d'ions énergétiques par temps ON est fortement réduite dans les plasmas pulsés à faibles rapports cycliques.

Dans la deuxième partie, l'impact de la polarisation du substrat et de la gravure du silicium sur les caractéristiques du plasma est analysé. Le spectre des neutres détectés par spectrométrie de masse est fortement élargi lorsque le substrat est gravé. Les produits de la gravure tels que le silicium atomique ou le $SiBr_x$ moléculaire sont responsables de l'élargissement du spectre. Avec un rapport cyclique faible, la proportion de HBr augmente, ce qui peut être expliqué par un taux de dissociation réduit et une vitesse de gravure plus faible. Pour les fréquences supérieures à environ 1 kHz la modulation de la densité des neutres pendant une période de pulse devient suffisamment petite pour pouvoir comparer les valeurs moyennes.
La composition du flux d'ions est dominée par $SiBr^+$, Si^+, $SiBr_3^+$ et BrH_{0-2}^+ lorsque le silicium est gravé, et de nombreuses autres espèces contenant du silicium sont également présentes sous forme d'ions. L'ion Br_3^+, d'autre part, n'est plus détecté et le pourcentage de Br_2^+ est presque négligeable.
En outre, les mesures de l'énergie des ions avec un analyseur électrostatique multigrilles indiquent une grande quantité de H^+ lorsqu'on ajoute de l'oxygène à un plasma de HBr. La contribution relative de BrH_{0-2}^+ augmente tandis que les ions Si^+ ne sont presque plus détectés lorsque le rapport cyclique diminue, ce qui suggère que la quasi-totalité du silicium gravé est incorporée dans des molécules plus grandes. Une augmentation de la fréquence, en particulier pour des rapports cycliques faibles, réduit le flux d'ions total, comme le ferait une (légère) diminution du rapport cyclique.
Les fonctions de distribution de l'énergie des ions (IEDF) en mode pulsé montrent deux pics à haute et à faible énergie qui correspondent respectivement aux ions du temps ON et du temps OFF du plasma. Lorsque le rapport cyclique diminue, le flux d'ions total diminue de façon proportionnelle, le pic de haute énergie se déplace à des énergies plus élevées et la contribution relative de ce pic au flux total est réduite. Ceci conduit à une diminution de l'énergie moyenne des ions, ce qui peut réduire l'endommagement de la surface.
Avec un rapport cyclique faible, l'épaisseur de la couche réactive de la gravure (REL) diminue en raison d'une disponibilité accrue de radicaux et d'une réduction de la puissance déposée par les ions (énergie moyenne des ions plus faible). La fréquence n'a pas une influence significative sur l'épaisseur de la REL.

La dernière partie de la thèse examine l'impact du plasma de HBr/O_2 pulsé sur la gravure des motifs de silicium qui peut être significativement modifiée par

l'utilisation des plasmas synchronisés (source et polarisation). En réduisant le rapport cyclique, l'évolution suivante du profil peut être observée et expliquée :

1. La vitesse de gravure du silicium en temps compensé, limitée par la disponibilité des radicaux, augmente. Une augmentation du flux de radicaux en temps compensé conduit à une augmentation nette de la quantité de radicaux disponibles lors de la gravure.
2. Le facettage et la consommation du masque sont réduits, ce qui est dû à une diminution de la pulvérisation physique.
3. La pente des profils gravés devient plus verticale, ce qui est attribué à une réduction de l'épaisseur de la couche de passivation sur les flancs. Sa formation est contrôlée par une combinaison du dépôt des produits de la gravure de silicium avec une probabilité de collage très élevée et par une oxydation ultérieure par des radicaux O de la phase gazeuse, ce dernier étant le facteur limitant.
4. La différence entre les profils denses et isolés est réduite. Ceci est également attribué à la réduction de l'épaisseur des couches de passivation, mais également à une répartition plus homogène des espèces neutres comme l'oxygène radicalaire.
5. Les micro-tranchées larges aux pieds des motifs, observées aux rapports cycliques élevés et en plasma continu, sont réduites. Par contre, des micro-tranchées très localisées se forment dans les motifs denses, en particulier à des rapports cycliques faibles, ce qui est lié à la focalisation localisée des ions réfléchis sur les flancs verticaux des tranchées, et à une plus forte sensibilité de la vitesse de gravure aux ions.

En augmentant la fréquence au-dessus d'une certaine limite qui dépend du rapport cyclique, la vitesse de gravure augment à la fois pour le silicium et pour le masque dur d'oxyde, indiquant que l'énergie des ions augmente dans ces conditions. Cependant, la raison de cette observation reste incertaine.

Sur la base de ces résultats, des conclusions générales ont été présentées pour les plasmas pulsés. Le taux de dissociation et l'énergie moyenne des ions sont réduits lorsque le plasma est pulsé à faible rapport cyclique. La diminution de l'endommagement provoqué par le plasma, le caractère chimique accru de la gravure, le taux de dissociation moyen réduit et la réduction de la température du plasma rendent les plasmas pulsés intéressant pour les procédés nécessitant une gravure ayant un très faible impact sur les couches d'arrêt. Ceci peut être le cas pour la gravure de la grille des transistors ou pour l'arrêt de la gravure sur des couches très fines comme du graphène.

Appendices

A. Résumé en français

La réduction constante de l'échelle des circuits intégrés impose des exigences croissantes sur les procédés plasmas en termes d'homogénéité de gravure, de contrôle dimensionnel des profils, d'endommagement des surfaces des matériaux à graver, de vitesse de gravure et enfin de reproductibilité. L'endommagement induit en surface devient notamment difficile à contrôler dans la mesure où les déformations des profils et les altérations de surface deviennent de moins en moins tolérables. Actuellement, les méthodes traditionnelles d'optimisation des procédés pour répondre aux exigences croissantes atteignent leurs limites. De nouvelles stratégies pour surmonter ces facteurs limitant sont nécessaires et des approches innovantes sont en cours d'élaboration. L'une d'elles est l'utilisation de plasmas pulsés.

Dans le cadre de cette thèse un plasma de HBr/O_2 pulsé dédié à la gravure du silicium est étudié. Nous nous sommes focalisés sur l'impact des paramètres de modulation, c'est à dire le rapport cyclique et la fréquence, sur les caractéristiques du plasma, les interactions plasma-surface ainsi que sur les profils des motifs gravés. Toutes les expériences sont réalisées dans une chambre de plasma à couplage inductif commercialisée par Applied Materials et dédiée à la gravure des substrats 300 mm. Elle a été modifiée pour utiliser plusieurs systèmes de diagnostic *in-situ*, et notamment la spectrométrie de masse des ions et des neutres, la spectrométrie d'absorption UV, une sonde de flux d'ions, une sonde d'énergie des ions, et la spectrométrie de photoélectrons des rayons X quasi *in-situ*. Les motifs gravés sont caractérisés par microscopie électronique à balayage.

Le résumé suivant de la thèse présente les effets de pulser un plasma sur le procédé étudié et présente les caractéristiques générales d'un plasma pulsé. En outre, les avantages et désavantages de pulser les plasmas de gravure sont discutés. Finalement, quelques perspectives pour les procédés pulsés sont données.

A.1. La gravure du silicium en plasma de HBr/O2 pulsé

A.1.1. Impact de pulser le plasma sur la phase gazeuse

La composition du plasma dépend fortement du mélange des gaz, du matériau gravé et des parois du réacteur. La différence majeure entre un plasma de HBr/O_2 avec et sans polarisation additionnelle du substrat est la gravure du silicium dans le premier cas. Dans cette situation, beaucoup de produits de gravure à base de silicium sont créés et sont détectés dans la phase gazeuse sous forme d'espèces neutres ou ionisées. Un grand nombre d'entre elles sont peu volatiles et peuvent être redéposées sur les parois du réacteur en formant une couche fine. Ceci peut changer les coefficients de collage et de recombinaison des espèces, ce qui conduit à une modification de l'équilibre entre les radicaux et les molécules, ainsi qu'à une modification du flux d'ions. Il faut donc garder ces changement en tête lorsqu'on compare des conditions avec et sans polarisation additionnelle du substrat.

Neutres

Dans le cas d'un plasma de HBr/O_2 sans polarisation du substrat, on observe principalement les espèces HBr, Br_2, Br et O_2 par spectrométrie de masse (Fig. A.1). Le dihydrogène (H_2) semble fortement présent mais le rapport signal sur bruit est trop faible pour obtenir des mesures valides. Ceci est également vrai pour les espèces OH_x. En réduisant le rapport cyclique, les densités de HBr et d'O_2 augmentent alors que la quantité de Br et de Br_2 reste plutôt constante pour des rapports cycliques supérieurs à 20 % et diminue très significativement pour des rapports cycliques plus faibles. La variation de la densité de HBr et O_2 est principalement expliquée par une diminution de la température du plasma. La plus faible dissociation lorsque le plasma est pulsé, particulièrement à des rapports cycliques faibles, participe également à l'augmentation de la densité de HBr et O_2.

Lorsque le substrat est polarisé, plusieurs produits de gravure contenant du silicium apparaissent dans le spectre de masse, notamment SiBr, $SiBr_3$ et $SiBr_4$. La molécule SiBr suit une évolution similaire à celle de Br : pour un rapport cyclique supérieur à environ 35-50 %, la densité reste constante, alors qu'elle baisse fortement pour des rapports cycliques plus faibles. En général, plus le rapport cyclique est faible, moins on observe d'espèces contenant du silicium, ce qui est attribué à une réduction de la vitesse de gravure moyenne.

En outre, l'analyse des expériences de la gravure des motifs indique une quantité réduite de l'oxygène radicalaire à des rapports cycliques faibles.

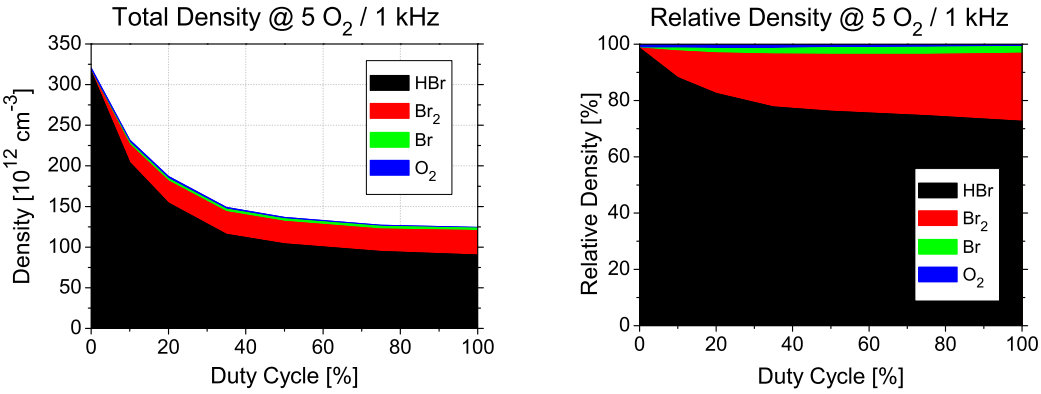

(a) (b)

Figure A.1.: *Ensemble des densités de toutes les espèces neutres mesurés* ***(a)*** *à une échelle absolue et* ***(b)*** *une échelle relative.*

Ions

Le flux d'ions en plasma HBr/O_2 sans polarisation du substrat est principalement constitué de Br_2^+ et de H_3O^+, et dans une moindre mesure de BrH_{0-2}^+ et de Br_3^+ (Fig. A.2). L'attachement des protons semble jouer un rôle important dans la formation de plusieurs des espèces observées.

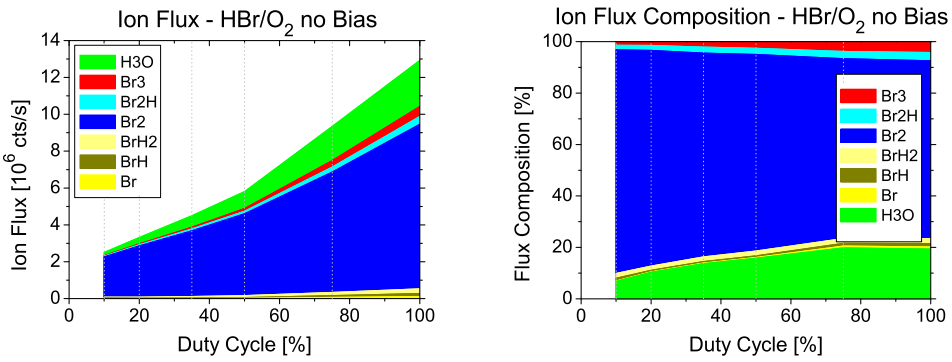

(a) (b)

Figure A.2.: ***(a)*** *Flux total d'ions d'un plasma HBr/O_2 sans polarisation du substrat et* ***(b)*** *sa composition relative.*

Lorsque le substrat est polarisé, le plasma contient beaucoup d'ions additionnels contenant au moins un atome de silicium. En revanche, Br_3^+ n'est plus détecté. La contribution majoritaire au flux d'ions vient de $SiBr^+$, Si^+, $SiBr_3^+$ et BrH_{0-2}^+ (Fig. A.3). Contrairement à un plasma sans polarisation du substrat, le pourcentage de Br_2^+ est faible. Ceci peut être expliqué par des conditions de parois du réacteur différentes qui influencent la composition globale du plasma. Avec un rapport cyclique plus faible, la contribution relative de BrH_{0-2}^+ au flux d'ions augmente. En même temps Si^+ n'est presque plus détecté à des rapports cycliques très faibles. Ceci semble indiquer que le silicium est principalement incorporé dans des molécules plus larges. De plus, la diminution de la vitesse de gravure moyenne du silicium à faible rapport cyclique réduit également sa présence globale dans le plasma.

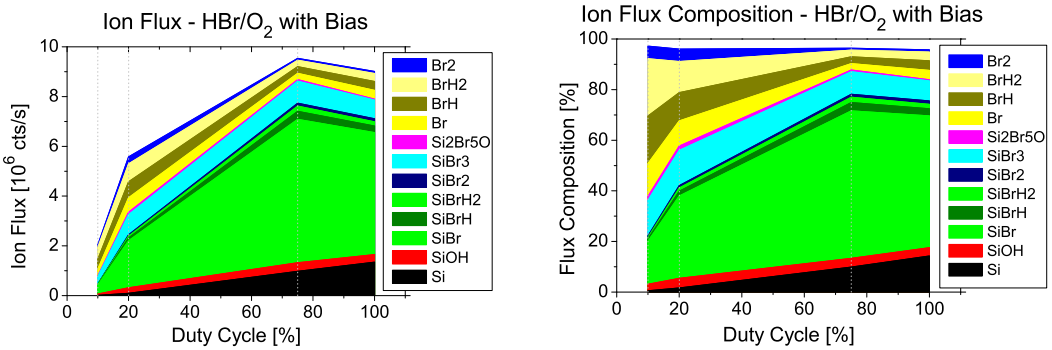

(a) (b)

Figure A.3.: ***(a)*** *Flux total d'ions d'un plasma HBr/O_2 AVEC polarisation du substrat et* ***(b)*** *sa composition relative.*

La fonction de distribution de l'énergie d'ions (IEDF) dans le plasma de HBr/O_2, mesurée par un analyseur électrostatique multi-grille (RFA) situé sur le substrat de silicium et montré en Fig. A.4, présente un double caractère bi-modal. Ceci indique qu'un flux significatif de H^+ arrive sur le substrat, ce qui n'est pas détecté proche des paroirs du réacteur en spectrométrie de masse. Par conséquent, une des espèces ionisées majoritaires dans le plasma HBr/O_2 qui contribue à la gravure du silicium est le proton H^+. En réduisant le rapport cyclique, moins de HBr est dissocié et la contribution de H^+ pourrait donc être réduite. En raison de sa masse très faible, l'ion hydrogène peut pénétrer profondément dans la surface gravée et endommager profondément le matériau. Une réduction du rapport cyclique pourrait alors aider à diminuer l'endommage de la surface en réduisant le flux de protons. Dans un

plasma de HBr pur, H^+ n'est pas observé. Cette différence est probablement liée à la composition différente du plasma et/ou à la différence de conditions des parois du réacteur.

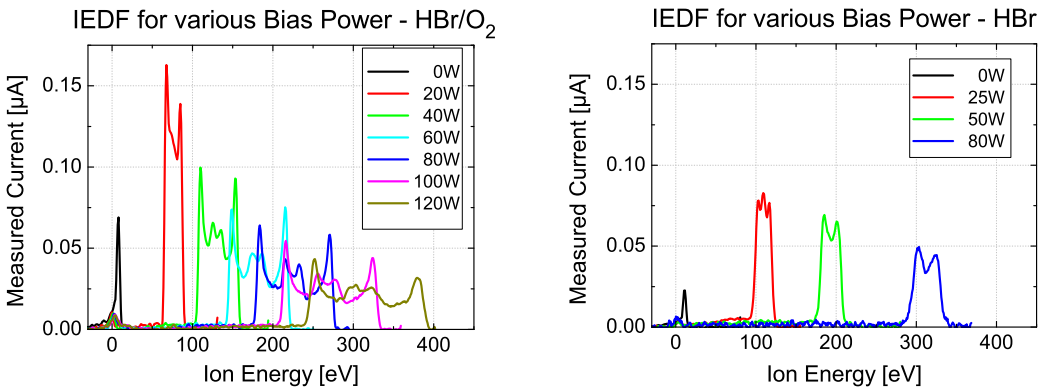

(a) **(b)**

Figure A.4.: *La fonction de distribution de l'énergie d'ions (IEDF)* ***(a)*** *d'un plasma de HBr/O_2 et* ***(b)*** *d'un plasma de HBr en continu AVEC polarisation.*

Dans le mode pulsé les IEDFs montrent un pic de haute et de basse énergie, qui correspondent respectivement aux ions des temps ON et OFF de la période de pulsation du plasma (Fig. A.5). Lorsque le rapport cyclique est réduit, le flux ionique total diminue proportionnellement au rapport cyclique et le pic de haute énergie se déplace vers les énergies plus élevées. La contribution relative des ions de la période ON au flux total est fortement réduite lorsque le rapport cyclique diminue, ce qui conduit à une énergie moyenne des ions plus faible.

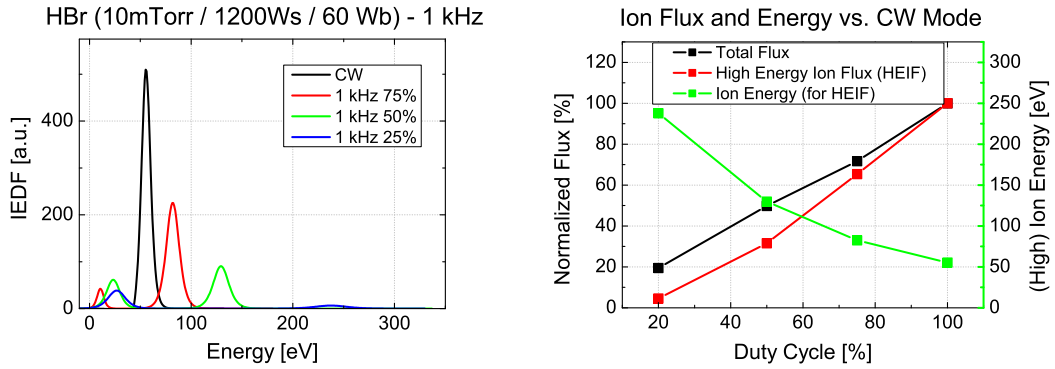

(a) **(b)**

Figure A.5.: ***(a)*** *L'IEDFs d'un plasma pulsé de HBr/O_2 à 1 kHz AVEC polarisation.* ***(b)*** *Flux total d'ions, flux d'ions de haute énergie et énergie moyenne des ions de haute énergie.*

A.1.2. Impact de pulser sur la gravure du silicium

Couche réactive à la surface du matériau gravée

Avec un rapport cyclique faible, l'épaisseur de la couche réactive à la surface du matériau gravé (REL) diminue, ce qui est montré en Fig. A.6. Ceci est lié au flux de radicaux élevé en temps compensé (c'est-à-dire par rapport au temps ON du plasma) et à une énergie déposée par les ions plus faible. Les radicaux de Br s'accumulent sur la surface gravée pendant le temps ON, mais également pendant le temps OFF de la période de pulsation du plasma. Ainsi le taux de gravure chimique du silicium amorphe de la REL augmente. La diminution de l'énergie déposée par les ions implique un taux d'amorphisation du silicium plus faible. Le nouvel équilibre entre les deux processus conduit à une réduction de l'épaisseur de la REL, ce qui correspond à une surface moins endommagée. Pour la même raison, la vitesse de gravure en temps compensé peut augmenter lorsque le plasma est pulsé à de faibles rapports cycliques.

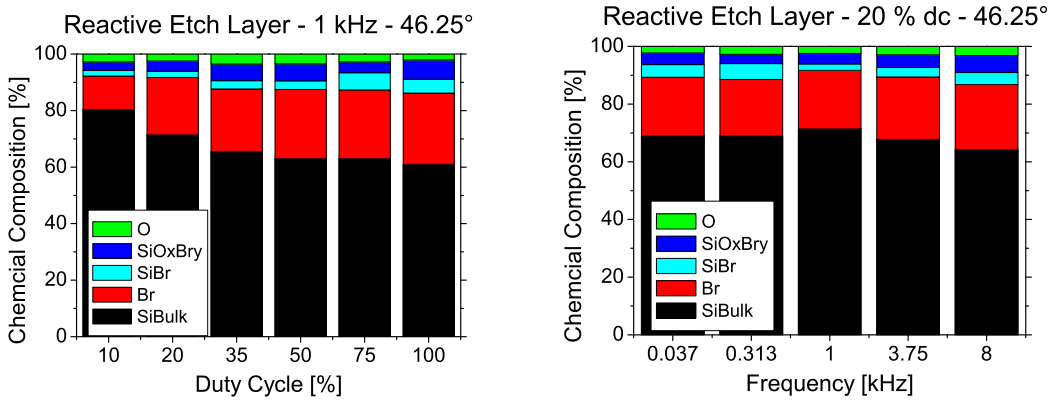

(a) (b)

Figure A.6.: ***(a)*** *Composition chimique du signal d'XPS (à 46.25°) de la couche réactive à la surface du matériau gravée pour des rapports cycliques (à 1 kHz) et* ***(b)*** *des fréquences (à un rapport cyclique de 20 %) variés. Un signal relatif plus élevée du silicium indique une couche réactive plus fine.*

Vitesse de gravure et sélectivité

La dépendance faible de la vitesse de gravure du silicium avec l'énergie des ions (liée à la puissance de la polarisation du substrat) indique un régime de gravure limitée par la disponibilité des radicaux. Le plus grand flux de radicaux (par rapport au temps de la période ON du plasma) à des rapports cycliques réduits implique une augmentation de la vitesse de gravure du silicium en temps compensé, ce qui est montré en Fig. A.7. En revanche, la diminution du flux d'ions à forte énergie conduit à une diminution de la vitesse de gravure du SiO_2 en temps compensé (Fig. A.8). La gravure du carbone amorphe en temps compensé augmente légèrement, probablement pour la même raison que pour le silicium (disponibilité de radicaux accrue). Puisque la gravure de silicium évolue plus rapidement que celle du carbone amorphe, la sélectivité augmente légèrement.

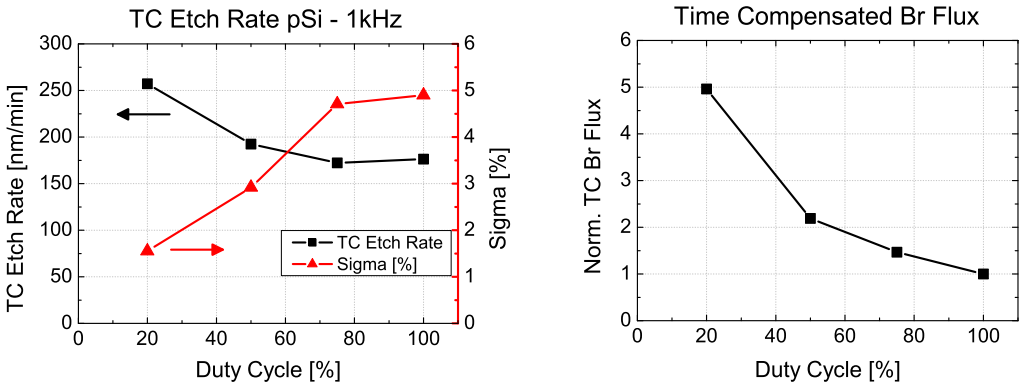

(a) (b)

Figure A.7.: ***(a)*** *Vitesse de la gravure en temps compensé de poly-silicium pour des rapports cycliques variés.* ***(b)*** *Flux de Br radicalaire en temps compensé.*

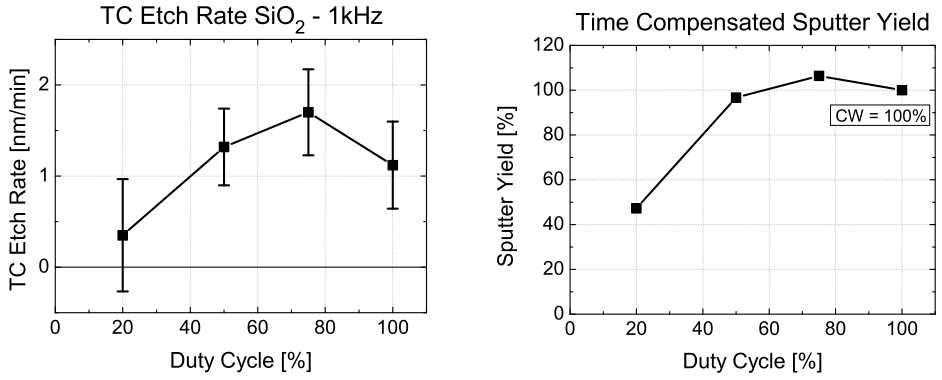

(a) (b)

Figure A.8.: ***(a)*** *Vitesse de la gravure en temps compensé de SiO_2 (matériau du masque) pour des rapports cycliques variés.* ***(b)*** *L'évolution approximée de la pulverisation par rapport à un plasma continu (100 %). Ce calcul est basé sur le flux d'ions de haute énergie et son énergie moyenne.*

Gravure des motifs

Lorsque des motifs de silicium sont gravés en utilisant un plasma pulsé (Fig. A.9), nous avons les évolutions suivantes lorsque le rapport cyclique diminue :

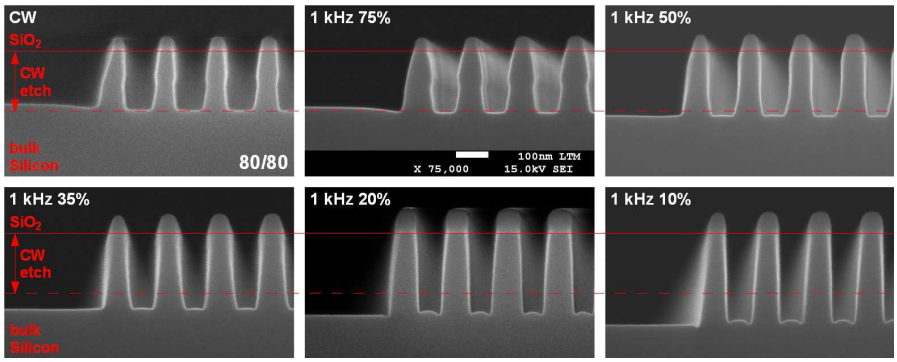

Figure A.9.: *Gravure des motifs en silicium dans un plasma pulsé de HBr/O_2.*

1. La vitesse de gravure de silicium en temps compensé augmente, ce qui est dû à une plus grande disponibilité des radicaux nécessaires pour la gravure.
2. Le facettage du masque en carbone amorphe diminue, ce qui est en contradiction avec les mesures de la gravure des substrats sans motifs. La différence peut être liée à la couverture réduit de carbone amorphe sur le substrat avec de motifs et en conséquence à une modification de la chimie du plasma. La réduction de la consommation et du facettage du masque en SiO_2 peut s'expliquer plus facilement car la gravure du SiO_2 nécessite une forte assistance ionique qui est réduite à faible rapport cyclique.
3. La pente des motifs gravés devient plus verticale. Comme la densité d'oxygène dans le réacteur diminue à faible rapport cyclique, des couches de passivation plus fines se forment sur les flancs des motifs. Ceci sera expliqué plus en détail dans la suite.
4. La différence entre les profiles denses et isolés est minimisée. Ceci peut s'expliquer par des couches de passivation plus fines, mais également par une meilleure répartition des espèces neutres telles que l'oxygène radicalaire lorsque le plasma est pulsé.
5. Les micro-tranchées larges localisées près des pieds des motifs, observées en plasma continu et en plasma pulsé à fort rapport cyclique, pourraient être liées à la différence de flux d'espèces ralentissant la gravure en fonction de la distance du pied. En s'éloignant du pied de la structure, l'angle de collection des espèces du plasma augmente. Par conséquent, si des espèces ralentissant la gravure proviennent de la phase gazeuse du plasma, la vitesse de gravure

diminue lorsqu'on s'éloigne du pied des motifs, ce qui forme de larges micro-tranchées près des motifs. En réduisant le rapport cyclique, moins d'espèces sont déposées et ces larges miro-tranchées disparaissent. Lorsque le rapport cyclique est très faible (<20 %) des micro-tranchées localisées apparaissent, ce qui peut être lié aux flancs des motifs plus verticaux qui focalisent les ions réfléchis très localement au pied des motifs, ce qui crée une micro-tranchée localisée au pied du motif. De plus, la vitesse de gravure est plus sensible au flux d'ions lorsque le plasma est pulsé à faible rapport cyclique (gravure de plus en plus limitée par les ions), ce qui favorise la formation de micro-tranchées dans les zones ou le flux d'ions est focalisé.

En résumant, la vitesse de gravure en temps compensé, la sélectivité par rapport au SiO_2 et l'homogénéité de la gravure sont améliorées lorsque le plasma est pulsé. De plus, le profil des motifs gravés peut être contrôlé par le rapport cyclique en modifiant la formation de la SPL sans les désavantages d'une baisse du flux d'oxygène en mode continue.

En augmentant la fréquence au-dessus d'une certaine limite qui dépend du rapport cyclique, la vitesse de gravure augmente à la fois pour le silicium et pour le masque dur d'oxyde, indiquant que l'énergie des ions augmente probablement dans ces conditions. Cependant, la raison de cette observation reste incertaine.

Une comparaison avec des motifs de plus petites dimensions montre la même évolution avec le rapport cyclique. Cependant, les résultats de la gravure à 1 kHz 10 % montrent des micro-tranchées très importantes et des flancs significativement courbés. La différence peut être attribuée au changement de masque. En effet, l'épaisseur des couches nécessaires pour ouvrir le masque de gravure est réduite, ce qui conduit à une évolution différente des couches formées sur les parois des réacteurs pendant les procédés nécessaires à l'ouverture du masque. De plus, les plaques avec des motifs de silicium présentent un taux d'ouverture plus faible (rapport entre la surface du silicium à graver et la surface total de la plaque) que les plaques avec des motifs plus larges, ce qui change également la composition du plasma de gravure.

Couche de passivation sur les flancs

L'épaisseur de la SPL, montrée en Fig. A.10, est probablement contrôlée par une combinaison de la déposition des produits non-volatiles de la gravure à base de silicium en ligne de mire et de l'oxydation de ces produits par les radicaux d'oxygène provenant de la phase gazeuse. Ces espèces déposées sur les flancs peuvent alors désorber spontanément ou être re-gravées par le brome radicalaire provenant du plasma. Si au contraire, elles sont oxydées par l'oxygène radicalaire provenant du plasma, elles se fixent sur les flancs et forment une couche de passivation empêchant la gravure latérale des motifs.

En l'absence d'oxygène dans le mélange de gaz, l'épaisseur de la SPL diminue fortement, ce qui est probablement lié à la diminution de la quantité de radicaux d'oxygène qui peuvent fixer les espèces peu volatiles déposées sur les flancs pour former la SPL.

En réduisant le rapport cyclique une évolution similaire peut être observée. Ceci peut s'expliquer par une diminution de la quantité de radicaux d'oxygène disponibles pour l'oxydation, mais également par une réduction de la quantité d'espèces peu-volatiles à base de silicium qui se déposent sur les flancs. En effet, plus de radicaux de brome sont disponibles pendant la gravure lorsque le plasma est pulsé à faible rapport cyclique, ce qui permet de former des produits de gravure plus volatils. De plus, la dissociation des produits volatils de gravure dans le plasma est réduite, ce qui limite fortement la formation d'espèces de faible volatilité dans le plasma susceptibles de coller sur les flancs. Nous avons remarqué que l'épaisseur de la couche de passivation sur les flancs dépend uniquement du rapport d'aspect dans les motifs et pas du temps d'exposition au plasma.

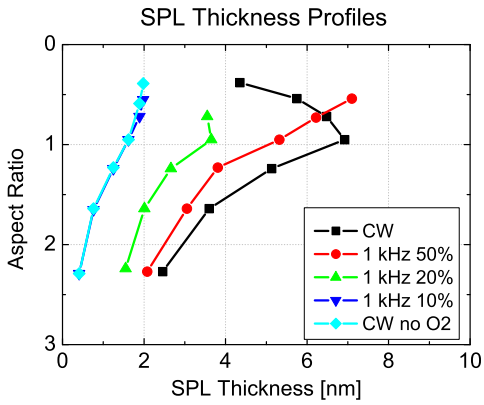

Figure A.10.: *Epaisseur moyenne de la couche de passivation sur les flancs des motifs gravés dans un plasma pulsé de HBr/O_2 avec des rapports cycliques variés et en mode continue avec et sans O_2.*

La composition chimique des couches de passivation montre un rapport constant entre Si et Br avec une fraction varié de l'oxygène (Fig A.11), ce qui indique que le processus de formation de la SPL reste comparable dans toutes les conditions. Lorsque le plasma est pulsé avec un rapport cyclique de 10 %, ou lorsque le plasma opère en mode continue sans flux d'oxygène, la quantité relative de l'oxygène dans la SPL est fortement réduite pour des rapports d'aspects très importants, ce qui est attribué à un flux de radicaux d'oxygène trop faible. Dans ce dernier cas, les motifs présentent des flancs courbés, du fait d'une couche de passivation trop fine pour empêcher la gravure latérale. On peut donc noter que la modification du flux d'O_2 en mode continue peut être utilisée pour obtenir une SPL avec une épaisseur plus fine. Néanmoins, le procédé est très sensible au flux d'oxygène, et cette solution conduirait à des risques en termes de stabilité du procédé, et probablement à une uniformité de gravure moins bonne. De plus, nous avons vu qu'en plasma continu avec une quantité d'oxygène intermédiaire, nous ne pouvions pas empêcher la gravure latérale avec des couches de passivation trop fine, du fait de la forte densité de radicaux très réactifs dans le plasma, et du fait de la déflection des ions par les charges différentielles sur le masque, qui conduit à une pulvérisation de cette fine couche de passivation et à une gravure latérale en plasma continu. En plasma pulsé, la densité de radicaux réactifs est fortement réduite, et les charges différentielles sont neutralisées pendant le temps OFF du pulse, ce qui permet d'obtenir des flancs pratiquement verticaux avec des couches de passivation très fines.

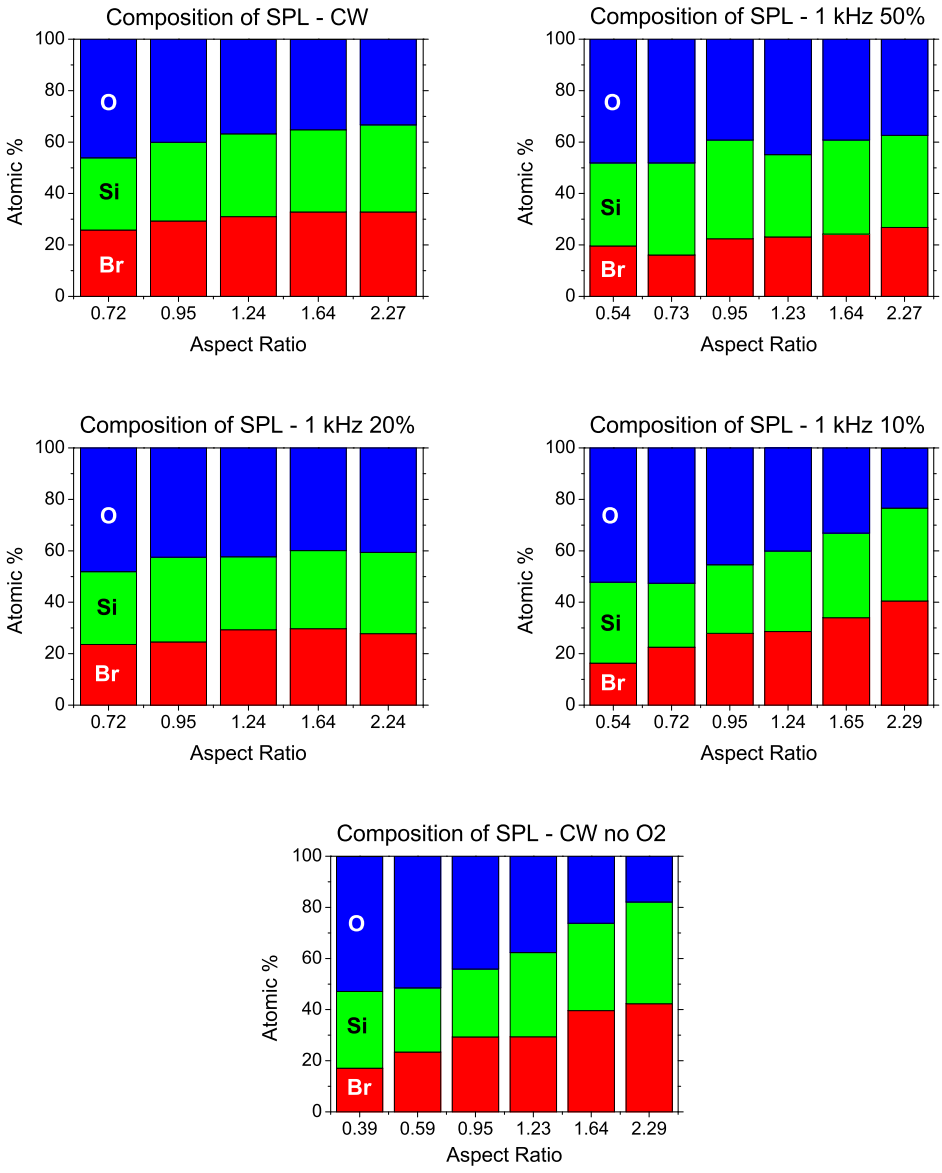

Figure A.11.: *Composition chimique moyenne de la couche de passivation sur les flancs des profils pour des rapports cycliques différents.*

A.1.3. Questions ouvertes

Les résultats présentés précédemment concernent l'étude de la gravure des motifs de silicium à base de plasma de HBr/O_2 pulsés. Ils ont montré l'impact de la modulation du plasma sur la phase gazeuse et sur la surface du matériau gravé. Bien que la plupart des observations puisse être expliquée, quelques questions restent ouvertes et pourraient être étudiées dans des expériences futures afin de vérifier les hypothèses proposées :

1. **Quel rôle joue l'hydrogène dans le procédé et comment se comporte-il par rapport aux paramètres de la modulation ?**
   L'hydrogène est une espèce particulièrement difficile à analyser car elle n'est pas détectée par XPS, et car notre spectromètre de masse n'est pas adapté pour sa détection. Au cours de nos expériences, nous avons observé par RFA que lorsque le plasma contient de l'O_2, le flux d'ions sur la plaque augmente fortement et contient des ions H^+. Les mesures de flux d'ions sur les parois ne montrent pas cette augmentation du flux d'ions avec l'ajout d'oxygène, ce qui semble contradictoire. Même si certains mécanismes comme le détachement d'un proton en entrant dans la gaine suite à la collision avec un électron secondaire pourraient expliquer ce phénomène, une étude plus poussée est nécessaire pour comprendre ce mécanisme. Le rôle de l'hydrogène sur la gravure reste donc aujourd'hui très spéculatif et une technique de mesure de l'hydrogène serait intéressante.
2. **Est-ce que la quantité d'oxygène radicalaire diminue vraiment avec le rapport cyclique ?**
   Les expériences réalisées pendant cette thèse concordent à indiquer que la densité d'oxygène radicalaire diminue avec le rapport cyclique. Cependant, la diminution de la densité d'oxygène radicalaire n'a pas été directement observée. Il serait donc intéressant de confirmer cette hypothèse par une mesure directe de la densité d'oxygène, par exemple en utilisant la spectroscopie d'absorption dans le V-UV.
3. **Comment pouvons-nous expliquer l'influence de la fréquence ?**
   La caractérisation du plasma, comme l'étude des motifs gravés, montre qu'à forte fréquence, à un rapport cyclique critique (qui dépend de la fréquence), le plasma évolue avec la fréquence. Pour des rapports cycliques plus forts (>20 %) ou à faible fréquence (<quelques kHz), la fréquence de pulsation n'a pas d'impact significatif. L'origine de cette évolution reste floue. La difficulté d'accorder le plasma à forte fréquence et faible rapport cyclique rend l'étude difficile, et peut également être à l'origine de cette évolution si les évolutions observées proviennent plus d'un problème d'accord du plasma que d'une évolution du plasma.

A.2. Caractéristiques générales des plasma pulsés

Les observations réalisées dans le cadre d'un plasma de HBr/O_2 pulsé pour la gravure du silicium peuvent être partiellement généralisées pour d'autres types de plasmas, et pour d'autres matériaux à graver.

Neutres

En diminuant le rapport cyclique, la puissance moyenne injectée dans le réacteur est réduite. Ceci conduit à une réduction de la température du gaz et, par conséquent, à une augmentation de la densité totale des neutres si la pression reste constant pendant le processus. Ainsi, le flux total des espèces neutres vers le substrat gravé va également augmenter. Un effet similaire pourrait être atteint par une augmentation de la pression totale ou par une réduction de la puissance injectée dans le plasma. Cependant, les propriétés du plasma seraient également significativement modifiées.

Le taux de dissociation moyen est également réduit lorsque le rapport cyclique diminue. Pendant le temps ON du plasma, la dissociation n'atteint pas une valeur constante (en comparant au mode continue) si la fréquence est assez élevée (~ 1 kHz). Pendant le temps OFF du plasma, la dissociation devient négligeable et seulement la recombinaison et d'autres mécanismes de perte se déroulent. Dans les plasmas à basse pression, la plupart des réactions chimiques ont lieu sur la surface des parois du réacteur. L'évolution de la concentration moyenne des produits de dissociation avec le rapport cyclique dépend du taux de dissociation et de recombinaison et des coefficients de collage de l'espèce sur la surface, ainsi que du changement de température du plasma. Par exemple, dans le cas d'un plasma de HBr/O_2, la densité du radical Br reste constante pour des rapports cycliques supérieurs à 50 %, mais chute brutalement pour des rapports cycliques inférieurs à 20 %. Au contraire, la densité du radical O semble diminuer plus rapidement, ce qui est dû à un coefficient de collage très élevé de l'oxygène radicalaire sur les parois du réacteur.

Au dessus d'une fréquence d'environ 1 kHz, la modulation de la densité pendant la période de pulsation devient assez faible pour les espèces neutres et des valeurs moyennes peuvent être utilisées pour caractériser le plasma.

Ions

L'ionisation dans un plasma pulsé se déroule uniquement pendant le tempts ON du plasma. De même que pour la dissociation des espèces neutres, la densité des ions dans le plasma a besoin d'un certain temps pour atteindre une valeur constante. Pendant le temps OFF les ions sont perdus rapidement sur les surfaces (plaque à graver et parois du réacteur). Par conséquent, il n'est pas surprenant que le flux d'ions moyen diminue plus que proportionnellement avec le rapport cyclique, comme observé dans le plasma HBr/O_2. Dans ce cas particulier, à une fréquence de pulsation de 1 kHz, le flux d'ions ne diminue pas à zéro, même pour un rapport cyclique de 10 %. La contribution relative des ions de la période ON du plasma au flux d'ions total est également environ proportionnelle au rapport cyclique. Par conséquent, le flux moyen des ions provenant du temps ON diminue plus qu'au carré du rapport cyclique.

Pendant la période OFF, la gaine entre le substrat et le plasma s'effondre et les ions qui arrivent sur le substrat ont des énergies fortement réduites. Pour un plasma pulsé de façon synchronisée, pour une puissance de polarisation donnée, la diminution du flux d'ions en plasma pulsé conduit à une augmentation de l'énergie des ions pendant le temps ON. Au contraire, l'énergie des ions provenant du temps OFF du plasma est très faible (inférieure au potentiel plasma d'un plasma continu). Pour cette raison, lorsque le plasma est pulsé avec un rapport cyclique faible, la majorité des ions ont des énergies beaucoup plus faible que celle obtenue en plasma continue, alors que peu d'ions (de la période ON) ont des énergies plus élevées. En moyenne, l'énergie des ions est donc significativement réduite.

Effets combinés

La forte diminution du flux d'ions avec le rapport cyclique, notamment des ions à forte énergie, réduit considérablement le rendement de pulvérisation physique en temps compensé. En parallèle, le flux des radicaux en temps compensé augmente. La combinaison des deux effets conduit à une gravure plus chimique lorsque le plasma est pulsé, et à une réduction de la composante physique de la gravure.

Les tendances présentées ci-dessus sont des tendances générales qui donnent des indications sur l'évolution de la densité des neutres et sur l'évolution du flux d'ions avec le rapport cyclique lorsque le plasma est pulsé. Cependant, ces évolutions dépendent fortement du mélange de gaz utilisé et du matériau gravé, et chaque procédé doit être analysé de façon individuelle et approfondie pour connaitre l'évolution exacte du flux d'ions et de la densité des espèces neutres lorsqu'il est pulsé.

A.3. Applications potentielles des plasmas pulsés

A.3.1. Avantages des plasmas pulsés

L'utilisation des plasmas pulsés offre des nouveaux paramètres de contrôle pour améliorer les procédés de gravure existant et pour rendre accessible de nouveaux régimes de la gravure. En comparaison avec le mode continue, pulser un plasma présente plusieurs avantages :

1. Moins d'endommagement par le plasma du fait de la réduction du flux d'ions de forte énergie.
2. Une caractère chimique du procédé de gravure plasma plus important
3. Une réduction du taux de dissociation moyen
4. Une réduction de la température du plasma

Endommagement réduit par le plasma

L'utilisation d'ions énergétiques pendant la gravure par plasma provoque toujours l'endommagement de la surface du matériau gravé. L'extrême surface est amorphisée, et mélangée avec les espèces du plasma neutres et avec les ions du plasma qui peuvent s'implanter à la surface. L'énergie des ions dans un plasma en mode continu est au minimum égale au potentiel plasma ($>15\,\mathrm{eV}$). En utilisant des plasmas pulsés, l'énergie moyenne des ions peut être réduite à une valeur inférieure au potentiel plasma d'un plasma continu, ce qui réduit l'endommagement de la surface des matériaux exposés au plasma.

Gravure chimique plus importante

Lorsque le plasma est pulsé à une fréquence de l'ordre du kHz, le flux de radicaux sur la surface est presque constant. Par conséquent, le flux de radicaux pendant le temps OFF du plasma peut participer à la gravure, et augmenter le caractère chimique de la gravure. Même si la densité de radicaux diminue lorsque le plasma est pulsé, la contribution du temps OFF peut compenser cette diminution de la densité et augmenter le flux de radicaux vers la surface en temps compensé (flux de radicaux divisé par le rapport cyclique). Lorsque deux matériaux présentent des mécanismes de gravure différents, comme c'est le cas pour silicium et SiO_2 dans un plasma HBr/O_2, l'augmentation du caractère chimique de la gravure par plasma peut conduire à une très forte augmentation de la sélectivité.

Réduction du taux de dissociation

La dissociation du plasma a lieu pendant le temps ON du plasma, alors que la perte des radicaux (recombinaisons, collage, pompage) a lieu pendant toute la période de pulsation. Par conséquent, le taux de dissociation moyen est réduit dans les plasmas pulsés. Ceci peut avoir différents effets sur la gravure. Dans le cas présent, la réduction de la dissociation diminue le flux d'oxygène vers la surface, et diminue le flux d'espèces peu volatiles à base de silicium. Le dépôt des couches de passivation qui contrôle la pente de gravure des motifs est donc fortement réduit, ce qui réduit l'épaisseur de la couche de passivation sur les flancs et conduit à des profils plus verticaux et plus homogènes. Pour d'autres procédés, pour lesquels la sélectivité de gravure entre deux matériaux est atteinte par la déposition sélective des molécules radicalaires [173], un taux de déposition réduit peut conduire au contraire à une perte de la sélectivité.

Réduction de la température du plasma

L'absence de puissance injectée dans le plasma pendant le temps OFF réduit la température du gaz. Cette réduction de la température, à pression constante, conduit à une augmentation de la densité des espèces neutres. Dans le cas d'un plasma de HBr/O_2, nous avons montré que la densité moyenne des radicaux ne change pas considérablement tant que le rapport cyclique est supérieur à 50 %. Pour des surfaces qui sont sensibles à la température et qui doivent être exposées à un flux de radicaux, les plasmas pulsés peuvent être utilisés à la place des réacteurs plasmas de diffusion. Ainsi, l'utilisation des plasmas pulsés peut permettre de rendre un réacteur plasma standard plus polyvalent.

A.3.2. Désavantages des plasmas pulsés

Naturellement, les plasmas pulsés n'ont pas que des avantages. Pour chaque procédé plasma, plusieurs inconvénients doivent être considérés en regard des avantages. Tout d'abord, la vitesse de gravure moyenne diminue généralement. Ceci n'est cependant pas automatique, puisque plusieurs études ont reporté une augmentation de la vitesse de gravure en pulsant le plasma. [50]. La pulsation des plasmas cible plutôt des procédés qui sont sensible à l'endommagement et dans lesquels la vitesse de gravure est d'une importance mineure, comme c'est le cas pour les étapes de "sur-gravure" qui sont utilisées pour finir la gravure de la grille des transistors en s'arrêtant sur l'oxyde de grille.

Un autre problème qui doit être adressé dans le futur est la difficulté d'obtenir une bonne adaptation d'impédance du générateur de puissance avec celle du plasma. Puisque le plasma a un caractère très transitoire, le réseau de la boite d'accord de l'impédance doit s'adapter très rapidement, ce qui est impossible du fait de l'utilisation de pièces mobiles. Pour résoudre ce problème, plusieurs techniques sont déjà développées, y compris un changement automatique de la fréquence du générateur de puissance. Néanmoins, les rapports cycliques et les fréquences de pulsation utilisables restent limités.

A.4. Perspectives

Etant donnés les avantages et inconvénients de la pulsation des plasmas présentés dans la partie précédente, quelques procédés de gravure susceptibles de bénéficier des plasmas pulsés peuvent être identifiés.

Petit-Etienne *et al.* [48] ont démontré comment le "silicon recess" peut être réduit pendant la gravure de la grille d'un transistor. Le "silicon recess" est la consommation de silicium par oxydation sous l'oxyde de grille pendant la fin de la gravure de la grille du transistor. La diminution du flux d'ions énergétiques, et la modification de la composition du flux d'ion (ions plus moléculaires et plus lourds et donc plus lents pour une même énergie) conduisent à une plus faible pénétration des espèces sous l'oxyde de grille, et donc à une plus faible oxydation du silicium sous l'oxyde.

Une autre application possible des plasmas pulsés est l'arrêt sans endommagement de la gravure sur une couche de graphène, ce qui pourrait être d'un fort intérêt pour l'électronique du futur à base de graphène. Ceci n'a pas encore été testé, mais des études en plasma de chlore sur silicium ont montré que l'amorphisation de l'extrême surface du silicium était très fortement réduite en pulsant le plasma à faible rapport cyclique. Une vitesse de gravure permettant un contrôle atomique (0.2 nm/min) a ainsi pu être obtenu [174].

Le meilleur contrôle des couches de passivation en plasma pulsé offre également une application potentielle pour les étapes de gravure critiques nécessitant un contrôle dimensionnel parfait. C'est notamment le cas pour la gravure des grilles de transistor, du canal des transistors dans le cas de transistors 3D (fin FET), ou encore pour la gravure des espaceurs utilisés pour contrôler le dopage ou dans les stratégies de double patterning.

Même si l'utilisation de plasmas synchronisés pulsés présente de nombreux intérêts et applications, une nouvelle stratégie de pulsation appelée "embedded pulsing" semble très prometteuse. Le concept est de pulser la source du plasma et la polarisation du substrat avec un rapport cyclique différent. Ainsi, il est possible de démarrer le plasma, puis la polarisation quelques dizaines ou centaines de microsecondes après que le plasma ait démarré. Ceci réduit les risques de pics d'énergie des ions. Ce type de plasma pourrait alors être utilisé pour réduire encore plus le risque d'endommagement des surfaces exposées aux plasmas de gravure.

List of Figures

Bibliography

[1] J. W. Coburn and H. F. Winters, *Ion- and electron-assisted gas-surface chemistry - an important effect in plasma etching.* J. Appl. Phys. 50 (1979) 3189.

[2] K. Hashimoto, *New phenomena of charge damage in plasma etching: Heavy damage only through dense-line antenna.* Jpn. J. Appl. Phys. 32 (1993) 6109.

[3] K. Hashimoto, *Charge damage caused by electron shading effect.* Jpn. J. Appl. Phys. 33 (1994) 6013.

[4] N. Fujiwara, T. Maruyama, M. Yoneda, K. Tsukamoto and T. Banjo, *Effect plasma transport on etched profiles with surface topography in diverging field electron cyclotron resonance plasma.* Jpn. J. Appl. Phys. 33 (1994) 2164.

[5] K. P. Giapis and G. S. Hwang, *Pattern-dependent charging and the role of electron tunneling.* Jpn. J. Appl. Phys. 37 (1998) 2281.

[6] T. J. Dalton, J. C. Arnold, H. H. Sawin, S. Swan and D. Corliss, *Microtrench formation in polysilicon plasma etching over thin gate oxide.* J. Electrochem. Soc. 140 (1993) 2395.

[7] M. A. Vyvoda, M. Li, D. B. Graves, H. Lee, M. V. Malyshev, F. P. Klemens, J. T. C. Lee and V. M. Donnelly, *Role of sidewall scattering in feature profile evolution during Cl_2 and HBr plasma etching of silicon.* J. Vac. Sci. Technol., B 18 (2000) 820.

[8] K. Giapis and G. Hwang, *Plasma interactions with high aspect ratio patterned surfaces: ion transport, scattering, and the role of charging.* Thin Solid Films 374 (2000) 175.

[9] A. P. Mahorowala and H. H. Sawin, *Etching of polysilicon in inductively coupled Cl_2 and HBr discharges. III. Photoresist mask faceting, sidewall deposition, and microtrenching.* J. Vac. Sci. Technol., B 20 (2002) 1077.

[10] M. A. Vyvoda, M. Li and D. B. Graves, *Hardmask charging during Cl_2 plasma etching of silicon.* J. Vac. Sci. Technol., A 17 (1999) 3293.

[11] K. Giapis, G. Hwang and O. Joubert, *The role of mask charging in profile evolution and gate oxide degradation.* Microelectron. Eng. 61 - 62 (2002) 835.

[12] N. Yabumoto, M. Oshima, O. Michikami and S. Yoshii, *Surface damage on Si substrates caused by reactive sputter etching*. Jpn. J. Appl. Phys. 20 (1981) 893.

[13] G. S. Oehrlein, R. M. Tromp, J. C. Tsang, Y. H. Lee and E. J. Petrillo, *Near-surface damage and contamination after CF_4/H_2 reactive ion etching of Si*. J. Electrochem. Soc. 132 (1985) 1441.

[14] G. S. Oehrlein, *Dry etching damage of silicon: A review*. Mater. Sci. Eng., B 4 (1989) 441 .

[15] S. J. Fonash, *An overview of dry etching damage and contamination effects*. J. Electrochem. Soc. 137 (1990) 3885.

[16] M. Okigawa, Y. Ishikawa and S. Samukawa, *Plasma-radiation-induced interface states in metal-nitride-oxide-silicon structure of charge-coupled device image sensor and their reduction using pulse-time-modulated plasma*. Jpn. J. Appl. Phys. 42 (2003) 2444.

[17] S. Uchida, S. Takashima, M. Hori, M. Fukasawa, K. Ohshima, K. Nagahata and T. Tatsumi, *Plasma damage mechanisms for low-k porous SiOCH films due to radiation, radicals, and ions in the plasma etching process*. J. Appl. Phys. 103 (2008) 073303.

[18] J. Lee and D. B. Graves, *The effect of VUV radiation from Ar/O_2 plasmas on low-k SiOCH films*. J. Phys. D: Appl. Phys. 44 (2011) 325203.

[19] H. Shi, H. Huang, J. Bao, J. Liu, P. S. Ho, Y. Zhou, J. T. Pender, M. D. Armacost and D. Kyser, *Role of ions, photons, and radicals in inducing plasma damage to ultra low-k dielectrics*. J. Vac. Sci. Technol., B 30 (2012) 011206.

[20] M. Fukasawa, Y. Miyawaki, Y. Kondo, K. Takeda, H. Kondo, K. Ishikawa, M. Sekine, H. Matsugai, T. Honda, M. Minami, F. Uesawa, M. Hori and T. Tatsumi, *Vacuum ultraviolet and ultraviolet radiation-induced effect of hydrogenated silicon nitride etching: Surface reaction enhancement and damage generation*. Jpn. J. Appl. Phys. 51 (2012) 026201.

[21] C.-C. Wei and T.-P. Ma, *Reduction of apparent dopant concentration in the surface space charge layer of oxidized silicon by ionizing radiation*. Appl. Phys. Lett. 45 (1984) 900.

[22] V. M. Donnelly, F. P. Klemens, T. W. Sorsch, G. L. Timp and F. H. Baumann, *Oxidation of Si beneath thin SiO_2 layers during exposure to HBr/O_2 plasmas, investigated by vacuum transfer X-ray photoelectron spectroscopy*. Appl. Phys. Lett. 74 (1999) 1260.

[23] L. Vallier, L. Desvoivres, M. Bonvalot and O. Joubert, *Thin gate oxide behavior during plasma patterning of silicon gates*. Appl. Phys. Lett. 75 (1999) 1069.

[24] M. Tuda, K. Shintani and J. Tanimura, *Study of plasma-surface interactions during overetch of polycrystalline silicon gate etching with high-density HBr/O_2 plasmas*. Appl. Phys. Lett. 79 (2001) 2535.

[25] S. A. Vitale and B. A. Smith, *Reduction of silicon recess caused by plasma oxidation during high-density plasma polysilicon gate etching*. J. Vac. Sci. Technol., B 21 (2003) 2205.

[26] M. Fukasawa, Y. Nakakubo, A. Matsuda, Y. Takao, K. Eriguchi, K. Ono, M. Minami, F. Uesawa and T. Tatsumi, *Structural and electrical characterization of HBr/O_2 plasma damage to Si substrate*. J. Vac. Sci. Technol., A 29 (2011) 041301.

[27] H. H. Goto, H.-D. Löwe and T. Ohmi, *Dual excitation reactive ion etcher for low energy plasma processing*. J. Vac. Sci. Technol., A 10 (1992) 3048.

[28] T. Kitajima, Y. Takeo, Z. L. Petrović and T. Makabe, *Functional separation of biasing and sustaining voltages in two-frequency capacitively coupled plasma*. Appl. Phys. Lett. 77 (2000) 489.

[29] T. Gans, J. Schulze, D. O'Connell, U. Czarnetzki, R. Faulkner, A. R. Ellingboe and M. M. Turner, *Frequency coupling in dual frequency capacitively coupled radio-frequency plasmas*. Appl. Phys. Lett. 89 (2006) 261502.

[30] T. Yamaguchi, T. Kimura, C. Koshimizu, K. Takeda, H. Kondo, K. Ishikawa, M. Sekine and M. Hori, *Spatial distributions of electron, CF, and CF_2 radical densities and gas temperature in DC-superposed dual-frequency capacitively coupled plasma etch reactor employing cyclic-$C_4F_8/N_2/Ar$ gas*. Jpn. J. Appl. Phys. 50 (2011) 056101.

[31] T. Goto, M. Hirayama, H. Yamauchi, M. Moriguchi, S. Sugawa and T. Ohmi, *A new microwave-excited plasma etching equipment for separating plasma excited region from etching process region*. Jpn. J. Appl. Phys. 42 (2003) 1887.

[32] T. Goto, K. Ikenaga, A. Teramoto, M. Hirayama, S. Sugawa and T. Ohmi, *Damage-free microwave-excited plasma etching without carrier deactivation of heavily doped Si under thin silicide layer*. J. Vac. Sci. Technol., A 26 (2008) 8.

[33] T. Goto, A. Inokuchi, K. Ishibashi, S. Yasuda, T. Nakanishi, M. Kohno, M. Okesaku, M. Sasaki, T. Nozawa, M. Hirayama and T. Ohmi, *Establishment of very uniform gas-flow pattern in the process chamber for microwave-*

excited high-density plasma by ceramic shower plate. J. Vac. Sci. Technol., A 27 (2009) 686.

[34] W. M. Manheimer, R. F. Fernsler, M. Lampe and R. A. Meger, *Theoretical overview of the large-area plasma processing system (LAPPS)*. Plasma Sources Sci. Technol. 9 (2000) 370.

[35] R. A. Meger, D. D. Blackwell, R. F. Fernsler, M. Lampe, D. Leonhardt, W. M. Manheimer, D. P. Murphy and S. G. Walton, *Beam-generated plasmas for processing applications*. Phys. Plasmas 8 (2001) 2558.

[36] D. Leonhardt, S. G. Walton, C. Muratore, R. F. Fernsler and R. A. Meger, *Etching with electron beam generated plasmas*. J. Vac. Sci. Technol., A 22 (2004) 2276.

[37] S. Samukawa, K. Sakamoto and K. Ichiki, *High-efficiency low energy neutral beam generation using negative ions in pulsed plasma*. Jpn. J. Appl. Phys. 40 (2001) L997.

[38] S. Samukawa, *Ultimate top-down etching processes for future nanoscale devices: Advanced neutral-beam etching*. Jpn. J. Appl. Phys. 45 (2006) 2395.

[39] T. Kubota, O. Nukaga, S. Ueki, M. Sugiyama, Y. Inamoto, H. Ohtake and S. Samukawa, *200-mm-diameter neutral beam source based on inductively coupled plasma etcher and silicon etching*. J. Vac. Sci. Technol., A 28 (2010) 1169.

[40] S. Samukawa, K. Sakamoto and K. Ichiki, *High-efficiency neutral-beam generation by combination of inductively coupled plasma and parallel plate DC bias*. Jpn. J. Appl. Phys. 40 (2001) L779.

[41] S. Samukawa and K. Terada, *Pulse-time modulated electron cyclotron resonance plasma etching for highly selective, highly anisotropic, and less-charging polycrystalline silicon patterning*. J. Vac. Sci. Technol., B 12 (1994) 3300.

[42] S. Samukawa and T. Mieno, *Pulse-time modulated plasma discharge for highly selective, highly anisotropic and charge-free etching*. Plasma Sources Sci. Technol. 5 (1996) 132.

[43] T. H. Ahn, K. Nakamura and H. Sugai, *Negative ion measurements and etching in a pulsed-power inductively coupled plasma in chlorine*. Plasma Sources Sci. Technol. 5 (1996) 139.

[44] G. S. Hwang and K. P. Giapis, *Mechanism of charging reduction in pulsed plasma etching*. Jpn. J. Appl. Phys. 37 (1998) 2291.

[45] J.-H. Kim, C.-J. Kang, T.-H. Ahn and J.-T. Moon, *Characteristics of self bias voltage and poly-Si etching in pulsed helicon wave plasma.* Thin Solid Films 345 (1999) 124 .

[46] S. Samukawa, K. Noguchi, J. I. Colonell, K. H. A. Bogart, M. V. Malyshev and V. M. Donnelly, *Reduction of plasma induced damage in an inductively coupled plasma using pulsed source power.* J. Vac. Sci. Technol., B 18 (2000) 834.

[47] C. Petit-Etienne, M. Darnon, L. Vallier, E. Pargon, G. Cunge, F. Boulard, O. Joubert, S. Banna and T. Lill, *Reducing damage to Si substrates during gate etching processes by synchronous plasma pulsing.* J. Vac. Sci. Technol., B 28 (2010) 926.

[48] C. Petit-Etienne, E. Pargon, S. David, M. Darnon, L. Vallier, O. Joubert and S. Banna, *Silicon recess minimization during gate patterning using synchronous plasma pulsing.* J. Vac. Sci. Technol., B 30 (2012) 040604.

[49] S. A. Voronin, M. R. Alexander and J. W. Bradley, *Time-resolved measurements of the ion energy distribution function in a pulsed discharge using a double gating technique.* Meas. Sci. Technol. 16 (2005) 2446.

[50] H. Ohtake, K. Noguchi, S. Samukawa, H. Iida, A. Sato and X. yu Qian, *Pulse-time-modulated inductively coupled plasma etching for high-performance polysilicon patterning on thin gate oxides.* J. Vac. Sci. Technol., B 18 (2000) 2495.

[51] S. Samukawa, Y. Ishikawa, S. Kumagai and M. Okigawa, *On-wafer monitoring of vacuum-ultraviolet radiation damage in high-density plasma processes.* Jpn. J. Appl. Phys. 40 (2001) L1346.

[52] P. Subramonium and M. J. Kushner, *Pulsed plasmas as a method to improve uniformity during materials processing.* J. Appl. Phys. 96 (2004) 82.

[53] G. Cunge, D. Vempaire and N. Sadeghi, *Gas convection caused by electron pressure drop in the afterglow of a pulsed inductively coupled plasma discharge.* Appl. Phys. Lett. 96 (2010) 131501.

[54] R. W. Boswell and D. Henry, *Pulsed high rate plasma etching with variable Si/SiO_2 selectivity and variable Si etch profiles.* Appl. Phys. Lett. 47 (1985) 1095.

[55] M. A. Lieberman and A. J. Lichtenberg, *Principles of Plasma Discharges and Materials Processing.* Wiley-Interscience (1994).

[56] F. F. Chen, *Introduction to plasma physics and controlled fusion. Vol. 1, 2nd ed.* Plenum Press (1984).

[57] J. H. Keller, J. C. Forster and M. S. Barnes, *Novel radio-frequency induction plasma processing techniques*. J. Vac. Sci. Technol., A 11 (1993) 2487.

[58] H. Takekida and K. Nanbu, *Particle modelling of inductively-coupled argon plasmas with wafer biasing*. J. Phys. D: Appl. Phys. 38 (2005) 3461.

[59] M. A. Sobolewski and J.-H. Kim, *The effects of radio-frequency bias on electron density in an inductively coupled plasma reactor*. J. Appl. Phys. 102 (2007) 113302.

[60] H.-C. Lee, M.-H. Lee and C.-W. Chung, *Effects of rf-bias power on plasma parameters in a low gas pressure inductively coupled plasma*. Appl. Phys. Lett. 96 (2010) 071501.

[61] H.-C. Lee, J.-Y. Bang and C.-W. Chung, *Effects of RF bias power on electron energy distribution function and plasma uniformity in inductively coupled argon plasma*. Thin Solid Films 519 (2011) 7009 .

[62] J. Schulze, E. Schüngel and U. Czarnetzki, *Coupling effects in inductive discharges with radio frequency substrate biasing*. Appl. Phys. Lett. 100 (2012) 024102.

[63] G. Cunge, R. L. Inglebert, O. Joubert, L. Vallier and N. Sadeghi, *Ion flux composition in $HBr/Cl_2/O_2$ and $HBr/Cl_2/O_2/CF_4$ chemistries during silicon etching in industrial high-density plasmas*. J. Vac. Sci. Technol., B 20 (2002) 2137.

[64] M. Hori and T. Goto, *Measurement techniques of radicals, their gas phase and surface reactions in reactive plasma processing*. Appl. Surf. Sci. 192 (2002) 135 .

[65] K. Miwa and T. Mukai, *Influences of reaction products on etch rates and linewidths in a poly-Si/oxide etching process using HBr/O_2 based inductively coupled plasma*. J. Vac. Sci. Technol., B 20 (2002) 2120.

[66] O. Joubert, G. Cunge, B. Pelissier, L. Vallier, M. Kogelschatz and E. Pargon, *Monitoring chamber walls coating deposited during plasma processes: Application to silicon gate etch processes*. J. Vac. Sci. Technol., A 22 (2004) 553.

[67] M. Hori and T. Goto, *Insights into sticking of radicals on surfaces for smart plasma nano-processing*. Appl. Surf. Sci. 253 (2007) 6657.

[68] G. Cunge, N. Sadeghi and R. Ramos, *Influence of the reactor wall composition on radicals' densities and total pressure in Cl_2 inductively coupled plasmas: II. During silicon etching*. J. Appl. Phys. 102 (2007) 093305.

[69] A. Agarwal and M. J. Kushner, *Seasoning of plasma etching reactors: Ion energy distributions to walls and real-time and run-to-run control strategies.* J. Vac. Sci. Technol., A 26 (2008) 498.

[70] G. Cunge, D. Vempaire, R. Ramos, M. Touzeau, O. Joubert, P. Bodard and N. Sadeghi, *Radical surface interactions in industrial silicon plasma etch reactors.* Plasma Sources Sci. Technol. 19 (2010) 034017.

[71] S. Samukawa and S. Furuoya, *Time-modulated electron cyclotron resonance plasma discharge for controlling generation of reactive species.* Appl. Phys. Lett. 63 (1993) 2044.

[72] M. Tuda and K. Ono, *Profile evolution during pulsed plasma etching.* Jpn. J. Appl. Phys. 35 (1996) L1374.

[73] P. J. Chantry, *A simple formula for diffusion calculations involving wall reflection and low density.* J. Appl. Phys. 62 (1987) 1141.

[74] D. Vempaire and G. Cunge, *Probing radical kinetics in the afterglow of pulsed discharges by absorption spectroscopy with light emitting diodes: Application to BCl radical.* Appl. Phys. Lett. 94 (2009) 021504.

[75] T. D. Bestwick and G. S. Oehrlein, *Reactive ion etching of silicon using bromine containing plasmas.* J. Vac. Sci. Technol., A 8 (1990) 1696.

[76] V. M. Donnelly and N. Layadi, *Halogen uptake by thin SiO_2 layers on exposure to HBr/O_2 and Cl_2 plasmas, investigated by vacuum transfer X-ray photoelectron spectroscopy.* J. Vac. Sci. Technol., B 16 (1998) 1571.

[77] T. Ito, K. Karahashi, S.-Y. Kang and S. Hamaguchi, *Evaluation of Si etching yields by Cl^+, Br^+ and HBr^+ ion irradiation.* J. Phys. Conf. Ser. 232 (2010) 012021.

[78] S. Kuroda and H. Iwakuro, *Abrupt reduction in poly-Si etch rate in HBr/O_2 plasma.* J. Vac. Sci. Technol., B 16 (1998) 1846.

[79] M. Nakamura, K. Koshino and J. Matsuo, *Mechanism of high selectivity and impurity effects in HBr RIE: In-situ surface analysis.* Jpn. J. Appl. Phys. 31 (1992) 1999.

[80] K. Ono, H. Ohta and K. Eriguchi, *Plasma-surface interactions for advanced plasma etching processes in nanoscale ULSI device fabrication: A numerical and experimental study.* Thin Solid Films 518 (2010) 3461 .

[81] S. A. Vitale, H. Chae and H. H. Sawin, *Silicon etching yields in F_2, Cl_2, Br_2, and HBr high density plasmas.* J. Vac. Sci. Technol., A 19 (2001) 2197.

[82] J. Coburn, *The influence of ion sputtering on the elemental analysis of solid surfaces*. Thin Solid Films 64 (1979) 371 .

[83] K. Koshino, J. Matsuo and M. Nakamura, *Chemical states of bromine atoms on SiO_2 surface after HBr reactive ion etching: Analysis of thin oxide*. Jpn. J. Appl. Phys. 32 (1993) 3063.

[84] S. Banna, A. Agarwal, K. Tokashiki, H. Cho, S. Rauf, V. Todorow, K. Ramaswamy, K. Collins, P. Stout, J.-Y. Lee, J. Yoon, K. Shin, S.-J. Choi, H.-S. Cho, H.-J. Kim, C. Lee and D. Lymberopoulos, *Inductively coupled pulsed plasmas in the presence of synchronous pulsed substrate bias for robust, reliable, and fine conductor etching*. IEEE T. Plasma. Sci. 37 (2009) 1730 .

[85] H. Singh, J. W. Coburn and D. B. Graves, *Mass spectrometric detection of reactive neutral species: Beam-to-background ratio*. J. Vac. Sci. Technol., A 17 (1999) 2447.

[86] S. Agarwal, G. W. W. Quax, M. C. M. van de Sanden, D. Maroudas and E. S. Aydil, *Measurement of absolute radical densities in a plasma using modulated-beam line-of-sight threshold ionization mass spectrometry*. J. Vac. Sci. Technol., A 22 (2004) 71.

[87] J. Benedikt, D. Ellerweg and A. von Keudell, *Molecular beam sampling system with very high beam-to-background ratio: The rotating skimmer concept*. Rev. Sci. Instrum. 80 (2009) 055107.

[88] G. Cunge, P. Bodart, M. Brihoum, F. Boulard, T. Chevolleau and N. Sadeghi, *Measurement of free radical kinetics in pulsed plasmas by UV and VUV absorption spectroscopy and by modulated beam mass spectrometry*. Plasma Sources Sci. Technol. 21 (2012) 024006.

[89] B. Pelissier and N. Sadeghi, *Time-resolved pulse-counting lock-in detection of laser induced fluorescence in the presence of a strong background emission*. Rev. Sci. Instrum. 67 (1996) 3405.

[90] H. Sugai and H. Toyoda, *Appearance mass spectrometry of neutral radicals in radio frequency plasmas*. J. Vac. Sci. Technol., A 10 (1992) 1193.

[91] A. Tserepi, W. Schwarzenbach, J. Derouard and N. Sadeghi, *Kinetics of F atoms and fluorocarbon radicals studied by threshold ionization mass spectrometry in a microwave CF_4 plasma*. J. Vac. Sci. Technol., A 15 (1997) 3120.

[92] W. Schwarzenbach, A. Tserepi, J. Derouard and N. Sadeghi, *Mass spectrometric detection of F atoms and CF_x radicals in CF_4 plasmas*. Jpn. J. Appl. Phys. 36 (1997) 4644.

[93] H. Singh, J. W. Coburn and D. B. Graves, *Appearance potential mass spectrometry: Discrimination of dissociative ionization products*. J. Vac. Sci. Technol., A 18 (2000) 299.

[94] S. G. Walton, R. F. Fernsler and D. Leonhardt, *Measurement of ion energy distributions using a combined energy and mass analyzer*. Rev. Sci. Instrum. 78 (2007) 083503.

[95] L. G. Christophorou and J. K. Olthoff, *Electron interactions with SF_6*. J. Phys. Chem. Ref. Data 29 (2000) 267.

[96] R. Rejoub, D. R. Sieglaff, B. G. Lindsay and R. F. Stebbings, *Absolute partial cross sections for electron-impact ionization of SF_6 from threshold to 1000 eV*. J. Phys. B: At., Mol. Opt. Phys. 34 (2001) 1289.

[97] W. M. M. Kessels, C. M. Leewis, M. C. M. van de Sanden and D. C. Schram, *Formation of cationic silicon clusters in a remote silane plasma and their contribution to hydrogenated amorphous silicon film growth*. J. Appl. Phys. 86 (1999) 4029.

[98] S. Candan, A. J. Beck, L. O'Toole, R. D. Short, A. Goodyear and N. St J. Braithwaite, *The role of ions in the continuous-wave plasma polymerisation of acrylic acid*. Phys. Chem. Chem. Phys. 1 (1999) 3117.

[99] P. Kae-Nune, J. Perrin, J. Guillon and J. Jolly, *Mass spectrometry detection of radicals in SiH_4-CH_4-H_2 glow discharge plasmas*. Plasma Sources Sci. Technol. 4 (1995) 250.

[100] K. Jouston (Editor), *Handbook of Vacuum Technology*. Wiley-VCH (2008).

[101] J. Benedikt, S. Agarwal, D. Eijkman, W. Vandamme, M. Creatore and M. C. M. van de Sanden, *Threshold ionization mass spectrometry of reactive species in remote Ar/C_2H_2 expanding thermal plasma*. J. Vac. Sci. Technol., A 23 (2005) 1400.

[102] J. W. Coburn and E. Kay, *Pressure considerations associated with ion sampling from glow discharges*. J. Vac. Sci. Technol. 8 (1971) 738.

[103] B. E. Thompson, K. D. Allen, A. D. Richards and H. H. Sawin, *Ion bombardment energy distributions in radio-frequency glow-discharge systems*. J. Appl. Phys. 59 (1986) 1890.

[104] J. Liu, G. L. Huppert and H. H. Sawin, *Ion bombardment in rf plasmas*. J. Appl. Phys. 68 (1990) 3916.

[105] J. Janes and C. Huth, *Energy resolved angular distribution of argon ions at the substrate plane of a radio frequency plasma reactor*. J. Vac. Sci. Technol., A 10 (1992) 3522.

[106] J. Benedikt, A. Consoli, M. Schulze and A. von Keudell, *Time-resolved molecular beam mass spectrometry of the initial stage of particle formation in an $Ar/He/C_2H_2$ plasma*. J. Phys. Chem. A 111 (2007) 10453.

[107] G. Cunge, D. Vempaire, M. Touzeau and N. Sadeghi, *Broadband and time-resolved absorption spectroscopy with light emitting diodes: Application to etching plasma monitoring*. Appl. Phys. Lett. 91 (2007) 231503.

[108] M. Kogelschatz, G. Cunge and N. Sadeghi, *Identification of halogen containing radicals in silicon etching plasmas and density measurement by UV broad band absorption spectroscopy*. J. Phys. D: Appl. Phys. 37 (2004) 1954.

[109] G. Cunge, M. Fouchier, M. Brihoum, P. Bodart, M. Touzeau and N. Sadeghi, *Vacuum uv broad-band absorption spectroscopy: a powerful diagnostic tool for reactive plasma monitoring*. J. Phys. D: Appl. Phys. 44 (2011) 122001.

[110] J. B. Nee, M. Suto and L. C. Lee, *Quantitative spectroscopy study of HBr in the 105–235 nm region*. J. Chem. Phys. 85 (1986) 4919.

[111] N. S. J. Braithwaite, J. P. Booth and G. Cunge, *A novel electrostatic probe method for ion flux measurements*. Plasma Sources Sci. Technol. 5 (1996) 677.

[112] J. P. Booth, N. S. J. Braithwaite, A. Goodyear and P. Barroy, *Measurements of characteristic transients of planar electrostatic probes in cold plasmas*. Rev. Sci. Instrum. 71 (2000) 2722.

[113] D. Gahan, B. Dolinaj and M. B. Hopkins, *Retarding field analyzer for ion energy distribution measurements at a radio-frequency biased electrode*. Rev. Sci. Instrum. 79 (2008) 033502.

[114] D. Gahan, S. Daniels, C. Hayden, D. O. Sullivan and M. B. Hopkins, *Characterization of an asymmetric parallel plate radio-frequency discharge using a retarding field energy analyzer*. Plasma Sources Sci. Technol. 21 (2012) 015002.

[115] D. Briggs and M. P. Seah (Editors), *Practical Surface Analysis by Auger and X-ray Photoelectron Spectroscopy*. John Wiley & Sons (1983).

[116] J. Scofield, *Hartree-slater subshell photoionization cross-sections at 1254 and 1487 eV*. J. Electron Spectrosc. Relat. Phenom. 8 (1976) 129 .

[117] P. J. Cumpson and M. P. Seah, *Elastic scattering corrections in AES and XPS. II. Estimating attenuation lengths and conditions required for their valid use in overlayer/substrate experiments*. Surf. Interface Anal. 25 (1997) 430.

[118] S. Tanuma, C. J. Powell and D. R. Penn, *Calculations of electron inelastic mean free paths. V. Data for 14 organic compounds over the 50-2000 eV range*. Surf. Interface Anal. 21 (1994) 165.

[119] W. H. Gries, *A universal predictive equation for the inelastic mean free pathlengths of X-ray photoelectrons and auger electrons*. Surf. Interface Anal. 24 (1996) 38.

[120] C. Powell and A. Jablonski, *Surface sensitivity of X-ray photoelectron spectroscopy*. Nucl. Instrum. Methods Phys. Res., Sect. A 601 (2009) 54 .

[121] M. P. Seah and S. J. Spencer, *Ultrathin SiO_2 on Si. II. Issues in quantification of the oxide thickness*. Surf. Interface Anal. 33 (2002) 640.

[122] B. Pelissier, A. Beaurain, J. Barnes, R. Gassilloud, F. Martin and O. Joubert, *Parallel angle resolved XPS investigations on 12 in. wafers for the study of W and WSi_x oxidation in air*. Microelectron. Eng. 85 (2008) 1882 .

[123] E. Pargon, M. Darnon, O. Joubert, T. Chevolleau, L. Vallier, L. Mollard and T. Lill, *Towards a controlled patterning of 10 nm silicon gates in high density plasmas*. J. Vac. Sci. Technol., B 23 (2005) 1913.

[124] G. S. Oehrlein and Y. Kurogi, *Sidewall surface chemistry in directional etching processes*. Mater. Sci. Eng., R 24 (1998) 153 .

[125] S. Hamaguchi and M. Dalvie, *Microprofile simulations for plasma etching with surface passivation*. J. Vac. Sci. Technol., A 12 (1994) 2745.

[126] G. S. Oehrlein, J. F. Rembetski and E. H. Payne, *Study of sidewall passivation and microscopic silicon roughness phenomena in chlorine-based reactive ion etching of silicon trenches*. J. Vac. Sci. Technol., B 8 (1990) 1199.

[127] L. Desvoivres, L. Vallier and O. Joubert, *X-ray photoelectron spectroscopy investigation of sidewall passivation films formed during gate etch processes*. J. Vac. Sci. Technol., B 19 (2001) 420.

[128] O. Luere, E. Pargon, L. Vallier, B. Pelissier and O. Joubert, *Etch mechanisms of silicon gate structures patterned in $SF_6/CH_2F_2/Ar$ inductively coupled plasmas*. J. Vac. Sci. Technol., B 29 (2011) 011028.

[129] F. H. Bell, O. Joubert and L. Vallier, *Polysilicon gate etching in high density plasmas. II. X-ray photoelectron spectroscopy investigation of silicon trenches etched using a chlorine-based chemistry*. J. Vac. Sci. Technol., B 14 (1996) 1796.

[130] K. V. Guinn, C. C. Cheng and V. M. Donnelly, *Quantitative chemical topography of polycrystalline Si anisotropically etched in Cl_2/O_2 high density plasmas*. J. Vac. Sci. Technol., B 13 (1995) 214.

[131] L. Vallier, J. Foucher, X. Detter, E. Pargon, O. Joubert, G. Cunge and T. Lill, *Chemical topography analyses of silicon gates etched in $HBr/Cl_2/O_2$ and $HBr/Cl_2/O_2/CF_4$ high density plasmas*. J. Vac. Sci. Technol., B 21 (2003) 904.

[132] M. Darnon, T. Chevolleau, T. David, J. Ducote, N. Posseme, R. Bouyssou, F. Bailly, D. Perret and O. Joubert, *Patterning of porous SiOCH using an organic mask: Comparison with a metallic masking strategy*. J. Vac. Sci. Technol., B 28 (2010) 149.

[133] M. Darnon, T. Chevolleau, D. Eon, R. Bouyssou, B. Pelissier, L. Vallier, O. Joubert, N. Posseme, T. David, F. Bailly and J. Torres, *Patterning of narrow porous SiOCH trenches using a TiN hard mask*. Microelectron. Eng. 85 (2008) 2226 .

[134] J. H. Thomas, C. E. Bryson and T. R. Pampalone, *X-ray photoelectron spectroscopy surface charge buildup used to study residue in deep features on integrated circuits*. J. Vac. Sci. Technol., B 6 (1988) 1081.

[135] M. P. Seah and S. J. Spencer, *Attenuation lengths in organic materials*. Surf. Interface Anal. 43 (2011) 744.

[136] E. Pargon, O. Joubert, N. Posseme and L. Vallier, *Resist-pattern transformation studied by X-ray photoelectron spectroscopy after exposure to reactive plasmas. I. Methodology and examples*. J. Vac. Sci. Technol., B 22 (2004) 1858.

[137] M. Haass, M. Darnon and O. Joubert, *Sidewall passivation layer thickness and composition profiles of etched silicon patterns from angle resolved X-ray photoelectron spectroscopy analysis*. J. Appl. Phys. 111 (2012) 124905.

[138] J. Cazaux, *Secondary electron emission and fundamentals of charging mechanisms in XPS*. J. Electron Spectrosc. Relat. Phenom. 178 - 179 (2010) 357 .

[139] M. P. Seah, *Ultrathin SiO_2 on Si. VI. Evaluation of uncertainties in thickness measurement using XPS*. Surf. Interface Anal. 37 (2005) 300.

[140] C. Powell and A. Jablonski, *Effects of elastic-electron scattering on measurements of silicon dioxide film thicknesses by X-ray photoelectron spectroscopy*. J. Electron Spectrosc. Relat. Phenom. 114 - 116 (2001) 1139 .

[141] M. Tuda, K. Shintani and H. Ootera, *Profile evolution during polysilicon gate etching with low-pressure high-density $Cl_2/HBr/O_2$ plasma chemistries*. J. Vac. Sci. Technol., A 19 (2001) 711.

[142] X. Detter, R. Palla, I. Thomas-Boutherin, E. Pargon, G. Cunge, O. Joubert and L. Vallier, *Impact of chemistry on profile control of resist masked silicon gates etched in high density halogen-based plasmas*. J. Vac. Sci. Technol., B 21 (2003) 2174.

[143] M. A. Ali and Y.-K. Kim, *Ionization cross sections by electron impact on halogen atoms, diatomic halogen and hydrogen halide molecules*. J. Phys. B: At., Mol. Opt. Phys. 41 (2008) 145202.

[144] H. N. Kothari, S. H. Pandya and K. N. Joshipura, *Electron impact ionization of plasma important $SiCl_x$ (x = 1-4) molecules: Theoretical cross sections*. J. Phys. B: At., Mol. Opt. Phys. 44 (2011) 125202.

[145] G. Cunge, R. Ramos, D. Vempaire, M. Touzeau, M. Neijbauer and N. Sadeghi, *Gas temperature measurement in CF_4, SF_6, O_2, Cl_2, and HBr inductively coupled plasmas*. J. Vac. Sci. Technol., A 27 (2009) 471.

[146] C. Lee, D. B. Graves and M. A. Lieberman, *Role of etch products in polysilicon etching in a high-density chlorine discharge*. Plasma Chem. Plasma Process. 16 (1996) 99.

[147] H. Deutsch, K. Becker, P. Defrance, U. Onthong, M. Probst, S. Matt, P. Scheier and T. Märk, *Calculated absolute cross section for the electron-impact ionisation of simple molecular ions*. Int. J. Mass Spectrom. 223 - 224 (2003) 639 .

[148] National Institute of Standards and Technology, *Chemistry WebBook*.

[149] A. G. Smolin, O. S. Vasyutinskii, G. G. Balint-Kurti and A. Brown, *Photodissociation of HBr. 1. Electronic structure, photodissociation dynamics, and vector correlation coefficients*. J. Phys. Chem. A 110 (2006) 5371.

[150] D. Ebbing and S. Gammon, *General Chemistry, 9th ed.* Brooks Cole (2010).

[151] Y. Itikawa, A. Ichimura, K. Onda, K. Sakimoto, K. Takayanagi, Y. Hatano, M. Hayashi, H. Nishimura and S. Tsurubuchi, *Cross sections for collisions of electrons and photons with oxygen molecules*. J. Phys. Chem. Ref. Data 18 (1989) 23.

[152] V. Poterya, M. Fárník, P. Slavíček, U. Buck and V. V. Kresin, *Photodissociation of hydrogen halide molecules on free ice nanoparticles*. J. Chem. Phys. 126 (2007) 071101.

[153] J. Erö, *Radiofrequency modulation in the thoneman ion source*. Nucl. Instrum. 3 (1958) 303 .

[154] J. W. Coburn and E. Kay, *Positive-ion bombardment of substrates in rf diode glow discharge sputtering*. J. Appl. Phys. 43 (1972) 4965.

[155] P. Benoit-Cattin and L.-C. Bernard, *Anomalies of the energy of positive ions extracted from high-frequency ion sources. A theoretical study.* J. Appl. Phys. 39 (1968) 5723.

[156] Y. Okamoto and H. Tamagawa, *Energy dispersion of positive ions effused from an RF plasma.* J. Phys. Soc. Jpn. 29 (1970) 187.

[157] E. Kawamura, V. Vahedi, M. A. Lieberman and C. K. Birdsall, *Ion energy distributions in rf sheaths; review, analysis and simulation.* Plasma Sources Sci. Technol. 8 (1999) R45.

[158] A. D. Kuypers and H. J. Hopman, *Ion energy measurement at the powered electrode in an rf discharge.* J. Appl. Phys. 63 (1988) 1894.

[159] A. D. Kuypers and H. J. Hopman, *Measurement of ion energy distributions at the powered rf electrode in a variable magnetic field.* J. Appl. Phys. 67 (1990) 1229.

[160] A. Manenschijn, G. C. A. M. Janssen, E. van der Drift and S. Radelaar, *Measurement of ion impact energy and ion flux at the rf electrode of a parallel plate reactive ion etcher.* J. Appl. Phys. 69 (1991) 1253.

[161] C. Böhm and J. Perrin, *Retarding-field analyzer for measurements of ion energy distributions and secondary electron emission coefficients in low-pressure radio frequency discharges.* Rev. Sci. Instrum. 64 (1993) 31.

[162] M. E. Barone and D. B. Graves, *Molecular-dynamics simulations of direct reactive ion etching of silicon by fluorine and chlorine.* J. Appl. Phys. 78 (1995) 6604.

[163] N. Layadi, V. M. Donnelly, J. T. C. Lee and F. P. Klemens, *Cl_2 plasma etching of Si(100): Damaged surface layer studied by in situ spectroscopic ellipsometry.* J. Vac. Sci. Technol., A 15 (1997) 604.

[164] P. Sigmund, *Theory of sputtering. I. Sputtering yield of amorphous and polycrystalline targets.* Phys. Rev. 184 (1969) 383.

[165] W. D. Wilson, L. G. Haggmark and J. P. Biersack, *Calculations of nuclear stopping, ranges, and straggling in the low-energy region.* Phys. Rev. B 15 (1977) 2458.

[166] P. C. Zalm, *Energy dependence of the sputtering yield of silicon bombarded with neon, argon, krypton, and xenon ions.* J. Appl. Phys. 54 (1983) 2660.

[167] H. F. Winters and E. Taglauer, *Sputtering of chemisorbed nitrogen from single-crystal planes of tungsten and molybdenum.* Phys. Rev. B 35 (1987) 2174.

[168] C. Steinbrüchel, *Universal energy dependence of physical and ion-enhanced chemical etch yields at low ion energy*. Appl. Phys. Lett. 55 (1989) 1960.

[169] E. J. H. Collart, J. A. G. Baggerman and R. J. Visser, *On the role of atomic oxygen in the etching of organic polymers in a radio-frequency oxygen discharge*. J. Appl. Phys. 78 (1995) 47.

[170] D. E. Rosner and J. P. Strakey, *High-temperature kinetics of pyrolytic graphite gasification by fluorine atoms and molecules*. J. Phys. Chem. 77 (1973) 690.

[171] J. M. Lane, K. H. A. Bogart, F. P. Klemens and J. T. C. Lee, *The role of feedgas chemistry, mask material, and processing parameters in profile evolution during plasma etching of Si(100)*. J. Vac. Sci. Technol., A 18 (2000) 2067.

[172] H. Hübner, *Calculations on deposition and redeposition in plasma etch processes*. J. Electrochem. Soc. 139 (1992) 3302.

[173] P. Bodart, G. Cunge, O. Joubert and T. Lill, *$SiCl_4/Cl_2$ plasmas: A new chemistry to etch high-k materials selectively to Si-based materials*. J. Vac. Sci. Technol., A 30 (2012) 020602.

[174] C. Petit-Etienne, M. Darnon, P. Bodart, M. Fouchier, G. Cunge, E. Pargon, L. Vallier, O. Joubert and S. Banna, *Control of Si etching at the atomic scale using pulsed Cl_2 plasma*. J. Vac. Sci. Technol., B (submitted).